COMPARATIVE STUDY OF HUMAN IMMUNODEFICIENCY VIRUS TYPE 1 AND TYPE 2 SINGLE AND DUAL INFECTIONS

A Dissertation

Presented to

The Faculty of the Graduate School

At the University of Missouri

In Partial Fulfillment

Of the Requirements for

the Degree Doctor of

Philosophy

By

Assi Vincent De Paul Yapo

Drs. Stefan G. Sarafianos and Marc C. Johnson, Dissertation Supervisors

May 2020

The undersigned, appointed by the Dean of Graduates School,

have examined the dissertation entitled

COMPARATIVE STUDY OF HUMAN IMMUNODEFICIENCY VIRUS TYPE 1 AND TYPE 2 SINGLE AND DUAL INFECTIONS

Presented by Assi Vincent De Paul Yapo

A Candidate for the Degree of

Doctor of Philosophy

And hereby certify that, in their opinion, it is worthy of acceptance

Professor Stefan G. Sarafianos

Professor Marc C. Johnson

Professor David Pintel

Professor Mark Hannink

Dr Emma Teixeiro-Pernas

To my children, David and Noah,

And my spouse, Sandra

ACKNOWLEDGEMENTS

First and foremost, I would like to thank Jesus Christ, who carried me to this point. I am grateful to Foreign Student Fulbright Program for the unique opportunity I was given through the scholarship that covered my expenses during the first two years in the Molecular Pathogenesis and Therapeutics PhD program. I am also thankful to Drs Stefan Sarafianos and Marc Johnson, my two mentors for their continuing support during these five years that led to the completion of my PhD. I would like to extend my appreciation to Drs Philip Tedbury and Kamlendra Singh for their insights, encouragement and advice. I am fortunate to have the committee members I have. I received support from each one of you in so many ways from access to your offices, laboratories, reagents, your lab team to so much more. Recounting everything you have done for me over these years would be an exercise in futility that runs the risk of leaving key things and moments aside. Allow me to let you know I am really glad I had you all as my committee members.

To all past and current members of the Sarafianos lab in Missouri and in Georgia, it has been a great ride, if I may. I want to acknowledge all of you for sharing your experience, your tips, and all the other things you did not shy away from letting me know. In that regard, I am fortunate for the opportunity to work with Dr Maritza Puray-Chavez, a former senior graduate student in the laboratory. Finally, all the data produced during my research as a Graduate Research Assistant in the Sarafianos laboratory in Missouri, then later in the Johnson laboratory would not be possible without the precious collaborations established by Dr Sarafianos and the help of the Johnson laboratory members that made possible the access to specific reagents.

TABLE OF CONTENTS

LIST OF FIGURES AND TABLES

LIST OF ABBREVIATIONS

ACD: advanced cell diagnostic

AIDS: acquired immune deficiency syndrome

APC: antigen presenting cells

ART: anti-retroviral treatment

ATP: adenosine tri-phosphate

CA: capsid protein

CCR5: CC chemokine receptor type 5

CD: cluster of differentiation

ChIP: chromatin immuno-precipitation

CPSF6: cleavage and polyadenylation signal factor 6

CRF: circulating recombinant form

CXCR4: CXC chemokine receptor type 4

DAPI: 4',6-diamidino-2-phenylindole

DMEM: Dulbecco's modified Eagle's medium

dsDNA: double stranded deoxy-ribose nucleic acid

EC_{50}: effective concentration for 50% inhibition

Env: envelope

FISH: fluorescent in situ hybridization

GAg: group Antigen

GAPDH: glyceraldehyde 3-phosphate dehydrogenase

Gp: glycoprotein

HAART: highly active anti-retroviral therapy

HIV: human immunodeficiency virus

HLA: human leukocyte antigens

HRP2: hepatoma-derived growth factor-related protein 2

IL: interleukin

IN: integrase

IRF5: interferon regulatory factor 5

LEDGF/p75: 75KDa isoform of the transcriptional coactivator lens epithelium-derived growth factor

LI = link protein

LNTP: long term non-progressors

LTR: long terminal repeat

MA: matrix protein

MDM: monocyte-derived macrophage

MHC: major histocompatibility complex

MLV: murine leukemia virus

MOI: multiplicity of infection

mRNA: messenger Ribose Nucleic Acid

NELF: negative elongation factor

NFAT: nuclear factor of activated T cells

NF-KB: nuclear factor-kappa beta

NIH ARP: national institutes of health AIDS repository program

NNRTI: non-nucleoside reverse transcriptase inhibitor

NPC: nuclear pore complex

pDC: plasmacytoid dendritic cell

PIC: pre-integration complex (PIC)

POL: polymerase

PR: protease

qPCR: quantitative polymerase chain reaction

RRE: Rev responsive element

RSV: Rous sarcoma virus

RT: reverse transcriptase

SP1: specificity protein 1

SAMHD-1: SAM and HD domain containing deoxynucleoside triphosphate triphosphohydrolase 1

SIVcpz: Chimpanzee simian immunodeficiency virus

SIVsmm: sooty managbey monkey simian immunodeficiency virus

TAR: transactivation protein responsive RNA element

Tat: transactivation protein

TM: transmembrane protein

TRIM5α: tripartite motif-containing protein 5

TLR: toll-like receptor

TNF: tumor necrosis factor

T.O.A: time of addition assay

URF: unique Recombinant Form

COMPARATIVE STUDY OF HUMAN IMMUNODEFICIENCY VIRUS TYPE 1 AND TYPE 2 SINGLE AND DUAL INFECTIONS

Assi Vincent De Paul Yapo

Drs. Stefan G. Sarafianos and Marc C. Johnson, Dissertation Supervisors

ABSTRACT

Human Immunodeficiency Virus (HIV) type 1 and type 2 are two related lentiviruses that have strikingly divergent features in terms of transmission rates, distribution, pathogenesis, and clinical outcomes. In places where both viruses coexist, individuals infected with HIV-2 showed less susceptibility to incident HIV-1 infection. Moreover, dual infected individuals may have better outcomes compared to their HIV-1 counterparts. Attempts to decipher the mechanisms underlying these stark differences between HIV-1 and HIV-2 have been underway since the discovery of these two infections in the 1980s. Many factors have been proposed including SAM and HD domain containing deoxynucleotides triphosphate triphosphohydrolase 1 (SAMHD1) and Vpx, type I interferon (IFN) responses, CD8+ cytotoxic T cells responses, and HIV-2 specific antibody responses.

We studied the kinetics of HIV-1 and HIV-2 single infection with fluorescent in situ hybridization (FISH) coupled with microscopy, and with qPCR. Our data indicated

that HIV-1 infection in TZM-bl cells proceeded quickly upon viral entry. It led to a faster integration into the host cell genome, and to higher rates of transcription with transcriptional bursts than those observed with HIV-2. On the other hand, HIV-2 was slower with a roughly two hours delay in reverse transcription completion and integration relative to HIV-1. Analysis the state of the chromatin around HIV-1 and HIV-2 long terminal repeat (LTR) promoters showed that both LTRs had similar active chromatin marker H3K9me2 levels, and should be equally accessible to host transcription machinery. Host RNA polymerase II (RNAP II) occupancy analysis at each LTR promoter start sites showed less occupancy in the case of HIV-2 LTR.

Secondly, we demonstrated that under laboratory conditions, HIV-1 and HIV-2 can infect the same target cell, a phenomenon known as dual infection. We found that when HIV-2 infects the target cell at the same time or before HIV-1 infection, HIV-1 infection is inhibited. Under these conditions, inhibition was non-reciprocal meaning that HIV-2 inhibits HIV-1 but the reverse was not true. It was also dose-dependent as the higher the HIV-2 multiplicity of infection (MOI) used the higher the inhibition of HIV-1 infection. We identified two mechanisms. The first mechanism involved type I IFN responses that had broad effects on gene expression in the target cell. We also identified a second mechanism that was selective for HIV-1, other retroviruses such as Murine Leukemia Virus (MLV) and Rous Sarcomas Virus (RSV) were not sensitive to HIV-2-mediated inhibition. HIV-1 selective inhibition was mediated through HIV-2 TAR. This latter mechanism used a block of HIV-1 LTR-driven transcription at the elongation phase by decreasing HIV-1 Tat protein availability through competition between HIV-1 TAR and HIV-2 TAR for HIV-1 Tat protein. Mapping the sequences of HIV-2 TAR element required for the

downmodulation showed that any two-stem loop structure including the HIV-2 stem loop 2 was inhibitory to HIV-1 infection.

CHAPTER I: GENERAL INTRODUCTION OF HIV/AIDS

I. 1. The epidemic of HIV/AIDS

Since its onset, human immunodeficiency virus (HIV) has infected roughly 75 million people, and claimed the lives of 32 million people worldwide (*1-2*). HIV is the etiological agent of acquired immune deficiency syndrome (AIDS) in which a weakened immune system in HIV-infected individuals (< 200 CD4+ T lymphocytes/ml of peripheral blood) renders those with the condition susceptible to opportunistic infections (*3-20*). With the development of highly active anti-retroviral therapy (HAART), HIV infection has moved from a death sentence to a chronic infection with a lifelong treatment (*1-20*). As of 2018 (**figure I-1**), roughly 38 million people were living with HIV around the world (*1-2*). Among them, 23.3 million had access to HAART, and the number of newly infected individuals was slowly decreasing, and estimated to be 1.7 million in 2018 versus 3.2 million in 1999 at the peak of the HIV/AIDS epidemic (*1-2*).

Two genetically related HIVs have been described, HIV type 1 and HIV type 2 (*21-28*). HIV-1 resulted from the zoonotic transmission of SIV chimpanzee, itself a product of recombination between SIVs from red capped mangabeys and guenons, while HIV-2 is derived from SIV sooty mangabey (*21-28*). HIVs diverge in terms of nucleotide sequences, geographic distribution, rates of transmission, pathogenesis, and mortality rates. HIV-1 is responsible for the current global pandemic (**figure I-2 and table I-1**), whereas HIV-2 is mainly restricted to West Africa, with sporadic cases outside of that region (*29-33*). HIV types 1 and 2 are further classified into groups (HIV-1), subtypes or clades (both), and

recombinant forms (both) based on their sequence homology (*4-7,17,20*), their frequency, and their geographical localization (*1-2,14,16,19*).

HIV-1 has four groups (**table I-1**), each resulting from a distinct zoonotic transmission, the main group also called group M, the outlier group (group O), the non-M and non-O group also referred to as group N, and finally the group P which is the latest to be described (*29,32*). HIV-1 group M is the most common group, and it includes ten subtypes (A, B, C, D, E, F, G, H, J, and K) and hundreds of circulating or unique recombinant forms (CRF or URF). HIV-1 group M, subtype B is the common clade found in Western countries (*29,32*), whereas non-B clades such as the HIV-1 subtype C predominates in South Africa (the most affected country in the world) and India (**figures I-1 and I-2**). The CRF02_AG is the prevalent strain of HIV-1 group M in Western Africa. HIV-2 is not divided into groups, but is subdivided into six subtypes (A, B, C, D, E, and F). Except for HIV-2 subtypes A and B, no other subtype has been reported to be transmitted from human to human. Subtypes C to F have been found in unique individuals and no cases of transmission exist so far (*29,32*). HIV-2 clades A and B are responsible for almost every case of HIV-2 infections around the world (*20*). And in 2010, a research group in Japan described the first recombinant HIV-2 virus to be isolated from a patient in the CRF01_AB virus (*17*).

HIV-2 has shown slower transmission rates for most transmission routes (*12,14,16,34*), lower pathogenesis with an asymptomatic phase before the advent of HAART twice as long as HIV-1's, and a slower progression to AIDS and lower mortality risks overall (*12-13,15,18,35-36,38-42,44*). Moreover, HIV-2 incidence and prevalence are rapidly declining pointing to a possible disappearance of the infection (*14,16,19*). In its

traditional epicenters such as Guinea Bissau, HIV-2 infection has been replaced by HIV-1 infection (*14,16,19*). In places where both types of HIV coexist, cases of patients infected with both viruses have been reported (*45-55*). These cases are referred to as HIV-1 and HIV-2 dual-infections.

Figure I-1: Global Distribution of adults (15-49 years old) living with HIV in 2017

The prevalence of HIV was estimated based on reports from participating countries and color-coded from light yellow corresponding to countries with very low prevalence in the population of 15 years old to 49 years old, to dark red corresponding to very high prevalence (*2*).

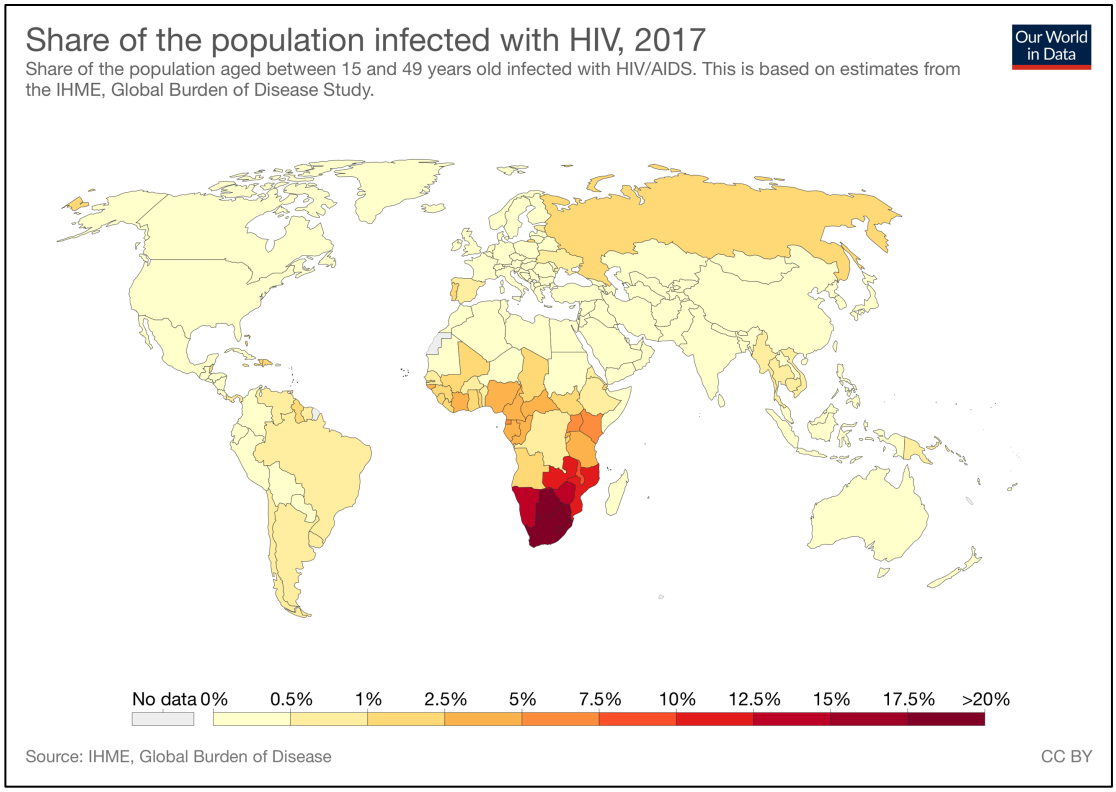
Share of the population infected with HIV, 2017
Share of the population aged between 15 and 49 years old infected with HIV/AIDS. This is based on estimates from the IHME, Global Burden of Disease Study.
Our World in Data
No data
0%
0.5%
1%
2.5%
5%
7.5%
10%
12.5%
15%
17.5%
>20%
Source: IHME, Global Burden of Disease
CC BY

Table I-1: Genetic diversity of HIV

The genetic diversity of HIV is illustrated through its classification into two types, HIV-1 and HIV-2. These two differ in their sequence homology, originate from different SIVs, have different distribution in the world. HIV-1 has a global repartition with several strains grouped into four different groups M, N, O and P. HIV-2 does not have groups. (*32*).

Type	Group	Origin	Isolates (%)[1]	Epidemiology	Comments
HIV-1	M	SIVcpz	259,678 (98.2%)	All continents with exception of Antarctica	Major group responsible for the AIDS pandemic; more fit than HIV-1 group O and HIV-2.
	O	SIVgor or SIVcpz	1,095 (0.4%)	Majorly found in Central and West Africa	Naturally resistant to NNRTI; less fit than group HIV-1 M and HIV-2.
	N	Recombinant group M ancestor / SIVcpz	22 (<0.001%)	Only found in Cameroon	Very rare epidemically; few studies on drug resistance published.
	P	SIVgor	Single case	Undetermined	Described in 2009 in a Cameroonian woman. The actual number of infections is unknown.
HIV-2	—	SIVsm	3,593 (1.4%)	Mainly found in Western and Central Africa; some cases in Western Europe, India, United States, Brazil and Japan	Apparently slower progression to AIDS; less susceptible to some anti-HIV-1 drugs; naturally resistant to NNRTI.

[1] Isolates sequenced and available at the Los Alamos HIV Sequence Database as of 18 July 2009.

Figure I-2: Global Distribution of HIV-1 clades (subtypes and CRFs)

HIV-1 clades or subtypes have different geographical distribution with the clade B representing the sole strain in the Americas and Western Europe. Non-clades B were the more frequent outside of these two regions with clades A, C and the CRF02_AG as major players (*32*).

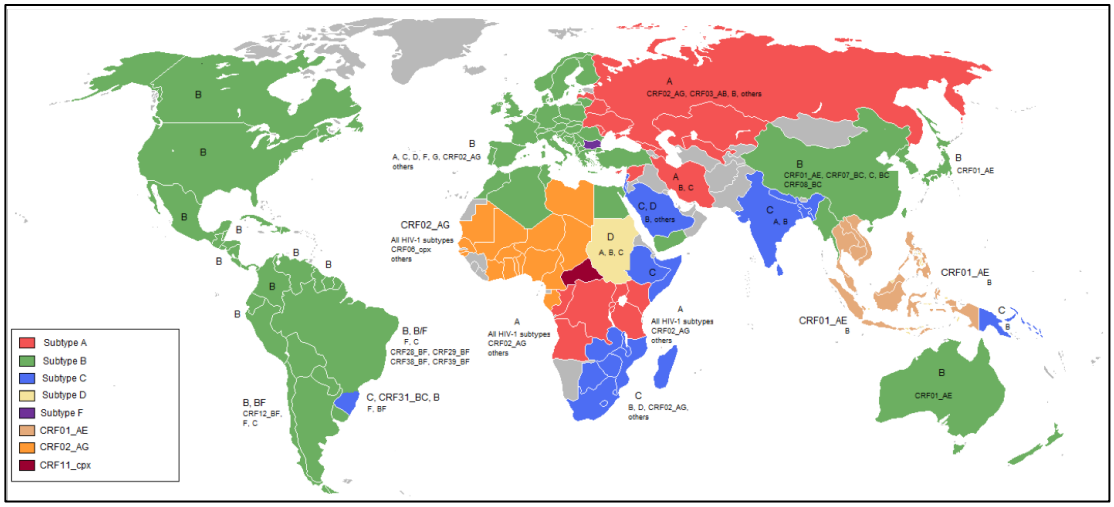
Subtype A
Subtype B
Subtype C
Subtype D
Subtype F
CRF01_AE
CRF02_AG
CRF11_cpx
A
CRF02_AG, CRF03_AB, B, others
B
A, C, D, F, G, CRF02_AG
others
A
B, C
C, D
B, others
B
CRF01_AE, CRF07_BC, C, BC
CRF08_BC
B
CRF01_AE
C
A, B
CRF02_AG
All HIV-1 subtypes
CRF06_cpx
others
D
A, B, C
C
A
All HIV-1 subtypes
CRF02_AG
others
A
All HIV-1 subtypes
CRF02_AG
others
C
B, D, CRF02_AG,
others
CRF01_AE
B
C
B
CRF01_AE
B
CRF01_AE
B, B/F
F, C
CRF26_BF, CRF29_BF
CRF38_BF, CRF39_BF
B, BF
CRF12_BF,
F, C
C, CRF31_BC, B
F, BF

I. 2. Human immunodeficiency viruses (HIVs)

HIV-1 and HIV-2 belong to the family of the Retroviridae, the subfamily of the Orthoretrovirinae, and to the genus of Lentiviruses (*3,5,8,12*). They evolved from non-human primate immunodeficiency viruses that infect either Central African chimpanzees (SIVcpz for HIV-1) or West African sooty mangabeys (SIVsm for HIV-2), and were introduced into the human populations between 1920 and 1940 (*21-28*). They are enveloped viruses with two copies of single stranded positive sense ribonucleic acid (RNA) of 9.2 to 9.6 kbps size for HIV-1 and approximately 9.8 kbps for HIV-2 (*3,8,12*). They also carry within their viral particle several viral factors and enzymes necessary for successful infection as shown in **figure I-3** (*33*).

HIV-1 and HIV-2 have very little sequence homology for any given viral genes. Yet, both viruses have an overall similar genome organization as the related SIVs (**figure I-4**) (*32*). They all have a capped 5' m^7 GpppU LTR that represents the regular viral promoter (*41*). That promoter is regulated by the cellular RNA polymerase II, and it drives viral gene expression during infection (*56-77*). HIV-2 LTR has a longer sequence of roughly 400 nucleotides whereas HIV-1 has a shorter sequence of roughly 200 nucleotides (**figure I-5**) (*41*). The transactivation RNA (TAR) element is around 60 nucleotides for HIV-1, and 160 nucleotides long in HIV-2 (*41,56-77*). Viral LTRs contain regulatory elements that are different in each one of the HIVs. For instance, HIV-2 lacks the NFAT binding sites that are present in HIV-1 LTR (*78*).

The viral promoter is followed by three main groups of viral genes (*GAG*, *POL* and *ENV*), and the viral genome ends with a polyadenylated 3' LTR that is a reverse replicate of the 5'LTR. HIV LTRs transcribe various viral RNAs. These RNA species are either

non-spliced as the subgenomic RNA, or singly spliced as the envelope mRNA, or multiple times spliced products as the Rev mRNA. The subgenomic RNA contains a stop codon within the *POL* gene, and in 95% of the cases, only the Gag polyprotein is synthesized. The Gag polyprotein contains the matrix protein, the capsid protein, the nucleocapsid protein, the late domain proteins and two spacer proteins. These components are involved in viral assembly and budding from the infected cells. In 5% of the cases, there is a ribosomal frameshift that produces a Gag-Pol polyprotein. Pol contains components such as reverse transcriptase with its Rnase H domain, protease, and integrase (*12,29,33,72*).

The third polyprotein produced during HIV infection is the HIV Env polyprotein. It is a glycoprotein that contains two subunits, the transmembrane subunit (gp41 for HIV-1) and the extra cellular subunit (gp120 for HIV-1). The Env glycoprotein is heavily glycosylated and trafficked to the viral assembly sites at the plasma membrane of the infected cells. Spliced RNA species give rise to viral regulatory genes: transactivation protein (Tat) and the unspliced and partially spliced RNA species export protein (Rev). Further spliced transcripts code for the accessory proteins Nef, Vif and Vpr that are common to both HIV-1 and HIV-2. Two other accessories genes are specific for each one of the HIVs, the Vpu (HIV-1) or Vpx (HIV-2), and specific antibodies raised against their products can be used to tell apart their respective infection in cell culture during dual infections (*12,29,31,33*).

Figure I-3: HIV-1 mature and immature viral particles

Schematic view of the HIV particle, corresponding electron micrograph (right) and immunoblot bands (left). Gp = Glycoprotein; p = protein; SU = surface protein; TM = transmembrane protein; gp160 (precursor of SU and TM); RT = reverse transcriptase; IN = integrase; CA = capsid protein; MA = matrix protein; PR = protease; NC = nucleic acid binding protein; LI = link protein. MHCs (major histocompatibility complexes) are HLA antigens. Graphic from Hans Gelderblom, at the Robert Koch Institute, Berlin, Germany. Reproduced with the permission #4735151500896 from Karger Publishers (*33*).

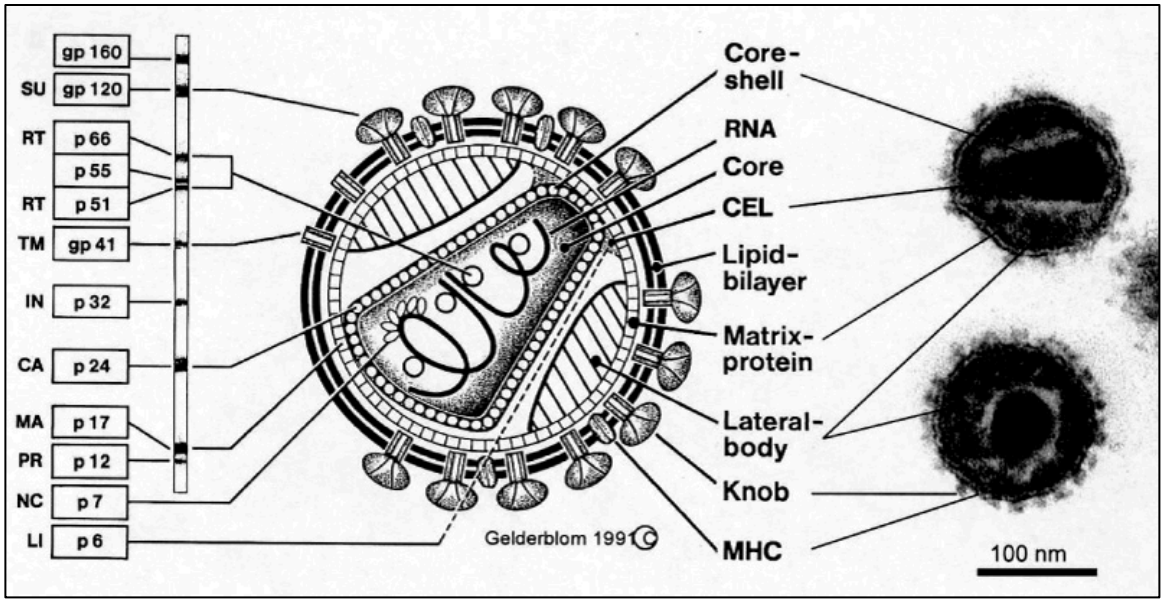
gp 160
SU
gp 120
RT
p 66
p 55
RT
p 51
TM
gp 41
IN
p 32
CA
p 24
MA
p 17
PR
p 12
NC
p 7
LI
p 6
Core-shell
RNA
Core
CEL
Lipid-bilayer
Matrix-protein
Lateral-body
Knob
MHC
Gelderblom 1991
100 nm

Figure I-4: Genome map and organization of HIV-1 and HIV-2

The genomes of HIV-1, HIV-2, SIVcpz, SIVagm, and SIVsm are organized in similar ways. From the 5' end to the 3' end, all have a 5' LTR that is shorter in HIV-1 than HIV-2. The *Gag* gene follows right after the LTR. Then come the *Pol* and *Env* genes. Besides the three main genes, HIV-1 and HIV-2 have in common several regulatory and accessory genes such as *Vif, Vpr, Tat, Rev, and Nef*. They differ by two accessory genes that are each specific of each virus, HIV-1 *Vpu* and HIV-2 *Vpx*. The 3' end has also an LTR that is an identical reverse of the 5' end LTR (*32*).

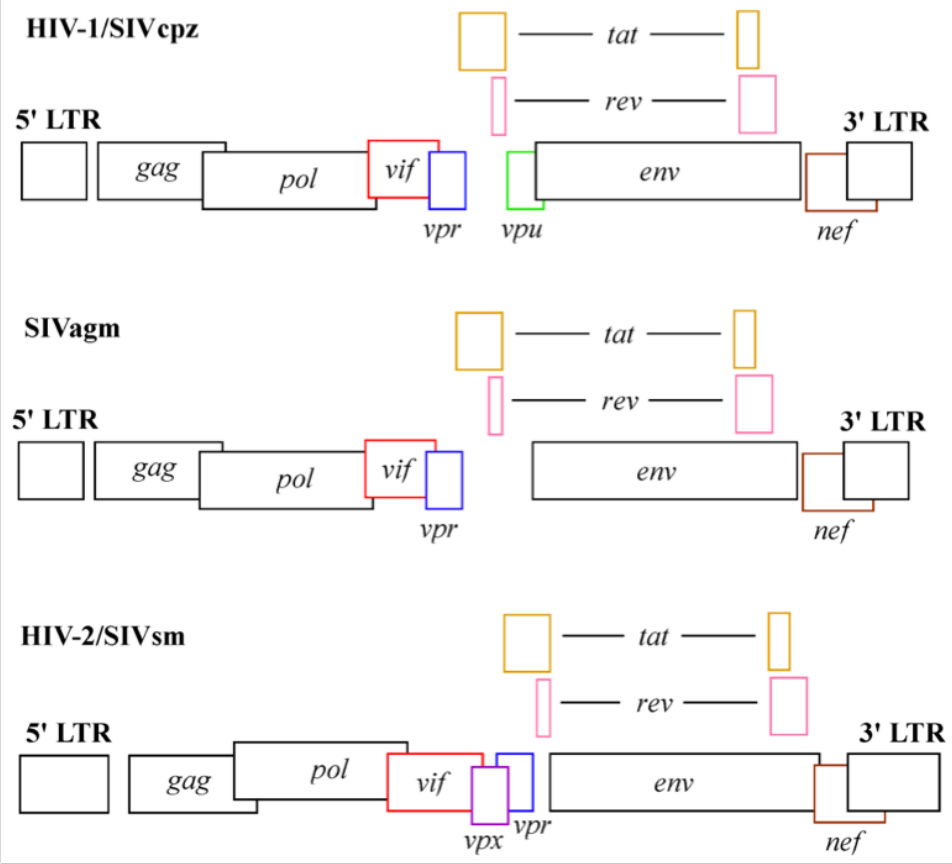
HIV-1/SIVcpz
tat
rev
5' LTR
3' LTR
gag
pol
vif
env
vpr
vpu
nef
SIVagm
tat
rev
5' LTR
3' LTR
gag
pol
vif
env
vpr
nef
HIV-2/SIVsm
tat
rev
5' LTR
3' LTR
gag
pol
vif
env
vpx
vpr
nef

Figure I-5: HIV 5' LTR promoters' structure

Both HIV-1 and HIV-2 genomes start with a 5' m7 G followed by the transactivation response RNA element (TAR). The predicted structure of HIV-2 TAR is twice as long as experimentally derived HIV-1 TAR. It has a duplicated stem loop 1 in stem loop 2, and an additional third stem loop 3 at its 3' end. HIV-1 TAR was resolved by NMR, and it has only one stem loop. The TAR in each virus is followed by the polyadenylation signal sequence second stem in HIV-1 LTR structure and fourth in HIV-2's. Then comes the primer binding site that is longer in HIV-2 than in HIV-1. The dimerization signal, the packaging signal, and the splice donor represent the next three stem loops found in HIV-1 5' LTR promoter right before the AUG start codon. HIV-2 has on top of these three stem loops, two additional stem loops (*41*). Reproduced with the permission #4731100977953 from Oxford University Press.

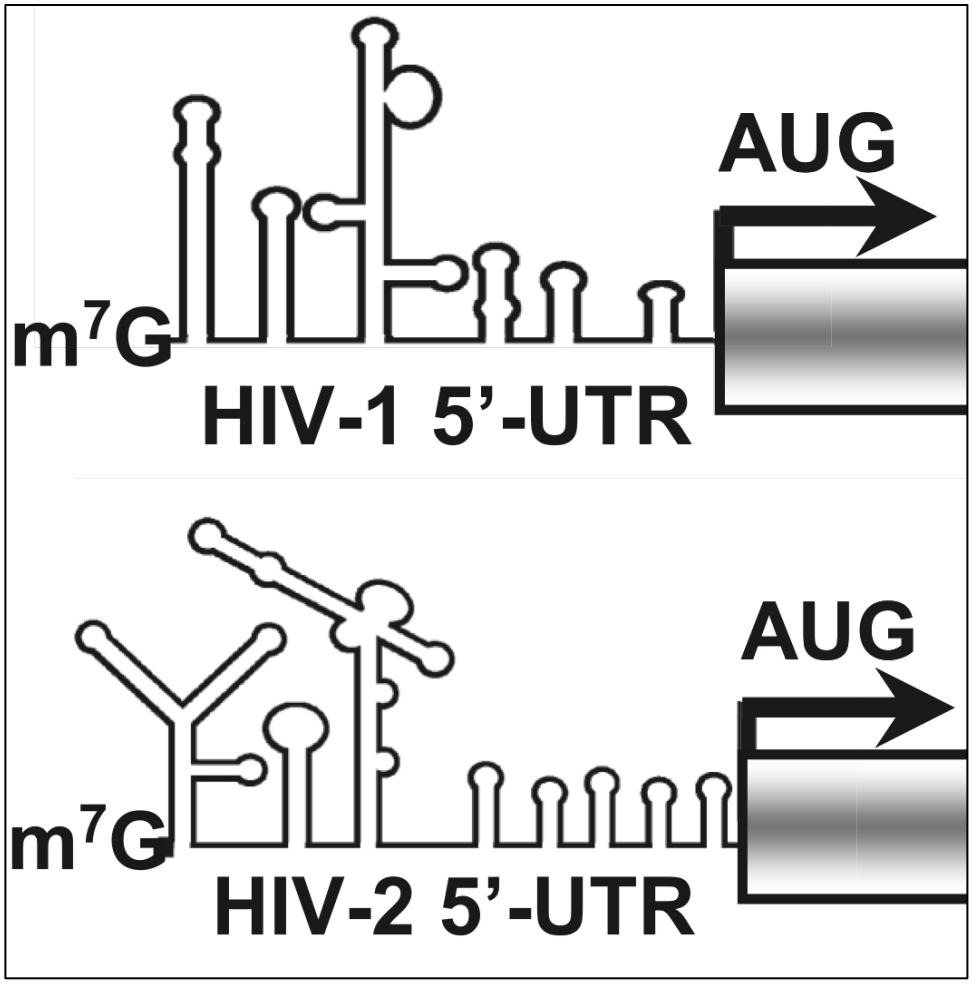
AUG
m7G
HIV-1 5'-UTR
AUG
m7G
HIV-2 5'-UTR

I. 3. The virus life cycle

Virus entry:

The primary target cell for HIVs are CD4+ T lymphocytes, and they have a lytic replication cycle in the infected cells (*29,33,79-82*). The cycle starts with the recognition and the attachment to the CD4 receptor on the surface of the target cell (**figure I-6**) (*29,33,79-82*) through their envelope glycoproteins (gp120). This attachment leads to conformational changes consisting of rearrangements of the variable loops V1-V3 of gp120. The gp120 through its V3 loop binds to either the CCR5 or CXCR4 coreceptor on the target cell surface. This binding exposes the second viral envelope glycoprotein (gp41) that inserts itself into the target cell plasma membrane. Upon insertion, gp41 forms a six-helix bundle that brings both viral and cellular membranes into contact. By doing so, gp41 triggers the fusion of the two membranes, and the release of the viral core into the cytoplasm of the target cell completing the entry phase of the viral life cycle (*29,33,79-82*).

Cytoplasmic trafficking:

Upon release of the viral core into the cytoplasm (**figure I-6**), HIV reverse transcriptase starts the process of synthesizing a double stranded viral DNA from the two copies of viral RNA to generate a viral pre-integration complex (PIC) (*83-84*). The PIC contains the viral DNA that has a CA dinucleotide at its 3' end. The CA dinucleotide is removed by HIV integrase (IN) in a process called 3' end processing before becoming a provirus (*83-84*). Viral DNA can be linear which constitutes the majority of the species present in an infected cell. It can have various aberrant forms resulting from autointegration events in which the HIV IN proceeds to the strand transfer reaction within the same linear

vDNA (*82*). The HIV PIC also contains other virally imported factors such as Vpr and capsid (p24). Although, it is still controversial, reverse transcription seems concurrent to the process of uncoating which involves cellular factors such as transportin-3 (TNPO3), cleavage and polyadenylation specific factor 6 (CPSF6), cyclophilin A, and kinesin that get recruited to the capsid core during the cytoplasmic transit (*80,85-91*). A partially uncoated core favors reverse transcription (*84*). It helps with the use of macromolecules transport mechanisms (*80*). And it shields the newly synthesized viral DNA from cellular cytoplasmic sensors (*93-96*) in order to evade immune sensors such as the cyclic GMP-AMP Synthetase (cGAS).

Cytoplasmic trafficking of the partial core uses the dynein motor protein and several host factors to bring the PIC towards the nucleus (*80*). TNPO3 is a karyopherin that carries SR protein family members to the nucleus (*87-88*). SR proteins are involved in splicing events, and CPSF6 is a member of that family (*85-86*). Recruitment of CPSF6 to HIV CA has been reported to result in a hyper stable capsid (*85-86*). Interestingly TNPO3 and CPSF6 both bind to the capsid lattice (*84-86*). Cyclophilin A is also recruited to HIV-1 CA but not HIV-2 CA lattice (*97-99*). Cyclophilin A binding has been proposed to destabilize HIV-1 CA lattice after recruitment. Cytoplasmic trafficking culminates with the passage of the PIC through the nuclear pore complexes (NPC) into the nucleus of non-dividing cells (*80,100-103*). Nuclear entry also happens with the breakdown of the nuclear envelope during mitosis in dividing target cells (*80,81,91*).

Of note, several host restrictions factors act between viral fusion and transit of the HIV PIC into the nucleus (*104-119*). For instance, the host SAMHD-1 restricts HIV infection by depleting the cytoplasmic pool of deoxyribonucleotides triphosphates (dNTP)

available for the synthesis of the viral DNA in non-dividing cells such as macrophages and resting CD4 T cells (*104*). It is counteracted by HIV-2 Vpx that targets it for proteasome degradation whereas HIV-1 which lacks Vpx, remains sensitive to its action in MDM and poorly infects those cells (*104-105*). The newly synthesized viral DNA can be subject to lethal hypermutations by some members of the human apolipoprotein B mRNA-editing enzyme catalytic polypeptide-like 3 (APOBEC3) family of proteins leading to an inactive provirus (*106-111*). It has been hypothesized that cellular APOBEC3 proteins can be packaged into viral particles in the producer cells (*110*). When those virions infect new target cells, viral DNA synthesis would be blocked by the impairment of HIV RT translocation along the viral RNA and DNA template by APOBEC3 according to the so-called road-block hypothesis (*110*). At any rate, HIV Vif targets APOBEC3 family protein members for degradation in the producer cell to prevent packaging into the virion, subsequent RT impairment, and hypermutations of the viral DNA from occurring (*111-117*). HIV capsid proteins can be targeted by various TRIM5 alpha proteins from Old World monkeys to human TRIM5 alpha (*118-121*). TRIM5 alpha is an interferon stimulated gene (ISG) that inhibits HIV-1 infection in old world monkeys. However, its human counterpart was shown to be less inhibitory power on HIV-1 while exerting a stronger restriction on HIV-2. Differences in sensitivity to human TRIM5 alpha originate from of their respective capsid proteins. And human TRIM5 alpha builds a mesh around the HIV capsid, leading to its premature breakdown and the inhibition of HIV reverse transcription (*118-121*). Another potent ISG that was identified through a comparative screening of cell lines that support or not type I IFN-mediated inhibition of HIV-1 is the Myxovirus resistance 2 protein (Mx2) (*122*). It is a human type I interferon-induced GTP-

binding protein that inhibits HIV-1 and a number of other lentiviruses. MX2 inhibits HIV-1 infection by blocking the capsid-dependent nuclear translocation of PICs, inhibiting infection at an early stage (*122*).

Nuclear trafficking:

Nuclear entry starts with the docking of the partial core containing the PIC to the NPC through interactions of the capsid lattice with the cytoplasmic filaments of Nup358 also called RanBP2 (*80,98-100*). Nup358 cytoplasmic filaments have a cyclophilin A domain allowing them to interact with capsid core (*80,98-100*). After docking to the NPC, the partial core goes through of the NPC via its interactions with numerous Nups such as Nup62 at the nuclear ring, and Nup153 at the nuclear basket (*88,123-124*). Inside the nucleus of the infected cell, the HIV linear unintegrated DNA is the target of the cellular DNA repair machinery (*125*) that makes from it episomes of 1 LTR circles and 2 LTR circles. Due to their exclusive nuclear localization, those episomes can serve as markers of nuclear entry for HIV.

HIV gene expression starts from the linear unintegrated vDNA (**figure I-6**) under the control of HIV Vpr in a Tat-independent manner (*82,126-128*). Early viral proteins needed for successful infection such as HIV Tat, HIV Rev, and HIV Nef are quickly expressed before gene expression from the integrated provirus can even start (*82,126-126*). The viral Nef protein downmodulates the surface receptor CD4, the coreceptor CCR5 and CXCR4, and MHC class I molecules. This serves a triple purpose. It prevents superinfection and its inherent toxicity. It allows proper trafficking of the viral envelope glycoprotein to the plasma membrane and the proper budding of progeny virions. It helps

avoid CD8+ cytotoxic T lymphocytes (*82,122-132*). The viral Tat protein increases the transcriptional activity of the integrated provirus LTR promoter by hijacking the cellular positive transcription elongation factor b (P-TEFb), a kinase to further phosphorylate the C-terminal domain (CTD) of RNAP II. The viral Rev protein binds to the Rev responsive element (RRE), present in the partially spliced and the unspliced transcripts in order to facilitate their export into the cytoplasm through the hijacking of the CRM-1 export pathway that otherwise would only export tRNAs, rRNA and other non-mRNAs (*82*).

Usually, nuclear translocation is followed by integration into the host cell genome of the proviral DNA (**figures I-6 and I-7**), mediated by HIV IN. By that point, an infected cell, the vDNA pool contains the linear unintegrated vDNA, the linear integrated provirus, episomes of 1 LTR circles and 2 LTR circles, and auto-integrants. Quantification of total vDNA measure all these forms together whereas specific PCR can quantify specific forms such as 2 LTR episomes (nuclear entry assessment) and the integrated linear provirus (integration assessment). HIV integration preferentially occurs at regions of the host genome within the body of highly expressed genes away from the gene promoter region (*135-137*). Highly expressed cellular genes are located within the euchromatin, a loosely packed chromatin, rich in gene concentrations, and genetically active (*136-137*). It has a high occupancy of the active histone markers such as H3K4me2, and it is accessible to the cellular transcription machinery (RNA polymerase II). Heterochromatin on the contrary is a firmly packed chromatin, poor in genes (epigenetic silencing), and genetically inactive (*136-137*). It has low occupancy of markers such as H3K4me2 and it is less accessible to the transcription machinery. Reports have shown that interactions of HIV capsid with CPSF6, TNPO3, Nup153, as well as HIV IN interactions with the p75 isoform of the

transcriptional coactivator lens epithelium-derived growth factor (LEDGF)/p75, help with integration sites selection and with the efficiency of the integration process (*138-142*).

From the integrated provirus (**figure I-7**), HIV late gene expression proceeds in two transcriptional and two nuclear export steps (*143*). The HIV LTR promoter drives transcription of viral mRNAs by RNAP II. The LTR promoter has been shown to be an efficient promoter at initiating transcription. However, transcription mostly stalls at the promoter region, and RNAP II is unable to efficiently clear the promoter and elongates the newly synthesized transcripts. That first transcriptional step is referred to as basal transcription, and it produces mainly abortive RNA transcripts (short transcripts containing sequences from the 5' LTR with no poly A tail) due to a block of the LTR-driven transcription by the cellular negative elongation factor (NELF). NELF prevents the further phosphorylation of the C-terminal domain (CTD) of RNAP II, thus blocking promoter clearance and the elongation phase of transcription (*57-78*). HIV Tat protein increases the phosphorylation state of RNAPII by binding to HIV TAR and recruiting (P-TEFb) complex. The P-TEFb complex contains among other factors the cyclin-dependent kinase 9 (cdk9) and the cyclin T1. Recruitment of the P-TEFb complex allows additional phosphorylation of RNAP II CTD serine 2 residues, which in turn allows for promoter clearance and for an increase in the transcriptional activity from the LTR. This marks the second transcriptional step and results in long and complete viral transcripts (*57-77,143*).

Some species of viral transcripts quickly accumulate in the nucleus of the infected cells, a phenomenon observed with the technique of *FISH* coupled to microscopy and referred to as transcriptional burst (*143*). These transcripts are categorized into fully spliced transcripts, partially spliced transcripts and non-spliced transcripts. Only fully spliced HIV

transcripts are exported outside the nucleus of the infected cells though the cellular NF1/NxT1 export pathway (*56,143*). This corresponds to the first nuclear export phase. HIV Rev mediates the nuclear export of all the partially spliced and non-spliced RNA species through interaction with the RRE present in all those transcripts (*57,143*). That interaction allows those transcripts to hijack the cellular CRM-1 export pathway to gain access to the cytoplasm of the infected cells in order to be translated into viral components. This marks the second nuclear export phase, and allows for the expression of all viral components required for virion release.

Viral components synthesis, assembly and budding:

The viral transcripts are translated into viral polyproteins either by polyribosomes in the cytoplasm (Gag-Pol and Pol) or at the endoplasmic reticulum (Env, Nef) to perform key duties necessary to successful infection (**figure I-7**). For instance, HIV-1 Vpu and HIV-2 envelope downmodulate the human CD4 protein (entry receptor) and tetherin also called bone marrow stromal protein 2 (BST2) from the plasma membrane to allow efficient budding and release (*144-145*). Envelope glycoproteins are highly glycosylated in the ER and the trans-Golgi network, and traffic to assembly sites at the plasma membrane. HIV Gag polyproteins also traffic to the same assembly sites as the envelope glycoproteins, and assemble into a lattice there, driven by hexamer formation by CA. HIV nucleocapsid (NC), a part of HIV Gag polyprotein recruits two copies of the viral genomic RNA through their packaging and dimerization signals (*146-147*).

During budding, the Gag polyprotein though its PTAP motif hijacks the endosomal sorting complexes required for transport (ESCRT) machinery at the plasma membrane to

favor timely budding and release of the maturing viral particles. Gag PTAP motif mimics the P(T/S)AP motif of hepatocyte growth factor-regulated tyrosine kinase substrate (HRS) to recruit TSG101 (member of ESCRT-I), the accessory protein Alix, the ESCRT-III complexes, and Vps4 to constrict and severe the neck of the budding virion from the producing cell surface (*146*). Virus maturation is performed by the viral protease that processes the viral polyproteins into their individual components. Virus maturation initial and critical step is the maturation of the Gag-Pol precursor. It consists in the folding/dimerization of the protease domain and the formation of an active site that is capable of catalyzing the hydrolysis of the peptide bonds at crucial sites to release the mature protease. Once the mature protease is released from the Gag-Pol polyprotein, it has an optimal enzymatic activity and a specificity that allow it to process the Gag and Gag-Pol polyproteins at precise sites to release a large number of mature proteins required for viral assembly and maturation. Mature HIV particles are able to start over the life cycle in a new target cell (*29,33,80,147*).

Figure I-6. Replication cycle of HIV and transcription from unintegrated DNA

Viral fusion and entry require the binding of glycoprotein gp120 to CD4 receptors at the cell surface as well as to CCR5 or CXCR4. The viral nucleocapsid enters the cytoplasm and uses cytoplasmic dynein to move toward the NPC. The viral RNA is retrotranscribed into proviral double-stranded DNA (dsDNA), which can stay in the cytosol, where it is highly unstable and exists in a transient, reversible pre-integration latent state, or can form a PIC consisting of dsDNA, viral proteins and some host cell proteins. When ATP levels are adequate, the pre-integration complex is transported into the nucleus through the NPC, and the dsDNA either circularizes as one or two long terminal repeat-containing circles or is integrated into a host cell chromosome. Prior to integration, or if integration is blocked, transcription from unintegrated cDNA may still occur, the template for which is unknown. Virally imported Vpr is important in the initial stages of viral gene transcription. Translation of multiply-spliced RNA (msRNA) transcripts leads to expression of Tat, Nef and Rev. Levels of Rev are insufficient to lead to the export of singly spliced and unspliced transcripts. Tat and Nef collectively lead to increased cellular activation in resting T-cells. Newly synthesized Tat will also promote viral gene transcription. Nef downregulates cell surface CD4, CXCR4, CCR5 and MHC-I (HLA class I) (*82*).

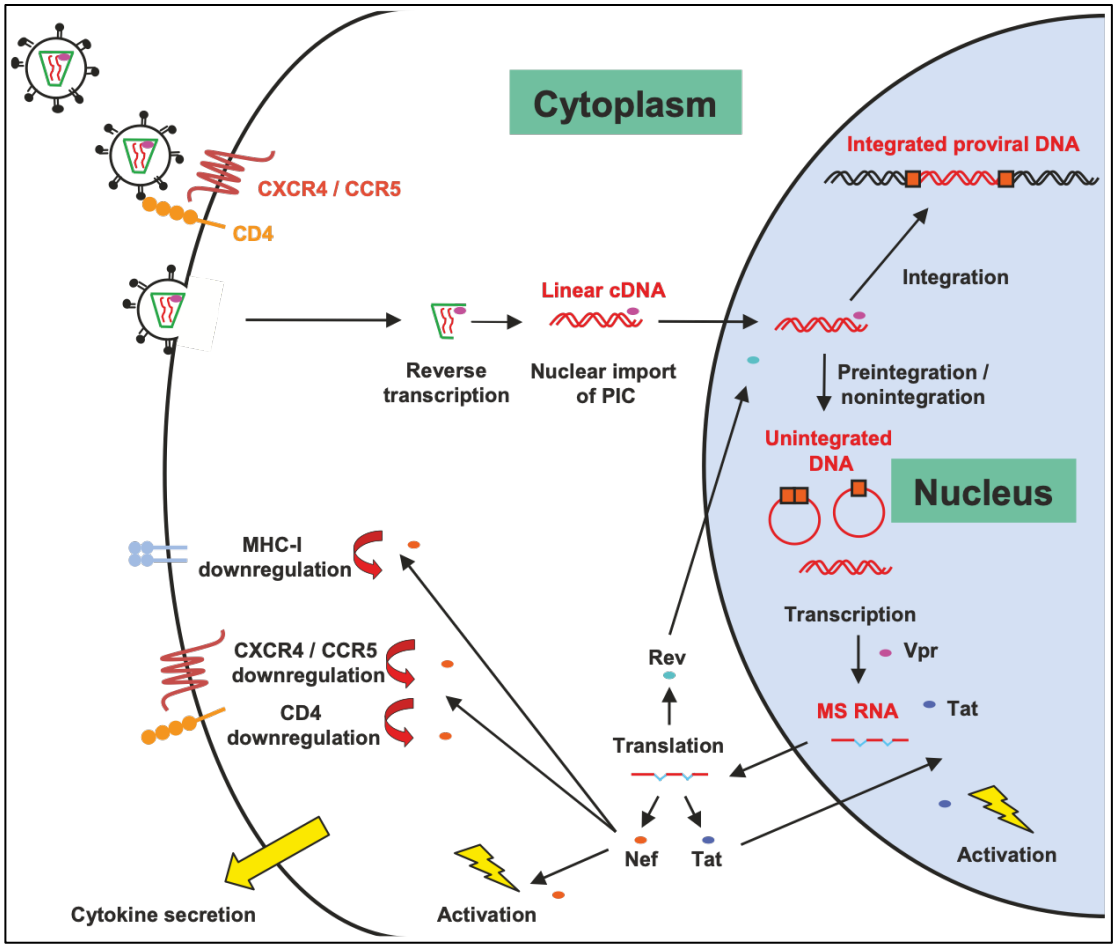
Cytoplasm
Nucleus
CXCR4 / CCR5
CD4
Linear cDNA
Reverse transcription
Nuclear import of PIC
Integrated proviral DNA
Integration
Preintegration / nonintegration
Unintegrated DNA
Transcription
Vpr
MS RNA
Tat
Rev
Translation
Nef
Tat
Activation
MHC-I downregulation
CXCR4 / CCR5 downregulation
CD4 downregulation
Cytokine secretion
Activation

Figure I-7. Replication cycle of HIV and transcription from integrated provirus

After integration, the provirus remains quiescent, existing in a post-integration latent state. On activation, the viral genome is transcribed by the synergic interaction of cellular transcription factors (nuclear factor-B - NF-B), nuclear factor of activated T cells (NFAT) and specificity protein 1 (SP1)) and the viral transactivator, Tat. Rev, a viral protein, regulates the cytosolic transport of some of the viral mRNAs, which are translated into regulatory and structural viral proteins. New virions assemble and bud through the cell membrane, maturing through the activity of the viral protease (*96*). Reproduced with the permission #4731110753580 from Springer Nature.

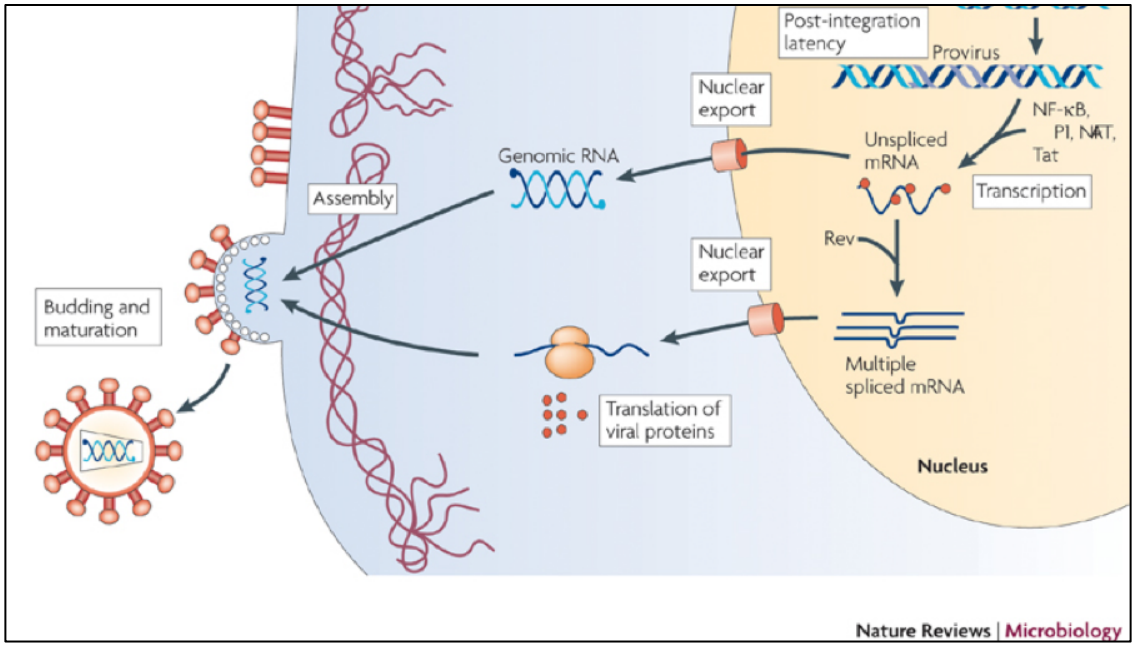
Post-integration latency
Provirus
Nuclear export
NF-κB, PI, NAT, Tat
Unspliced mRNA
Transcription
Genomic RNA
Assembly
Rev
Nuclear export
Budding and maturation
Multiple spliced mRNA
Translation of viral proteins
Nucleus
Nature Reviews | Microbiology

I. 4. HIV-1 infection versus HIV-2 infection

Both types of HIV have the same transmission routes, the same main target cells (CD4+ T lymphocytes), and cause AIDS and death in infected individuals (*1-2,30-34,54*). However, they have several noticeable differences (*35-45*). With regard to their genome, HIV-2 LTR promoter is larger that HIV-1's (**figures I-4 and I-5**). It lacks the NFAT binding sites and the negative regulatory elements present in HIV-1 LTR promoter making it less responsive to cellular activation signals (*42*). In addition, HIV-2 TAR element is much more structured with three TAR stem loops instead one in HIV-1 (*42*). That peculiar feature prevents efficient translation of its viral RNAs, a phenomenon known as post-transcription control of HIV-2 gene expression (*42,149-150*).

HIV-2 is five times less transmissible by sexual route, and 20 to 30 times less transmissible from infected mothers to their newborn babies in the absence of antiretroviral treatment (ART) due to lower plasma/semen/breastmilk viral loads than HIV-1 (*13,19,32,34-35,37,45*). HIV-1 is responsible for the global pandemic whereas HIV-2 is sporadic and geographically restricted to Western Africa (*1-2,17*). During entry, HIV-1 usually binds to the CD4 receptor and mainly uses two coreceptors in CCR5 and CXCR4. HIV-2 uses a variety of coreceptors, and can oftentimes enter the target cells in a CD4-independent manner (*30,34,45,78*). That feature might make HIV-2 more susceptible to neutralizing antibodies, and increase the host ability to control HIV-2 infection in vivo (*45,78*).

During cytoplasmic trafficking, HIV-2 uses Vpx to counteract the host restriction factor SAMHD-1, and successfully infects monocytic lineage cells (*100-101*). Whereas HIV-1 poorly infects those cells. HIV-1 and HIV-2 differ by their ability to recruit several

host factors and/or to evade several host factors and innate immunity (*84,151-164*). HIV-1 is less susceptible to the human TRIM5 alpha than HIV-2 (*118-121*). HIV-2 capsid does not recruit cyclophilin A (CypA) likely leading to its DNA being sensed by the host innate immunity (*44,156-163*). Type I IFN response ensues. To counteract that response, HIV-2 downregulates the functions of interferon regulatory factor 5 (IRF5) (*164*). HIV-2 Vpx reduces expression of toll-like receptor (TLR)-dependent Interleukin 6 (IL6), IL12p40, tumor necrosis factor (TNF) alpha (*163*). Genome-wide expression analysis showed that HIV-2 infection preferentially drives plasmacytoid dendritic cells (pDC) differentiation into Antigen Presenting Cells (APC) instead of type I interferon-producing cells (*163*).

Upon nuclear entry, HIV-1 recruits LEDGF/p75 or hepatoma-derived growth factor-related protein 2 (HRP2) (*138-142*). These two host factors tether the viral pre-integration complex to the host cell DNA to facilitate integration (*45*). HIV-2 interactions with these factors are still completely known (*45*). Unlike HIV-1, HIV-2 tends to integrate in the opposite direction of the transcriptional direction of the host gene, making it susceptible to transcriptional interference and latency (*38,45*).

The duration of HIV-1 clinical asymptomatic phase is 9.8 year-median with only 5-15% of long term non-progressors (LTNP) versus more than 18 year-median for HIV-2 and 86-95% of LTNPs (*36-37,39,43,45*). LTNPs are infected individuals that maintain a plasma viral load below 5,000 copies/ml without antiretroviral treatment. Despite similar proviral loads (*11-12,14,41*), HIV1-infected individuals have higher virus replication rates, and higher plasma viral loads than their HIV2-infected counterparts (*11-12,14,16*) due the post-transcriptional block of HIV-2 replication (*42,149-151*). In term of incidence, HIV-1 is slowly decreasing (from more than 10% at the beginning of the epidemic to less than 4%

currently) in the era of HAART whereas HIV-2 is disappearing (from 8% at the beginning of the epidemic to less than 1% currently) (*1-2,15,20,45,49*).

Efforts have been made over the years to decipher the mechanisms that underlie HIV-2 low pathogenicity in the hope of learning cues from the retroviral biology that might help in addressing challenges in HIV-1 cure, in HIV vaccine strategies, and in the design of safe and effective lentiviral delivery vectors for gene therapy. It has been reported that HIV-2 low pathogenicity could be related to low transcription rates in vivo which in turn could explain the low plasma viral load measured in HIV2-infected individuals (*12,14,16,36,37,40,46*). Transcriptional interferences have been described to be often associated with HIV-2 infection in vivo due to its propensity to integrate in the opposite direction of the host cell genes (*39*). Moreover HIV-2 unlike HIV-1 was subject to a strong immunological control with potent type I interferon responses, potent HIV-2 specific antibody responses, and potent HIV-2 specific CD8+ T cell responses (*129-140,162*). Determinants of these observations were proposed to be related to events during the initial HIV-2 infection including the induction of type I IFN responses.

Previous studies of the kinetics of HIV-1 and HIV-2 infection have shown differences in human monocytes-derived macrophages (MDM) and dendritic cells which HIV-1 was unable to efficiently infect. The restriction of infection in those cells was attributed to SAMHD1, a restriction factor that is counteracted by the viral factor Vpx present only present in HIV-2 particles (*104-105*). Successful HIV-2 infection of macrophages led to a type I interferon response (*151-157*) which in turn primed HIV-2 specific adaptive immunity (*127-132,165*). In CD4+ T lymphocytes, infection kinetics seemed similar, but there are differences in replication rates, and in integration sites

selection that clearly point to deeper trafficking differences. It has been proposed that HIV-1 recruits CPSF6 and CypA as key factors for trafficking upon entry (*98-99*). Unlike HIV-1, HIV-2 was unable to recruit CypA due to differences in its capsid protein.

I. 5. HIV-1/HIV-2 dual infections

Shortly after the discovery of HIV-2, cases of HIV-1 and HIV-2 dual infection were reported in patients from Western Africa (*45-55*). However, to our knowledge, no cases of single cells infected with both viruses have been reported in HIV-infected individuals. Even though there is indirect evidence that coinfections and superinfections occur at the single cell level (**figures I-8 and I-9**), in HIV-infected patients (*4,6-7,161*). The challenges and ethical issues related to identifying dually infected single cells seem unsurmountable as most HIV-infected cells reside in deep tissues that cannot be collected on living individuals. Nonetheless, understanding the interplay between these two viruses during dual infections is still of interest.

One of the first report that attempted to shed light on the interplay between HIV-1 and HIV-2 infections was a report by *Travers et al* (*166-167*). It revealed that HIV-2 protects HIV2-monoinfected individuals against HIV-1 infection. HIV-2 protection against HIV-1 infection appeared independent of the CD4+ cells count in the HIV-2-infected individuals, but seemed related to neutralizing antibodies against HIV-2 that cross-reacted with HIV-1 (*166-167*). In 2012 and 2014, two other reports demonstrated that HIV-2 in some HIV-1/HIV-2 dual-infected individuals led to better clinical outcomes in terms of long survival rates, and low mortality risks (*168-169*). However, the authors could not show a direct correlation between immunity and the protective status conferred by HIV-2.

In vitro studies have also reported on HIV-1 and HIV-2 interplay in cell culture (*170-176*). The HIV-2 Rev protein was shown to be a dominant negative of HIV-1 Rev that inhibits its function when it is overexpressed (*170*). In addition to HIV-2 Rev, two independent groups have shown that HIV-2 Vpx also inhibited HIV-1 infection upon overexpression (*171,176*). The incorporation of the Vpx protein into HIV-1 viral particles during viral assembly led to a drop in their infectivity. Of note, none of these two viral factors (HIV-2 Rev and Vpx) reported to be involved in HIV-1 inhibition had an inhibitory effect on the HIV-1 LTR activity (*170-171,176*).

HIV-1 and HIV-2 LTR promoters can be efficiently transactivated by HIV-1 Tat protein (*41,172*). However, the reverse was not true as HIV-2 Tat protein efficiently transactivates only the cognate HIV-2 LTR. In their report, *Rappaport et al* suggested that HIV-2 directly inhibited HIV-1 LTR activity when both viruses infected the same target cell (*171*). They suggested a mechanism by which HIV-2 appears to discriminate between its own LTR and the non-cognate HIV-1 LTR. They demonstrated that HIV-2 transactivation requires less stem loops than those present in the normal HIV-2 TAR. And they ruled out HIV-2 Tat protein as a factor involved in HIV-1 inhibition (*171*).

In an attempt to map the HIV-2 sequences involved in the HIV2-mediated inhibition of HIV-1 LTR activity, *Arya et al* performed extensive deletions of the HIV-2 genome (*172*). They showed that the first 321 nucleotides of HIV-2 genome (5' end to the PBS) to the exclusion of any other part of the viral genome, were enough to downmodulate HIV-1 LTR activity (*172*). The use of gene therapy strategies against HIV-1 infection to target the transactivation mechanism of HIV-1 transcription in order to block replication

in cell culture was explored (*173-174*). Of all the decoys of HIV-1 Tat protein tested, HIV-2 TAR was the most potent.

Figure I-8: Coinfections and superinfections

Evolution of Diversity in HIV-1 during the typical viral life cycle and creation of unique recombinant forms in the context of coinfection with two subtypes. RT denotes reverse transcriptase. Recombinant virus is referred to as a Unique Recombinant Form (URF) when they restricted to one geographical location, and as a Circulating Recombinant Form when they are found in at least two geographically distinct regions of the world (CRF). The frequency of recombination (number of recombination events at a particular gene per total number of recombination events throughout the HIV-1 genome) varies according to viral gene involved: 35% for *Env*, 25% for *Gag*, 20% for *Pol*, and 10% for the accessory genes (*7*).

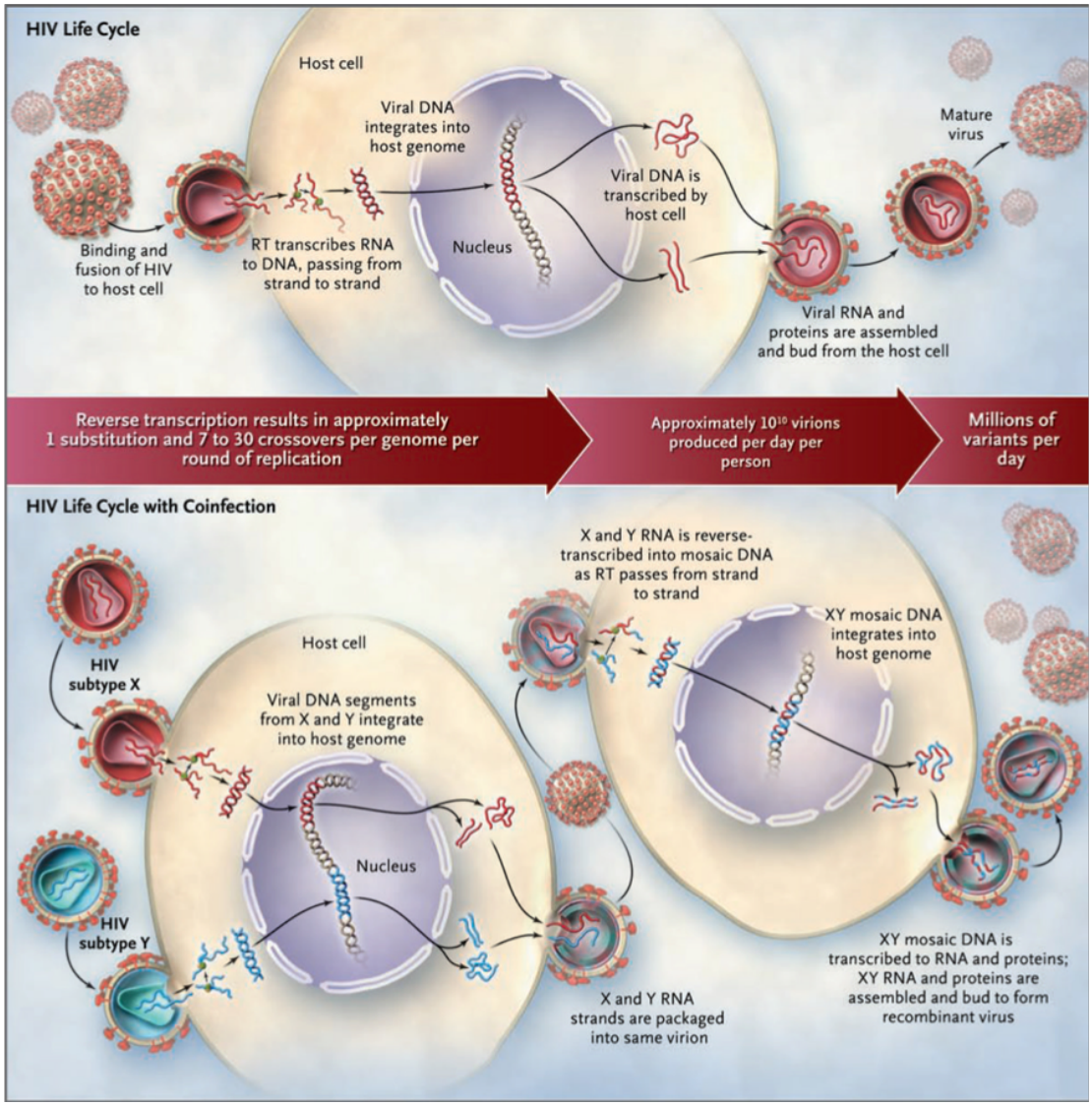
HIV Life Cycle
Host cell
Viral DNA integrates into host genome
Viral DNA is transcribed by host cell
Mature virus
Binding and fusion of HIV to host cell
RT transcribes RNA to DNA, passing from strand to strand
Nucleus
Viral RNA and proteins are assembled and bud from the host cell
Reverse transcription results in approximately 1 substitution and 7 to 30 crossovers per genome per round of replication
Approximately 10^{10} virions produced per day per person
Millions of variants per day
HIV Life Cycle with Coinfection
X and Y RNA is reverse-transcribed into mosaic DNA as RT passes from strand to strand
XY mosaic DNA integrates into host genome
Host cell
HIV subtype X
Viral DNA segments from X and Y integrate into host genome
Nucleus
HIV subtype Y
X and Y RNA strands are packaged into same virion
XY mosaic DNA is transcribed to RNA and proteins; XY RNA and proteins are assembled and bud to form recombinant virus

Figure I-9: HIV-1 circulating and unique recombinant forms

(a) Mosaic structures of HIV-1 circulating recombinant forms (CRF) documented in Africa. For instance, CRF01-AE has various sequences originating from two distinct subtypes of HIV-1, subtype A and subtype E that were recombined during reverse transcription as explained in figure I-8. The sequences are color-coded based on the subtype of origin as follow subtype A in red, subtype E in green, subtype G in dark blue, subtype D in light magenta, subtype F in light blue, subtype J in yellow, subtype K in orange; and subtype C in light green. Unclassified sequences are represented with empty squares, and portions that were not analyzed with sequencing are drawn in grey.

(b) Mosaic structures of HIV-1 from unique complex recombinants involving two CRFs, and mosaic structure of an intergroup M/O recombinant HIV-1 strain. Sequences from HIV-1 CRF02-AG are in dashed red; those from CFR06-cpx are in dashed blue; those from the HIV-1 group O are in green. Unclassified sequences and none sequenced portions are drawn as described in (b) (*165*). Reproduced and adapted with the permission #4731550184050 from Wolters Kluwer.

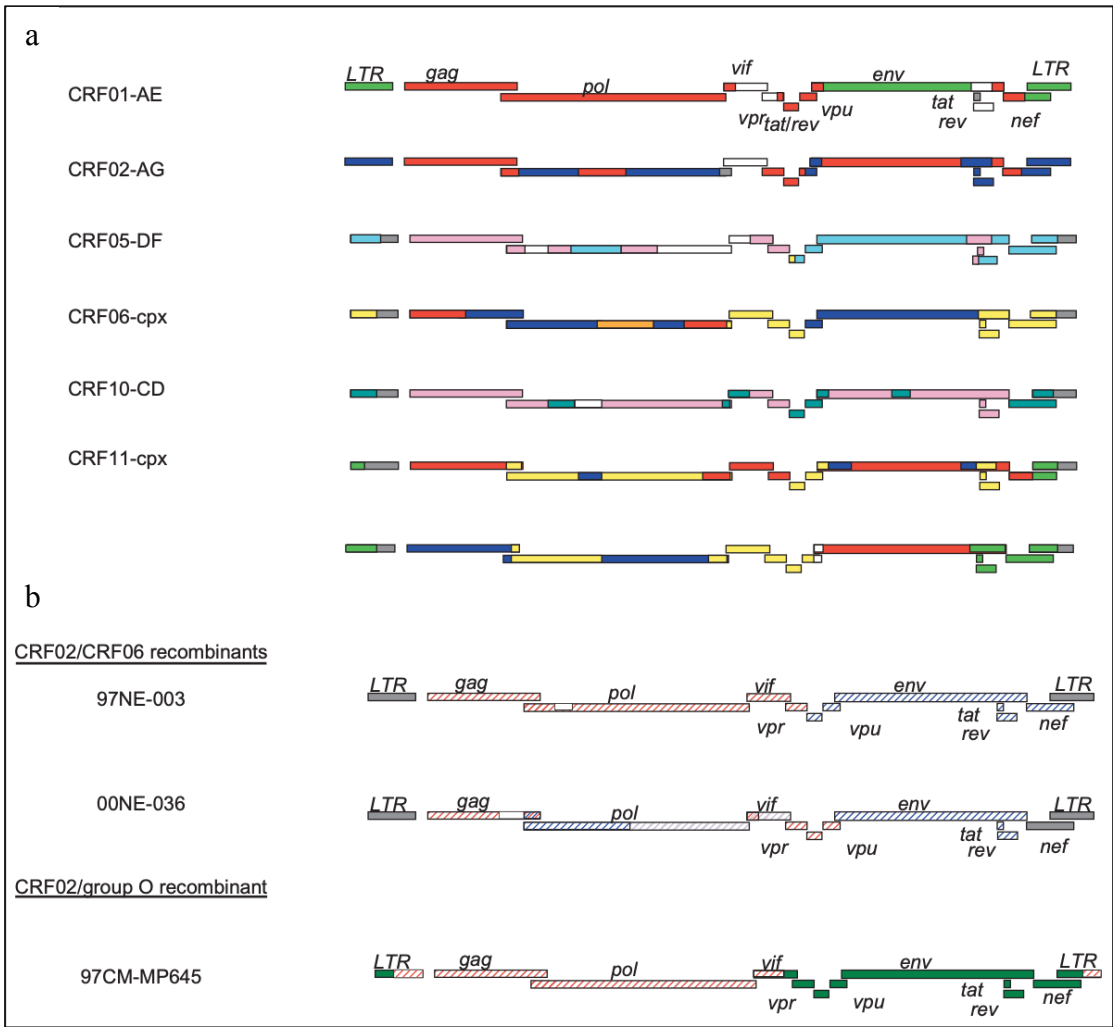
a
CRF01-AE
CRF02-AG
CRF05-DF
CRF06-cpx
CRF10-CD
CRF11-cpx
LTR
gag
pol
vif
vpr
tat/rev
vpu
env
tat
rev
nef
LTR
b
CRF02/CRF06 recombinants
97NE-003
00NE-036
CRF02/group O recombinant
97CM-MP645

CHAPTER II: MATERIALS AND METHODS

II. 1. Materials

Cell lines and drug treatments

HeLa-derived TZM-bl cells expressing CD4, CXCR4 and CCR5 at their surface and carrying two reporter genes (beta-galactosidase and luciferase) were used in this study. They were obtained from the NIH AIDS Repository Program (NIH ARP) (catalog #8129) (*177-180*). The TZM-GFP cells were derived from the TZM-bl cell line by stably transducing a gene coding eGFP under HIV-1 LTR (*181*). Human embryonic kidney cancer cells (HEK 293 FT) were from Fischer Thermo Scientific (Invitrogen, Carlsbad, CA). HEK 293 cells are adenovirus transformed, and the HEK 293 T variants additionally express the SV 40 large T antigen. Vero cells are a kidney epithelium cell line derived from African green monkeys, and lack a cluster of genes (~ 9 Mbps deletion) coding for type I interferons (*182*). Anti-HIV drugs raltegravir (RAL), tenofovir (TDF), and nelfinavir (NFV) were obtained the NIH ARP. Human recombinant interferon beta (IFN) was obtained from STEMCELL Technology (catalog #78113, Saint Louis, Missouri, USA).

Viral infectious clones, reporter constructs, and other plasmids

The following two plasmids were provided by the NIH ARP, HIV-1 subtype B laboratory-adapted clone plasmid pNL4.3 (catalog #114) (*183*), and HIV-2 subtype B molecular clone plasmid pST (catalog #12444) (*184-185*). A chimeric Nef pNL4.3 construct with part HIV-2 (amino acids 1 to 61) and part HIV-1 (amino acids 62 to 206) Nef genes was generated. The dual fluorescence reporter eGFP/mKO2 HIV-1 pNL4.3

plasmid was built as described for the ARP reagent DuoFluo (R7GEmC), catalog #12595 (*186*) with mKO2 driven by the eIF1α promoter instead of m-Cherry. An eGFP/E2-Crimson pNL4.3 construct was also used. Unlike the eGFP/mKO2 pNL4.3, it contains eGFP in frame within HIV-1 Nef gene and consequently under control of the HIV-1 LTR, and E2-Crimson outside of the HIV-$1_{NL4.3}$ backbone after the 3'LTR, under control of the CMV early-immediate promoter, to serve as a control for transfection efficiency.

A dual reporter eGFP/E2-Crimson Rous Sarcomas Virus (RSV) plasmid was built as described for the eGFP/E2-Crimson pNL4.3 construct with eGFP under control of the RSV LTR promoter. Three single reporter plasmids were used in this study (eGFP pNL4.3, and a tandem-dimer (td)-tomato murine leukemia virus, and a CMV-driven td-tomato expressing plasmids). Reporter viruses have either eGFP under HIV-1 LTR, or td-tomato under MLV LTR promoter. The vesicular stomatitis virus (VSV) glycoprotein-expressing plasmid (pVSV-G) used in these studies, was obtained from Invitrogen (pMD-G, Carlsbad, CA). HIV-2 full-length (FL) TAR element (TAR-2, 160 nucleotides) and several mutants of its, were cloned into an expression vector pTZU6+27 to generate pTAR-2 and mutants pTAR-2. The td-tomato expressing plasmid served as an external control for transfection efficiency and had a CMV early-immediate promoter. Reporter viruses have either eGFP under HIV-1 LTR, or td-tomato under MLV LTR promoter.

Microscopes, flow cytometer, and other instruments

Two epifluorescence microscopes were used to image live and fixed samples, the ix80 (Olympus, Center Valley, PA) and the Cytation 5 automated epifluorescence microscope (BioTek, Winooski, VT). The confocal microscope sp8 (Leica Microsystems, Wetzlar, Germany) was also used to produce images from fixed cells. The flow cytometer Accuri C6? (Becton Dickinson, Warwick, RI) was used to analyzed stained cells in lieu of microscopes where indicated. The spectrophotometer Nanodrop (Thermo Fischer Scientific, Rockford, IL) was used to quantify nucleic acid concentration of DNA and RNA preparations. The Enspire plate reader (Perkin-Elmer, Walthman, MA) was used to measure optical densities (O.D), and fluorescence signals where indicated. The sonicator Bioruptor (Diagneode, Sparta, NJ) was used to breakdown genomic DNA samples during the ChIP assays. Two real time PCR machines were used in these projects, the PIKO Real PCR machine (Thermo Fischer scientific, Rockford, IL) and the CFX Connect Real-Time PCR Detection System (Bio Rad, Hercules, CA). For regular PCR runs, the PIKO PCR machine (Thermo Fischer scientific, Rockford, IL) was used.

II. 2. Methods

Cell culture, transfection and virus preparation

The cell lines used in these projects were grown and maintained in Dulbecco's modified Eagle's medium (DMEM) supplemented with 10 % of fetal bovine serum (TZM-bl cells, TZM-GFP cells, and Vero cells) or in DMEM supplemented with 10 % FBS, non-essential amino acids, sodium pyruvate, L-glutamine, and penicillin/streptomycin (HEK 293 FT cells). Transfection was performed in 75 T flask with 14 µg of plasmid DNA to

make replication competent viruses (wild-type HIV-2, wild type HIV-1 and Nef chimeric HIV-1) or in small dishes (6-well and 12-well plates) with 0.8 to 2 µg of plasmid DNA for other applications. Lipofectamine 3000 was used along with DMEM only and Opti-MEM to make the DNA mixture before transfection. Non-replication competent viral preparations were made using the respective reporter virus plasmids. Reporter viruses have either eGFP under HIV-1 LTR, or td-tomato under MLV LTR promoter. The vesicular stomatitis virus (VSV) glycoprotein-expressing plasmid used for viral pseudotyping, referred to herein as pVSV-G, was obtained from Invitrogen (pMD-G, Carlsbad, CA). The next day after transfection, the medium was replaced with growth medium described above supplemented with geneticin (Gibco?). Virus preparations were collected at days 3 and 4 post-transfection and filtered through 0.2 µm sterile filters. Filtrates (4 parts) were mixed a lentiviral concentration solution (1 part) and placed at 4 °C for 4 days to precipitate viral particles in filtrates. Mixtures were spun down at 1,640g for 30 minutes at 4 °C to pellet down precipitates, and supernatants were discarded. A second centrifugation at the same speed for 5 minutes at 4 °C helped in eliminating droplets stuck on the edges of the centrifugation tube with a pipette. Dry pellets were resuspended into 5 mL of serum-free DMEM, aliquoted into smaller volumes, and stored at -80 °C before use.

Design and cloning of the HIV-2 TAR expression vectors

HIV-2 full-length (FL) TAR element (TAR-2, 160 nucleotides) was cloned into pZTU6+27, a small nucleolar RNA expression vector that uses a U6 promoter, obtained from Addgene, (Cambridge, MA, USA; catalog #25573) (*174-176,187*). That plasmid is referred to as FL pTAR-2. RNA structure predictions were performed with the UNAFold

software from Integrated DNA Technologies (IDT, Coralville, IA, USA) (*188*) to guide mutational deletions within the FL TAR-2. The resulting TAR-2 mutants were cloned into the pTZU6+27 backbone as described above. These plasmids are referred to as based upon the specific stem loops they contain. For instance, the full-length TAR deleted of the poly A sequence contains stem loops 1, 2, 3. It will be referred to as SL_{1+2+3} pTAR-2. The pNL4.3 construct with a chimeric Nef was generated by inserting the c-terminus domain of HIV-2 Nef sequence in lieu of HIV-1 Nef c-terminus. The pNL4.3 backbone kept its HV-1 Nef N-terminus.

Infection assays and drug treatment

Cells were plated onto glass coverslips, 96, 24, 12 and 6-well plates, and left to attach overnight. Attached cells were infected with HIV-1 and/or HIV-2 at MOI of 2 at 24 hours post-infection (hpi). Infected cells were incubated for various incubation times depending on the purpose of the experiments. Infection was performed in 4 x 10^4 TZM-bl cells on a glass coverslip format for the time course of infection using either the replication competent HIV-$1_{NL4.3}$ or HIV-2_{ST}. Time of addition assays (TOA) with RAL and TDF were performed in 1 x 10^6 TZM-GFP cells on in 6-well plate format with either the replication competent HIV-$1_{NL4.3}$ or HIV-2_{ST}. The glass coverslip samples and the 6-well plates were fixed with 4% paraformaldehyde every 2-hr. starting from 2 hpi up to 24 hpi. Fixed coverslips were processed with RNAscope reagents and fixed 6-well plates were counterstained with DAPI and imaged with the Cytation 5.

For the study of HIV-1 and HIV-2 dual infections, the infection assays were performed in 1 x 10^4 TZM-bl cells in 96-well plate format for 36 to 48 hr. with replication

competent HIV-$1_{NL4.3}$ and HIV-2_{ST} to assess the effects of the order of infection on HIV-1 inhibition during dual infections. VSV glycoprotein-pseudotyped dual reporter eGFP/mKO2 HIV-$1_{NL4.3}$ and the replication competent HIV-2_{ST} were used to infect 5 x 10^3 TZM-bl cells for one to five days. For the infection of Vero cells, VSV(G)-pseudotyped HIV-2_{ROD} and the dual reporter HIV-$1_{NL4.3}$ were used as described for the TZM-bl cells. To test the effects of FL TAR-2 and its mutants, VSV(G)-pseudotyped eGFP reporter HIV-1 and td-Tomato MLV were produced in HEK 293 FT cells in the presence of the control pTZU6 or FL pTAR-2 or one of its mutants. Virus supernatants were collected at 48 hr. post-transfection and frozen at -80 °C before their use. Single reporter HIV-1 and MLV were used to infect fresh HEK 293 FT cells for 48 hr. For chromatin immunoprecipitation (ChIP), HIV-1 infections and HIV-1/HIV-2 dual infections were performed in 1 x 10^6 TZM-bl cells for 24, 48 and 72 hr. Two anti-HIV drugs, the strand transfer inhibitor raltegravir (RAL) and the nucleoside inhibitor of HIV reverse transcriptase tenofovir (TDF) were used at 1 μM and 2 μM respectively. They were added 1 hr before infection. Recombinant IFN was used at 1000 units/mL to treat non-infected TZM-bl cells for 24 hr., 48 hr. and 72 hr.

Time course of infection and fluorescence in situ hybridization (FISH)

Every two hours, starting from 4 hpi, the coverslips were fixed with 4% paraformaldehyde for 30 minutes at room temperature, then washed twice with sterile PBS. The fixed coverslips were dehydrated at room temperature for 5 minutes with successively ethanol 50%, ethanol 70% and ethanol 100%. The last dehydration step consisted to incubate coverslips at room temperature for 10 minutes with ethanol 100%. Dehydrated

coverslips were stored for up to 6 months at -20 °C before further processing. Stored coverslips were rehydrated at room temperature with successively ethanol 70% (2 min.), ethanol 50% (2 min.) and PBS (10 min.). Rehydrated samples were permeabilized with 1% PBS-tween 20% for 10 min. Samples were protease-digested at 40 °C with protease III from the RNAscope kit (Advanced Cell Diagnostic – ACD, Newark CA). Protease-digested samples were incubated with the corresponding vRNA probe targeting the sense genomic vRNA for 2 hrs. at 40 °C. Unbound probe was removed with two successive washes. The vDNA probe (ACD, Newark, CA) combined with equal volume of a hybridization buffer was added to samples and incubated at 40 °C for 2 hrs. That probe targets the antisense strand of the double stranded viral DNA. The hybridization buffer contains ethylene carbonate, dextran sulfate, Triton X-100, milliQ water. Unbound probe was washed away twice. A series of amplifiers were added to the samples (Amp 1 to 4) to visualized the nucleic acid signals. DAPI staining completed the staining procedure. Stained coverslips were mounted on slide with prolong gold antifade (Invitrogen, Carlsbad, CA). The antifade was allowed to hardened overnight. The slides were sealed with nail polish before imaging.

Microscopy and flow cytometry assays

Infected cells were either imaged live or fixed with 4% PFA for 30 min., immunostained with specific antibodies, then image. TZM-bl cells infected with replication competent viruses were stained using specific antibodies against HIV-1 Vpu and HIV-2 Vpx. TZM-bl cells and Vero cells infected with eGFP/mKO2 reporter virus were imaged live because the mKO2 fluorescence signal is lost upon fixation. Samples

were imaged with the Olympus ix80 inverted manual epifluorescence microscope or with the Cytation 5 inverted automated epifluorescence microscope at 4X, 10X, and 20X magnification. HEK 293 cells transfected with eGFP/E2-Crimson plasmids (HIV-1 and RSV) and single reporter virus (HIV-1 and MLV) transduced HEK 293 FT cells were harvested, fixed, and analyzed using an Accuri C6 flow cytometer (Becton Dickinson, Warwick, RI). RNAscope samples were imaged with the inverted manual confocal microscope Leica sp8 equipped with a 60 X/1.4 glycerol immersion objective, and tunable supercontinuum white light LASER. Twenty to 30 frames were taken per time point and per run. Each time point was repeated at least once. Images were analyzed with the Leica application software version X (*LASX*), and the complementary deconvolution module *Huygens Professional* software version X (scientific volume imaging software). Nucleic acid dots were counted, and their cytoplasmic or nuclear localization assessed with the open source *Cell Profiler* software.

Enzyme linked immunosorbent assay (ELISA)

Supernatants (2 mL) were collected from transfected TZM-GFP cells for p24 (capsid) ELISA, and lysed with 200 µL of lysis buffer (phosphate buffer saline – PBS, 10% triton X-100, trypan blue). Anti-HIV-1 capsid (anti-p24) antibody was made from NIH ARP hybridoma (catalog #1513) (*189*). Corner-notched Pierce 96-well plates (catalog #15041, Thermo Scientific, Rockford, IL) were coated overnight with 4 µg/ml of the anti-p24 antibody, in presence of a coating buffer (30 mM $NaCO_3$, 68 mM $NaHCO_3$, pH 9.4-9.8). Coated plates were treated with a blocking buffer (PBS, 1% bovine serum albumin, 5% sucrose, 0.05% NaN_3) for 3 hr. HIV-1 capsid protein was expressed in *E. coli* to

generate a recombinant p24 stock of 11 mg/ml (*190-191*). To construct a standard curve, the stock solution was diluted with a capsid dilution buffer (25 mM Tris-HCl pH 8.1, 40 mM NaCl), then a series of 2-fold dilutions was done, starting at 60 ng/ml. Subsequently, 100 µL of the culture supernatants or the diluted recombinant p24 solutions were added to each well (triplicates per sample), and incubated overnight at 4 °C. A home-made biotinylated secondary Ig anti-HIV-1 polyclonal antibody (non-biotinylated Ig, NIH ARP catalog #3957) (*192*), was added to each well (100 µL, 37 °C for 1 hr.). Streptavidin conjugated to horseradish peroxidase – (HRP, 100 µL) was added to the well, and incubated at 37 °C for 30 min. A substrate for the HRP, trimethylbenzidine (catalog #555214, Becton Dickinson, Warwick, RI) was added to each well (100 µL) for 30 min. at room temperature. The reaction was stopped with 50 µL of 2 N sulfuric acid, followed by reading the optical density at 450 nm. Quantities of p24 in samples were determined using the standard curve from the recombinant p24 serial dilutions. Values were corrected to the starting volume of sample collected for analysis.

Transcription assessment

The effects of HIV-2 TAR expression were studied following transfection of constructs into in 1 x 10^6 TZM-GFP cells for 48 hr in 6-well plate format. These cells were transfected with 2 µg of pTZU6 control or FL pTAR-2, and 50 ng of the fully infectious molecular clone pNL4.3, and 10 ng of pCMV_td-tomato (transfection efficiency control) in the presence of lipofectamine 3000 transfection reagent (catalog #3000008, Invitrogen, Carlsbad, CA). Successfully transfected cells became red (transfection+) and green (HIV-1+). HEK 293 FT cells and Vero cells were transfected under the same conditions. For

flow cytometry, transfections were done for 48 hr on 1 x 10^5 HEK 293 FT cells in 12-well plates with 800 ng of pTZU6 control or pTAR-2 (or mutants) plus 20 ng of dual reporter pNL4.3 or RSV. The next day after transfection, the medium was replaced with the fresh culture medium supplemented with geneticin (Sigma, Saint-Louis, MO) to enhance viral particles production. Analysis of flow cytometry data normalized the mean fluorescence intensity (MFI) of LTR-driven eGFP expression (successful LTR transactivation) to the MFI of the CMV-driven E2-Crimson expression (transactivation independent control) to determine the ratio of eGFP MFI to E2-Crimson MFI for successfully transfected cells (flow chart gate. Subsequently, the ratios from cells co-transfected with pTAR-2s (FL and mutants) were normalized to the ratios from the pTZU6 control cells. The latter were set to 1 to plot the data.

RT-qPCR and qPCR techniques

Transfected or infected TZM-bl cells were harvested and divided into 200 µL cellular vDNA samples in sterile PBS, and 200 µL of cellular vRNA samples in RNAlater (Invitrogen, Carlsbad, CA). Samples were stored at -80 °C before further processing. Nucleic acids were extracted with the QiaAmp DNA Blood mini Kit and RNeasy minikit (Qiagen, Germantown, MD). Nucleic acids extracts were quantified with NanoDrop spectrophotometer (Invitrogen, Carlsbad, CA) and 200 ng of them was used in each RT-qPCR or qPCR assay. Two types of RT-qPCR and qPCR were used in this study. The first one is a SYBR green-based assay and the second type is a Taqman molecular beacon-based assay using sets of primers and probes (table II-1). Amplification conditions are listed in table II-2. The high capacity cDNA synthesis kit, the one-step SYBR green-based RT-

qPCR cell-to-Ct kit, the PowerUp SYBR green qPCR, and the Absolute qPCR Low Rox – based qPCR kits (Invitrogen, Carlsbad, CA) were used following the manufacturer's recommendation. PCR conditions used in these studies are listed in table II-2.

Chromatin immuno-precipitation (ChIP) assay

In a 6-well plate, $1x10^6$ TZM-bl cells were plated per well. The following day, HIV-1 and HIV-2 infection were performed at MOI ~0.2 at 24 hrs. post-infection (hpi) each for 24, 48 and 72 hr. Infected cells were fixed with 1% formaldehyde for 10 min. The fixation reaction was quenched with glycine 125 mM for 5 min. And the cells were washed twice with sterile ice-cold PBS. The cells were harvested using a single-use cell scraper, and collected with PBS into 1.5 mL microtube. Cells suspensions were spun down to recover cell pellet, which were lysed in the presence of 300 µL of ChIP lysis buffer (1% SDS, 10 mM EDTA, 50 mM Tris HCl pH 8.0) supplemented with protease inhibitor cocktail (PIC) (catalog #P8340, Sigma-Aldrich, Saint Louis, MO) for 20 min. on ice. Lysates were sonicated for 75 min. (75 sonication cycles of 30 s on/30 s off) with the Bioruptor (Diagneode, Sparta, NJ). Sonicated lysates were cleared at 1 x 10^4 g for 15 min., and cleared supernatants were transferred into new 1.5 mL microtubes. 10% of cleared supernatant was stored at -80 °C as input sample. The remaining supernatant was split equally into samples for IP.

Rabbit anti-Histone H3K4me2 antibody (catalog #ab32356, Abcam, Cambridge, MA) and rabbit normal IgG conjugated to agarose (catalog #2729S, Invitrogen, Carlsbad, CA) antibodies were used at 0.5 µg/IP to control for H3K4me2, and at 1 µg/IP otherwise. Mouse anti-full-length RNAPII antibody (catalog #ab817, Abcam, Cambridge, MA),

mouse anti-serine-2 phosphorylated RNAPII antibody (catalog #ab5095, Abcam, Cambridge, MA), mouse anti-serine-5 phosphorylated RNAII antibody (ab5408, Abcam, Cambridge, MA), mouse normal IgG conjugated to agarose (sc-2343, Santa Cruz, Dallas, TX) antibodies were used at 1 µg/IP. Rabbit anti-threonine 186-phosphorylated cyclin-dependent kinase 9 (p-cdk9 – catalog #2449S, Cell Signaling Technology, Danvers, MA, USA), and rabbit IgG isotype control (ab37415, Abcam, Cambridge, MA) were used at 3 µg/IP. Protein G beads (catalog #10004D, Invitrogen, Carlsbad, CA) were coated overnight at 4 °C with these antibodies. 50 µL of antibody-coated beads were added to corresponding IP samples and incubated overnight at 4 °C. Samples were washed successively with 1 mL each of four different washing buffers, the low salt wash buffer (SDS 0.1%, Triton X-100 1%, EDTA 2 mM, TrisHCl pH 8.0 20 mM, NaCl 150 mM, H2O), the high salt wash buffer (SDS 0.1%, Triton X-100 1%, EDTA 2 mM, TrisHCl pH 8.0 20 mM, NaCl 500 mM, H2O), the lithium chloride (LiCl) wash buffer (LiCl 0.25 mM, NP40 1%, sodium deoxycholate 1%, EDTA 1 mM, TrisHCl pH 8.0 10 mM, H2O), and the Tris-EDTA wash buffer (TrisHCl pH 8.0 5 mM, EDTA 0.5 mM). Elution was performed twice with 125 µL freshly made ChIP elution buffer (SDS 1%, $NaHCO_3$ 0.1 M, H2O) at 37 °C for 15 min. each. Input samples were thawed on ice, and 250 µL of ChIP dilution buffer supplemented with PIC was added to them. IP eluates and input samples were de-crosslinked overnight at 65 °C with 10 µL of 5 M NaCl. The samples underwent proteinase K digestion (1 µL of 20 mg/mL stock solution) at 45 °C for 90 min. Digested samples were cleaned up with the Wizard SV Gel and PCR Clean-Up system from Promega (catalog# A9282) and eluted into 80 µL of nuclease-free water. qPCRs using primers and probes against regions flanking HIV-1, and GAPDH transcription start sites were performed with 2-3 µL of eluates.

Statistical analysis

Experiments were independently repeated two to three times. Replicate values from each independent experiment were plotted. Statistical significance was assessed with the p value for binary comparison (unpaired t test) and with one-way ANOVA tests for multiple comparisons of the mean ± standard errors of the means as described in each case. The specific corrected one-way ANOVA tests are indicated in the figure legends.

Table II-1: Primers, oligonucleotides and gene blocks used in this study

Assay	Primers (5' to 3')		Probe
	Forward	**Reverse**	**FAM – NQF**
GAPDH mRNA	CGCTCTCTGCTCCTCC TGTTC	CGCCCAATACGACCAA ATCCG	-
HIV-1 Gag RNA quantification	CGAGAGCGTCGGTATT AAGC	AACAGGCCAGGATTAA GTGC	CCCTGGCCTT AACCGAATT
HIV-1 abortive transcripts quantification	CGCGAGAAACTCCGTC TTG	GCTGCCCACACAATAT GTTTTA	CCGGGCCGTA ACCT
HIV-1 TSS	AGTGGCGAGCCCTCAG ATCCTGCATATAAGCA	GTGGGTTCCCTAGTTAG CCAGAGAGCTCCC	TGGGTCTCTC TGGTTAGACC AGATCTGAGC
GAPDH TSS	CGCCCCCGGTTTCTAT AAATTGAGCCCGCA	CACCTGGCGACGCAAA AGAAGATGCGGC	-
HIV-1 TSS + 1kbp	AGTGGCGAGCCCTCAG ATCCTGCATATAAGCA	GTGGGTTCCCTAGTTAG CCAGAGAGCTCCC	TGGGTCTCTC TGGTTAGACC AGATCTGAGC
GAPDH TSS + 1 kbp	CGCCCCCGGTTTCTAT AAATTGAGCCCGCA	CACCTGGCGACGCAAA AGAAGATGCGGC	-
HIV-2 Nef DNA and RNA quantification	GTCCCAAGAAGGATC AGGCAGGG	GCTTGTACGAGCCTTTC TCCCC	TCGCCCTCCT GTGAGGGA
HIV-2 Gag mRNA quantification	CGCGAGAAACTCCGTC TTG	GCTGCCCACACAATAT GTTTTA	CCGGGCCGTA ACCT
FL HIV-2 TAR generation	GCAGCACATATACTAG TCGACCAGTCGCTCTG CGGAGAGGCT	CGGACCGAAGTCCGCT CTAGAAGCTTTATTAAG AGGTCTTTT	-
SL1+2+3 TAR generation	GCAGCACATATACTAG TCGACCAGTCGCTCTG CGGAGAGGCT	CGGACCGAAGTCCGCT CTAGACCAGTGCCGGC CAAGCACTGG	-
SL1+2 TAR generation	GCAGCACATATACTAG TCGACCAGTCGCTCTG CGGAGAGGCT	CGGACCGAAGTCCGCT CTAGACTAGCAGGGAA CACCCAGGCT	-
SL2+3+polyA TAR generation	GCAGCACATATACTAG TCGACCAGTCGCTCTG CGGAGAGGCT	CGGACCGAAGTCCGCT CTAGACCAGTGCCGGC CAAGCACTGG	-
SL2+3 TAR generation	GCAGCACATATACTAG TCGACCTAGCAGGTAG AGCCTGGGTG	CGGACCGAAGTCCGCT CTAGACCAGTGCCGGC CAAGCACTGG	-

SL1+3 TAR generation (gene block from IDT)	GCAGCACATATACTAGTCGACGTCGCTCTGCGGAGAGGCTGGCAGA TTGAGCCCTGGGAGGTTCTCTCCAGCCTCTCACCAGTGCTTGGCCGG CACTGGGCAGACGGCTCTAGAGCGGACTTCGGTCCG		
SL1 TAR generation	GCAGCACATATACTAG TCGACCAGTCGCTCTG CGGAGAGGCT	CGGACCGAAGTCCGCT CTAGAGCTGGAGAGAA CCTCCCAGGG	
SL2 TAR generation (hybridization at RT for 1 hour)	GCAGCACATATACTAG TCGACCTAGCAGGTAG AGCCTGGGTGTTCCCT GCTAG	CGGACCGAAGTCCGCT CTAGACTAGCAGGGAA CACCCAGGCTCTACCTG CTAG	
SL3 TAR generation (hybridization at RT for 1 hour)	GCAGCACATATACTAG TCGACCCAGTGCTTGG CCGGCACTGG	CGGACCGAAGTCCGCT CTAGACCAGTGCCGGC CAAGCACTGG	
HIV-2 TAR RNA quantification	AGTCGCTCTGCGGAGA GGCTG	AGCTTTATTAAGAGGTC TTTA	
pTZU6 and pTAR DNA quantification	GCACATATACTAGTCG ACAGTCGCTCTGCGGA GAGGC	ACCGAAGTCCGCTCTA GATCTGCCAATCCGAA TCTGT	
pTAR constructs sequencing primer (hU6)	GAGGGCCTATTTCCCATGATT		
Chimeric HIV-1/HIV-2 Nef generation (gene block from IDT)	CTAAAGAATAGTGCTGTTAACTTGCTCAATGCCACAGCCATAGCAG TAGCTGAGGGGACAGATAGGGTTATAGAAGTATTACAAGCAGCTTA TAGAGCTATTCGCCACATACCTAGAAGAATAAGACAGGGCTTGGAA AGGATTTTGCTATAAGATGGGGGCGAGTGGATCCAAGAAGCGTTCC GAGCCTTCGCGAGGGCTACGGGAGAACTCTTACAAACGCCTGGAG AGGCTTCTGGGGGACACTGGGACAAATTGGGAGGGGAATACTTGC AGTCCCAAGAAGGATCAGGCAGGGGGCAGAAATCGCCCTCCTGTG AGGGACGGCGGTATCAACAGGGAGATTTTATGAATACCCCATGGA GAGCCCCAGCAGAAGGGGAGAAAGGCTCGTACAAGCAACAAAATA TGGATGATGTAGATTCAGATGATGATGACCTAGTAGGGGTCCCTGT CACACCAAGAGTACCATTAAGAGAAATGACATATAGATTGGCAAG AAATATGTCACATTTGATAAAAGAAAAGGGGGGACTGGAAGGGCT AATTCACTCCCAAAGAAGACAAGATATCCTTGATCTGTGGATCTAC CACACACAAGGCTACTTCCCTGATTGGCAGAACTACACACCAGGGC CAGGGGTCAGATATCCACTGACCTTTGGATGGTGCTACAAGCTAGT ACCAGTTGAGCCAGATAAGGTAGAAGAGGCCAATAAAGGAGAGAA		

	CACCAGCTTGTTACACCCTGTGAGCCTGCATGGAATGGATGACCCT GAGAGAGAAGTGTTAGAGTGGAGGTTTGACAGCCGCCTAGCATTTC ATCACGTGGCCCGAGAGCTGCATCCGGAGTACTTCAAGAACTGCTG ACATCGAGCTTGCTACAAGGGACTTTCCGCTGGGGACTTTCCAGGG AGGCGTGGCCTGGGCGGGACTGGGGAGTGGCGAGCCCTCAGATGC TGCATATAAGCAGCTGCTTTTTGCCTGTACTGGGTCTCTCTGGTTAG ACCAGATCTGAGCCTGGGAGCTCTCTGGCTAACTAGGGAACCCACT GCTTAAGCCTCAATAAAGCTTGCCTTGAGTGCTTCAAGTAGTGTGT GCCCGTCTGTTGTGTGACTCTGGTAACTAGAGATCCCTCAGACCCTT TTAGTCAGTGTGGAAAATCTCTAGCAGCCGGCTGTGCGGGAGAACG G

Table II-2: PCR conditions used in this study

	Reverse transcription	Initial step	Step 3	Step 4	Step 5	Step 6	Step 7
Phusion PCR	-	-	98 °C 30 s	98 °C 10 s	60 °C 30 s	72 °C 150 s	72 °C 7 min.
GoTaq PCR	-	-	95 °C 120 s	95 °C 30 s	60 °C 30 s	72 °C 120 s	72 °C 7 min.
PowerUp qPCR	-	50 °C 120 s	95 °C 120 s	95 °C 30 s	60 °C 60 s		-
SYBR-green RT-qPCR	48 °C 30 min.	-	95 °C 120 s	95 °C 30 s	60 °C 60 s		-
High capacity cDNA synthesis	37 °C 2 hr.	-	-	-	-		-

Step 3: Heat stable Taq polymerase activation step

Step 4: Denaturation step

Step 5: Hybridization step

Step 6: Elongation step

Steps 4-6 were repeated 35 times (35 cycles).

Step 7: Final elongation step (Phusion and GoTaq PCRs) or SYBR green melting curve step (others)

CHAPTER III: HIV-2 INHIBITS HIV-1 GENE EXPRESSION VIA TWO INDEPENDENT MECHANISMS DURING CELLULAR CO-INFECTION

III. 1. Introduction

Since its onset, human immunodeficiency virus (HIV) has infected roughly 75 million people, and claimed the lives of 32 million people worldwide (*1-2*). Two genetically related HIVs have been described, HIV type 1 and HIV type 2 (*21-28*). HIV-1 and HIV-2 diverge in terms of nucleotide sequences, geographic distribution, rates of transmission, pathogenesis, and mortality rates. HIV-1 is responsible for the current global pandemic, whereas HIV-2 is mainly restricted to West Africa, with sporadic cases outside of that region (*29-33*). HIV-2 has shown slower transmission rates for most transmission routes (*12,14,16,34*), lower pathogenesis with an asymptomatic phase before the advent of HAART twice as long as HIV-1's, and a slower progression to AIDS and lower mortality risks overall (*12-13,15,18,35-36,38-42,44*). In places where both types of HIV coexist, cases of patients infected with both viruses have been reported (*45-55*). These cases are referred to as HIV-1 and HIV-2 dual-infections.

The present study assessed the specific roles of type I interferon responses (innate immunity), and HIV-2 TAR element in controlling concurrent or subsequent HIV-1 infection during dual infections. It showed that the order in which HIV-1 and HIV-2 infections occur, was relevant to HIV-1 inhibition by HIV-2. It also demonstrated that both type I interferon responses and HIV-2 TAR mediate inhibition of HIV-1 infection. Importantly, these two mechanisms were not mutually exclusive. As each of them occurred

independently at specific time points after infection. Direct inhibition was mapped to a minimum two stem loops structure from HIV-2 TAR involving its second stem loop. Moreover, this study provides evidence that HIV-2 TAR-mediated inhibition did not target other retroviruses such as Murine Leukemia Virus (MLV) and Rous Sarcoma Virus (RSV), and was not cytotoxic in that the cellular promoters tested were not affected.

III. 2. Results

Inhibition of HIV-1 infection by HIV-2 is dependent on order of addition.

We set out to visualize dual infection in cell culture using specific markers of HIV-1 and HIV-2. The two viruses have each a unique accessory gene (HIV-1 Vpu and HIV-2 Vpx) for which specific antibodies are available. Anti-Vpu and anti-Vpx antibodies were tested for cross-reactivity against the non-cognate HIV and showed none (data not shown). They also showed no reactivity against non-infected samples. Therefore, immunostaining of HIV-infected cells with these antibodies is specific and can be used to identify HIV-1 and HIV-2 infected cells. Next, infection, immunostaining, and imaging conditions were optimized to consistently achieve 75-80% infection of TZM-bl cells at 48 hours post infection (data not shown).

To determine whether infection with either of the two viruses (HIV-1 or HIV-2) influences infection by the other, a time-of-addition assay was performed to compare simultaneous and sequential infections. Based on a previous report (*139*), we estimated that the window between viral entry and CD4 receptor downmodulation during HIV-1 infection would be approximately 12 hours. We thus performed dual infections within that time window. For sequential infection, the second virus was added to the target cells 12 hours

after the first virus. Infected cells were incubated for 48 hours following addition of the first virus (fig. III-1). We found that HIV-2 strongly inhibited HIV-1 infection when added before HIV-1 (drop from 80% to 8% HIV-1-positive cells) or at the same time (from 80% to 20%) (fig. III-1 and III-2). Notably, HIV-1 did not affect HIV-2 infection, when added simultaneously with, or prior to HIV-2 (fig. III-1 and III-2). These data indicate that HIV-2 infection inhibits HIV-1 infection, but HIV-1 infection does not inhibit HIV-2 infection.

Figure III-1: Effect of the order of HIV-1 and HIV-2 infection on viral replication in co-infected TZM-bl cells.

TZM-bl cells were infected with replication competent HIV-1 and HIV-2 (MOI of 2 each virus titrated in TZM-bl cells). In co-infection experiments i, ii, and iii (rows 2, 3, and 4) HIV-1 was added at t_0, t_0, and t_{12}, (zero, zero, and 12 hours post infection by the first virus), whereas HIV-2 was added at t_{12}, t_0, and t_0. All experiments were terminated at t_{48}. Images were acquired by an automated Cytation 5 epifluorescence microscope. Sample images from three independent experiments for each condition are shown. Anti-Vpu (Alexa Fluor 550) and anti-Vpx (Alexa Fluor 488) antibodies are shown in red and green, respectively; DNA was stained with DAPI (blue). Scale bar represents 100 μm.

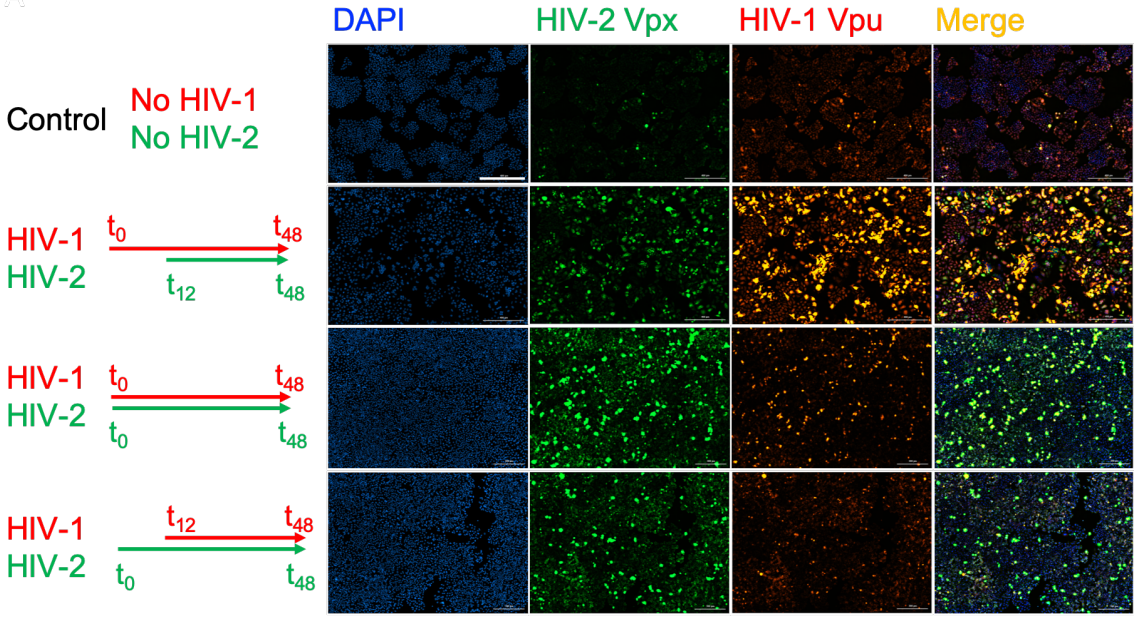

Cytation 5 epifluorescence automated microscope 20X

Figure III-2: Quantitation of HIV-1 and HIV-2 in co-infected cells

The proportion of Vpu-positive (HIV-1-infected) cells (filled bars) and the proportion of Vpx-positive (HIV-2-infected) cells (empty bars) for dual infection conditions i, ii, and iii (described in A) are shown. Averages from three independent experiments are shown ± standard errors of the means.

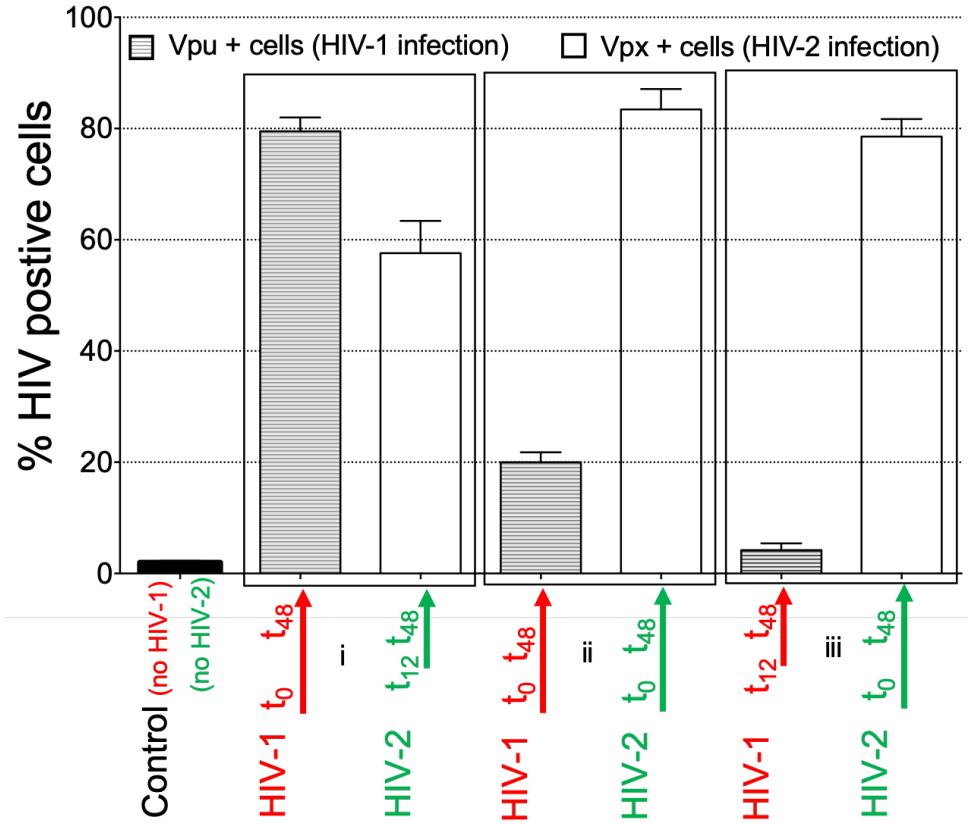
100
80
60
40
20
0
% HIV postive cells
Vpu + cells (HIV-1 infection)
Vpx + cells (HIV-2 infection)
Control (no HIV-1)
(no HIV-2)
HIV-1 t0 t48
i
HIV-2 t12 t48
HIV-1 t0 t48
ii
HIV-2 t0 t48
HIV-1 t12 t48
iii
HIV-2 t0 t48

HIV-2 infection affects both HIV-1 transduction and gene expression.

Having demonstrated the inhibitory effect of HIV-2 on HIV-1 infection using replication-competent viruses, we sought to determine the specific step of infection at which inhibition occurs. Previous reports have suggested that the HIV-2 Vpx protein can interfere with HIV-1 replication by inhibiting HIV-1 reverse transcription and by decreasing infectivity of HIV-1 viral particles produced during co-infection (*166,171*). To address confounding effects from possible secondary infections as well as the challenges involved in accurately determining transduction efficiencies, we used a system that enables concomitant measurement of HIV-1 transduction as well as HIV-1 transcriptional activity. Our approach was based on a VSV(G)-pseudotyped eGFP/mKO2 dual reporter HIV-1 (fig. III-3) in lieu of the replication competent HIV-1. In this system, fluorescent mKO2 is expressed under control of the constitutively active eukaryotic translation initiation factor 1 α (eIF1α) core promoter, and is directly proportional to the transduction rates of HIV-1 (fig. III-3). In contrast, signal intensity of eGFP is dependent on HIV-1 LTR promoter activity and is correlated to HIV-1 gene expression. Any cell transduced with the reporter virus fluoresces red, and transduced cells with an active provirus additionally fluoresce green (fig. III-4). Non-transduced cells do not fluoresce, while transduced cells with latent or defective provirus fluoresce red only. Simultaneous transduction with HIV-1 and infection with HIV-2 were performed in TZM-bl cells for one to five days, infections were staggered such that the entire 96 well plate could be live imaged at day 6 post-infection (fig. III-5). Simultaneous transduction of HIV-1 with HIV-2 infection decreased both cellular promoter-driven mKO2 signal and HIV-1-associated eGFP signal at 48 hpi and 72 hpi, respectively (fig. III-6, III-7).

Figure III-3: Genome organization of DuoFluo HIV-1 pNL4.3 plasmid used for HIV-1 transduction experiments.

The mKO2 fluorescent protein expression is under the control of the eIF-1α core promoter and is expressed in transduced cells. The eGFP protein expression is under the control of the HIV-1 LTR promoter.

A

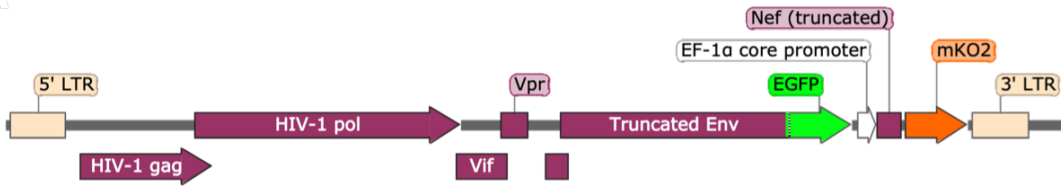
Nef (truncated)
EF-1α core promoter
mKO2
5' LTR
Vpr
EGFP
3' LTR
HIV-1 pol
Truncated Env
HIV-1 gag
Vif

Figure III-4: Dual fluorescence HIV-1 transduction outcomes

Schematic indicating possible outcomes of transduction with the HIV-1 reporter virus shown in (figure III-3).

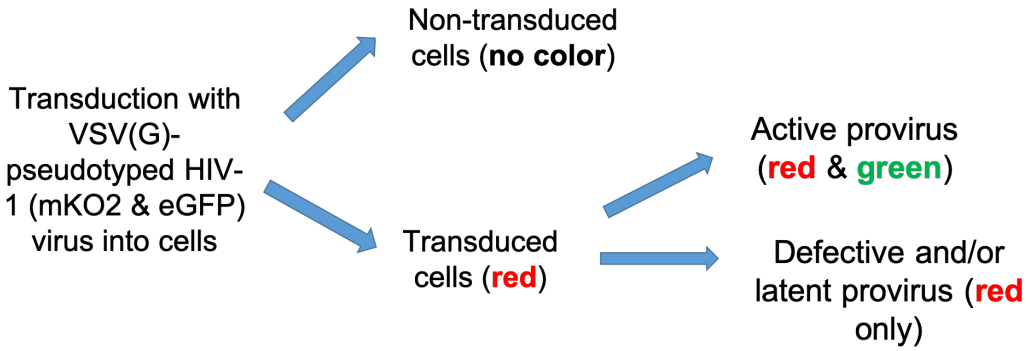
Transduction with VSV(G)-pseudotyped HIV-1 (mKO2 & eGFP) virus into cells
Non-transduced cells (no color)
Transduced cells (red)
Active provirus (red & green)
Defective and/or latent provirus (red only)

Figure III-5: Dual infection images in TZM-bl cells

Representative images for each time point of infection (HIV-1 transduction + HIV-2 infection) in TZM-bl cells are shown. Scale bar represents 100 μm.

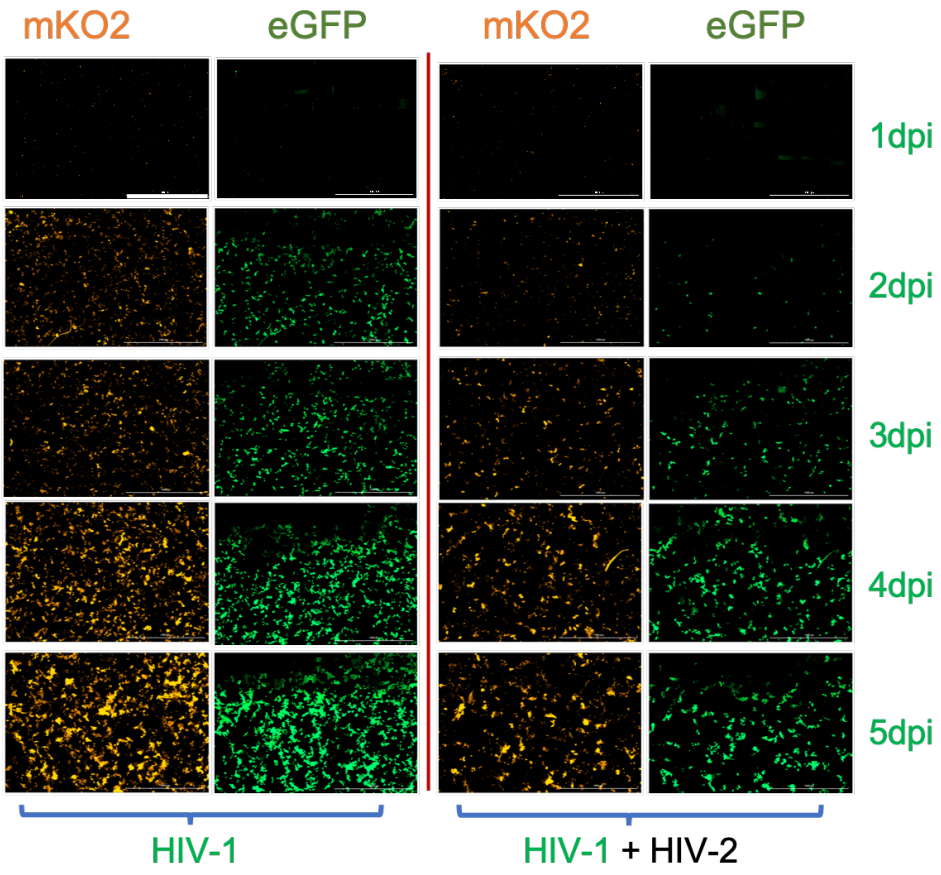
mKO2
eGFP
mKO2
eGFP
1dpi
2dpi
3dpi
4dpi
5dpi
HIV-1
HIV-1 + HIV-2

Figure III-6: Effects of HIV-1 transduction + HIV-2 infection on eIF1α-driven mKO2 expression in TZM-bl cells

The percentage of HIV-1-transduced cells was determined from the images shown in (C). Representative images for each time point of infection (HIV-1 transduction + HIV-2 infection) in TZM-bl cells are shown. Scale bar represents 100 μm.

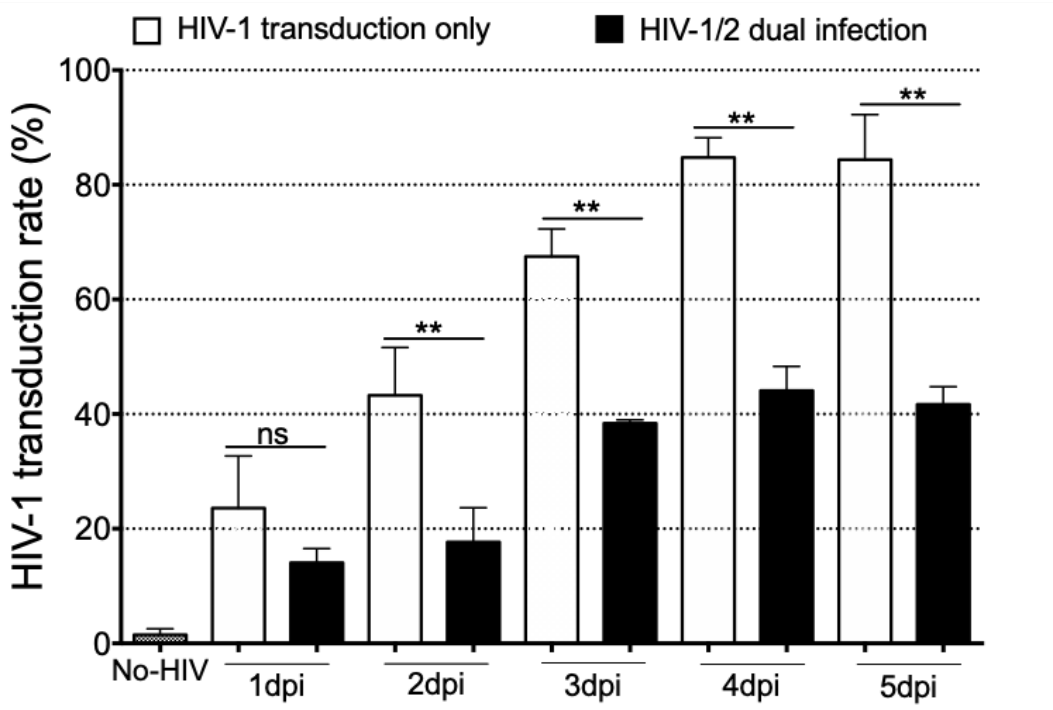
HIV-1 transduction only
HIV-1/2 dual infection
HIV-1 transduction rate (%)
100
80
60
40
20
0
ns
**
**
**
**
No-HIV
1dpi
2dpi
3dpi
4dpi
5dpi

Figure III-7: Effects of HIV-1 transduction + HIV-2 infection on HIV-1 LTR-driven eGFP expression in TZM-bl cells

The percentage of HIV-1-transduced cells with an active provirus was determined from the images shown in (C), n = 3 independent experiments. The Sidak's (corrected one-way ANOVA test) multiple comparison test was used.

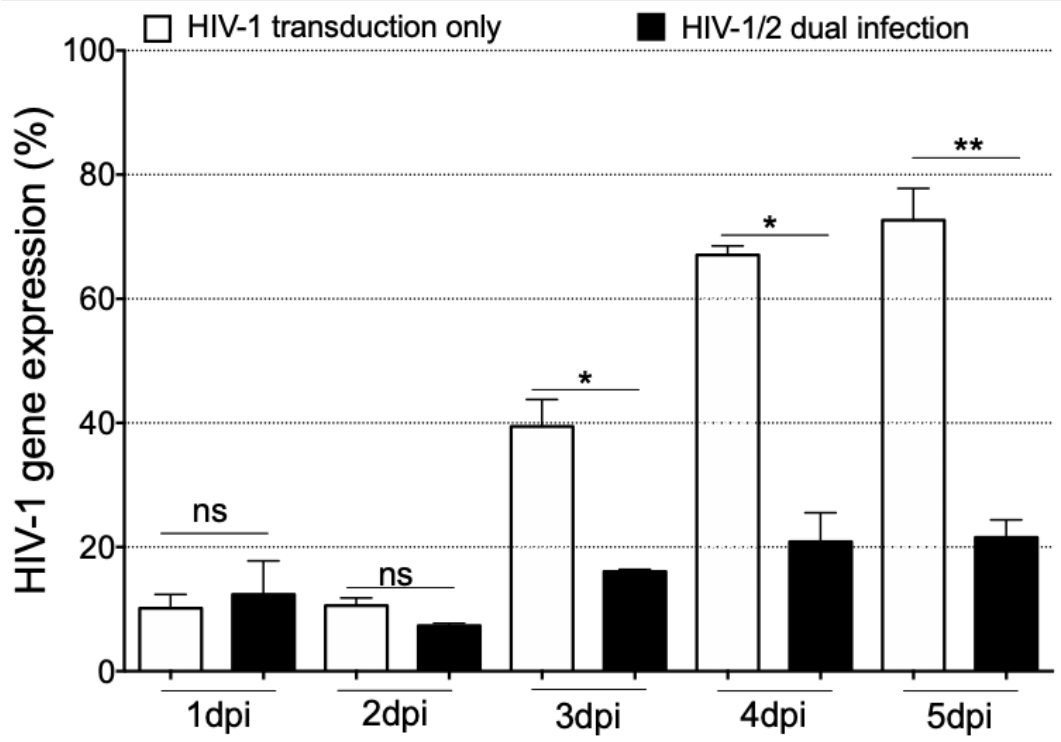
HIV-1 transduction only
HIV-1/2 dual infection
HIV-1 gene expression (%)
100
80
60
40
20
0
ns
ns
*
*
**
1dpi
2dpi
3dpi
4dpi
5dpi

HIV-2 infection triggered type I interferon responses by 48 hours post-infection.

Having observed an effect of HIV-2 infection not only on HIV-1 gene expression but also on HIV-1 transduction (fig. III-8), we examined whether HIV-2 infection results in induction of cellular innate immunity, such as the type I interferon (IFN) response, which in turn could suppress HIV-1 transduction and possibly replication. Notably, it has been previously reported that HIV-2 successfully infects target cells while eliciting innate immunity (*97-98,189-191*). We first measured IFN beta (IFNβ) mRNA expression levels during individual HIV-1 or HIV-2 infections (fig. III-8). Our data showed that HIV-1 infection elicited a modest increase in IFNβ mRNA at 48 and 72 hpi, whereas HIV-2 infection resulted in a strong IFNβ response (substantially more than HIV-1), especially at 48 hpi. That increase matched the levels of IFNβ mRNA measured in TZM-bl cells treated with recombinant IFNβ protein (fig. III-8). It also coincided with the decrease in the cellular promoter activities (eIF1α-driven mKO2 expression) (fig. III-5, III-6).

Figure III-8: Interferon (IFN) β mRNA analysis by RT-qPCR

Data were plotted as fold-change of IFNβ mRNA relative to the negative control and normalized to GAPDH mRNA. Infected HIV samples were compared to IFNβ-treated control cells and non-treated cells (n = 3 independent experiments). The Tukey's (corrected one-way ANOVA test) multiple comparison test was used.

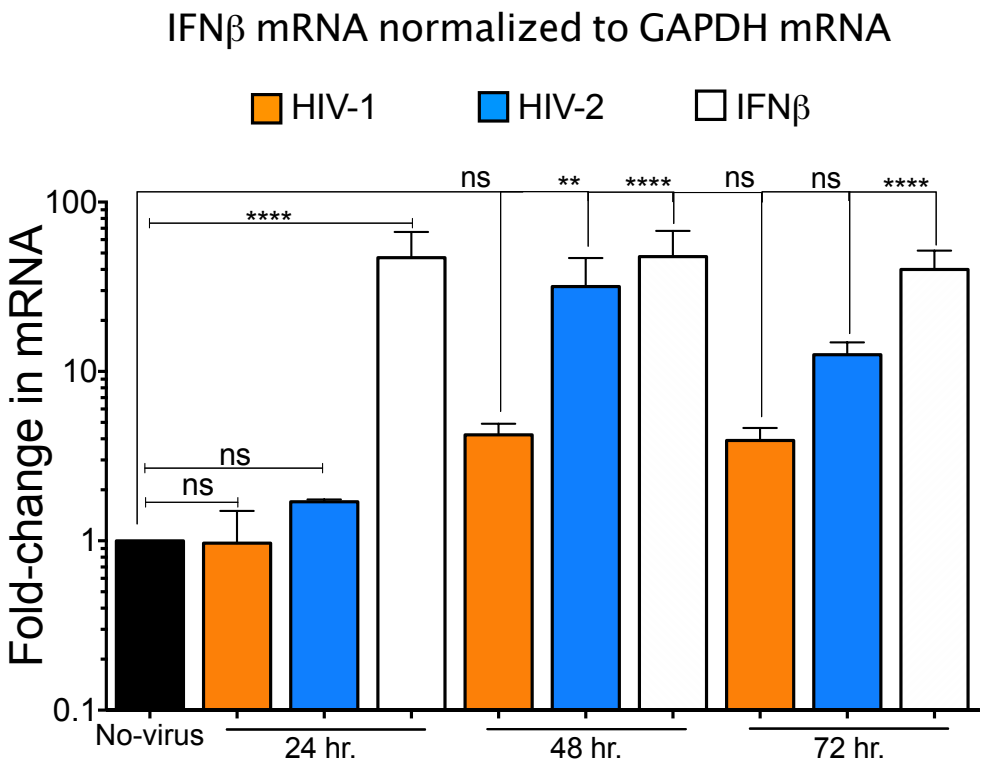
IFNβ mRNA normalized to GAPDH mRNA
HIV-1
HIV-2
IFNβ
Fold-change in mRNA
100
10
1
0.1
ns
**
****
ns
ns
****
****
ns
ns
No-virus
24 hr.
48 hr.
72 hr.

HIV-2 inhibition of HIV-1 is independent of type I interferon responses.

Having shown that HIV-2 can efficiently upregulate IFN response in the time-frame of our co-infection experiments, we next determined whether the inhibitory effect of HIV-2 infection on HIV-1 replication is solely dependent on IFN production. To do this we repeated the experiment in Vero cells. Vero cells have a deletion in chromosome 12 that has removed the genes coding for type I IFNs. Consequently, they cannot produce IFNα and IFNβ (*177*). To ensure that no type I IFNs were provided to target cells through the inoculum, virus preparations were pelleted by centrifugation, the supernatants removed, and viruses were resuspended into 5 mL of fresh DMEM. Vero cells were processed as described for TZM-bl cells. Importantly, we observed that in the absence of type I IFN production, the eIF1α-driven mKO2 signal from the HIV-1 reporter virus was no longer inhibited by co-transduction with HIV-2 (fig. III-9 and III-10). Remarkably, HIV-1 LTR-driven eGFP expression was still inhibited by co-transduction with HIV-2 (fig. III-11). These data strongly suggest that HIV-2 suppresses LTR-driven HIV-1 replication independently of type I IFN responses.

Figure III-9: Dual infection images in Vero cells

Images were obtained as described in figures 1G and 1H. Sample images for each time point of infection in Vero cells are shown (scale bar = 100 μm).

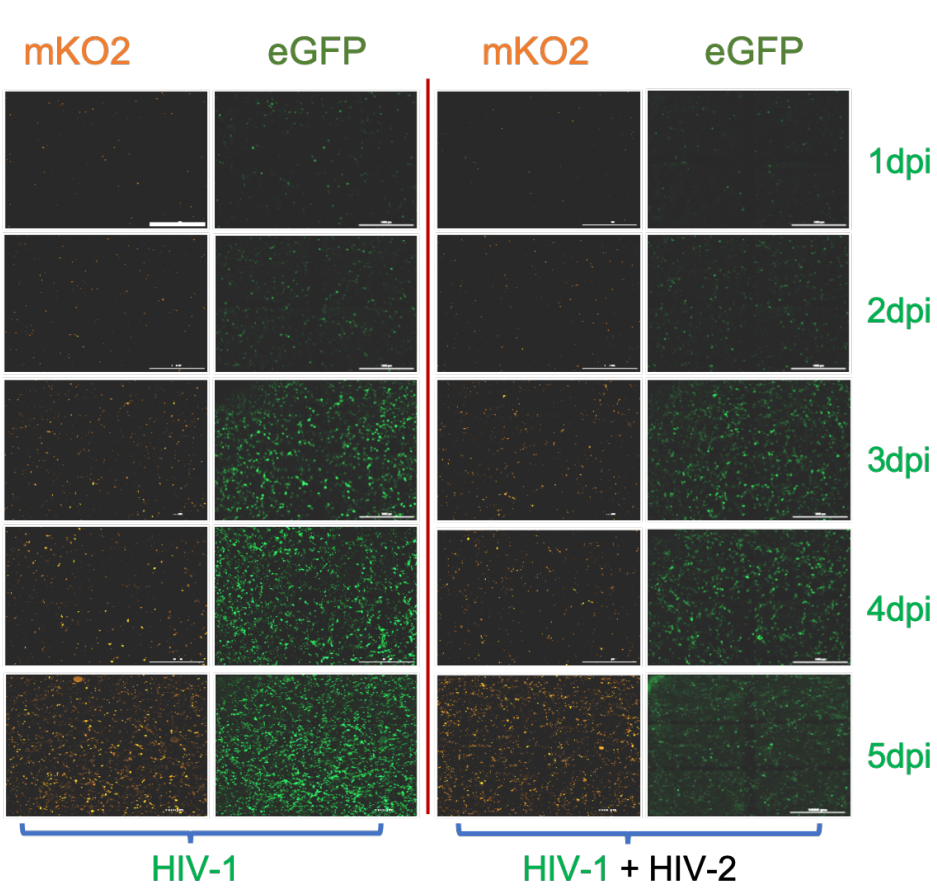
A
mKO2
eGFP
mKO2
eGFP
1dpi
2dpi
3dpi
4dpi
5dpi
HIV-1
HIV-1 + HIV-2

Figure III-10: Effects of dual transduction on eIF1α-driven mKO2 expression in Vero cells

Quantification was performed as described in figure III-9.

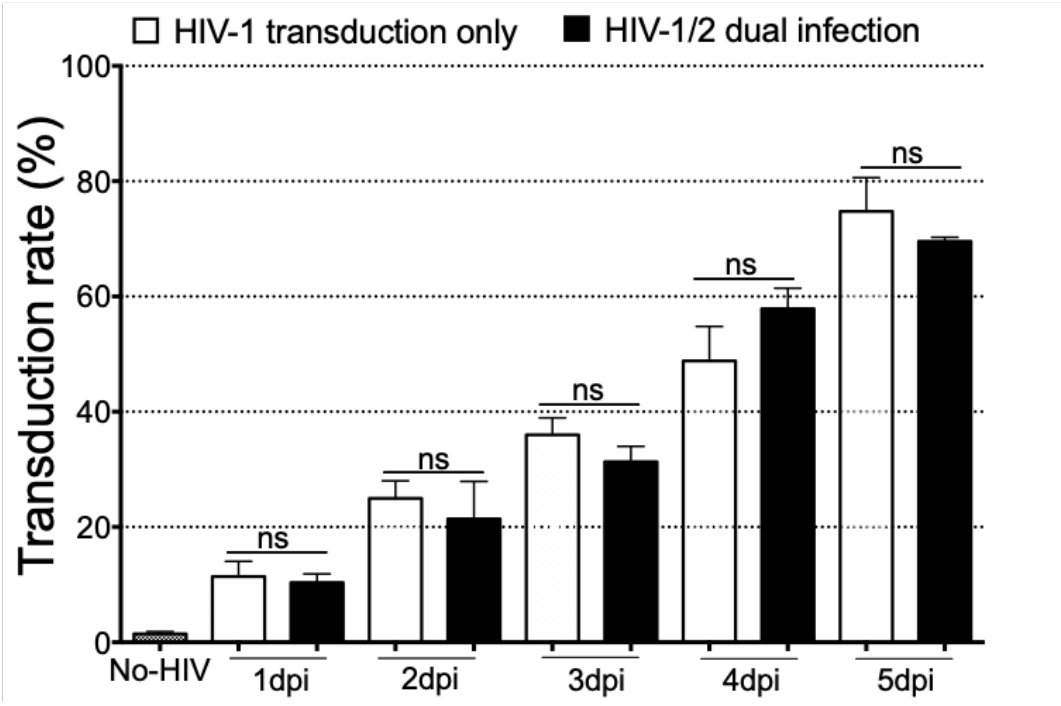
HIV-1 transduction only
HIV-1/2 dual infection
Transduction rate (%)
100
80
60
40
20
0
ns
ns
ns
ns
ns
No-HIV
1dpi
2dpi
3dpi
4dpi
5dpi

Figure III-11: Effects of dual transduction on HIV-1 LTR-driven eGFP expression in Vero cells

Quantification was performed as described in figure 1I. Error bars are standard errors (n = 3 independent experiments). Sidak's multiple comparison test was used in figure III-8 and figure III-9.

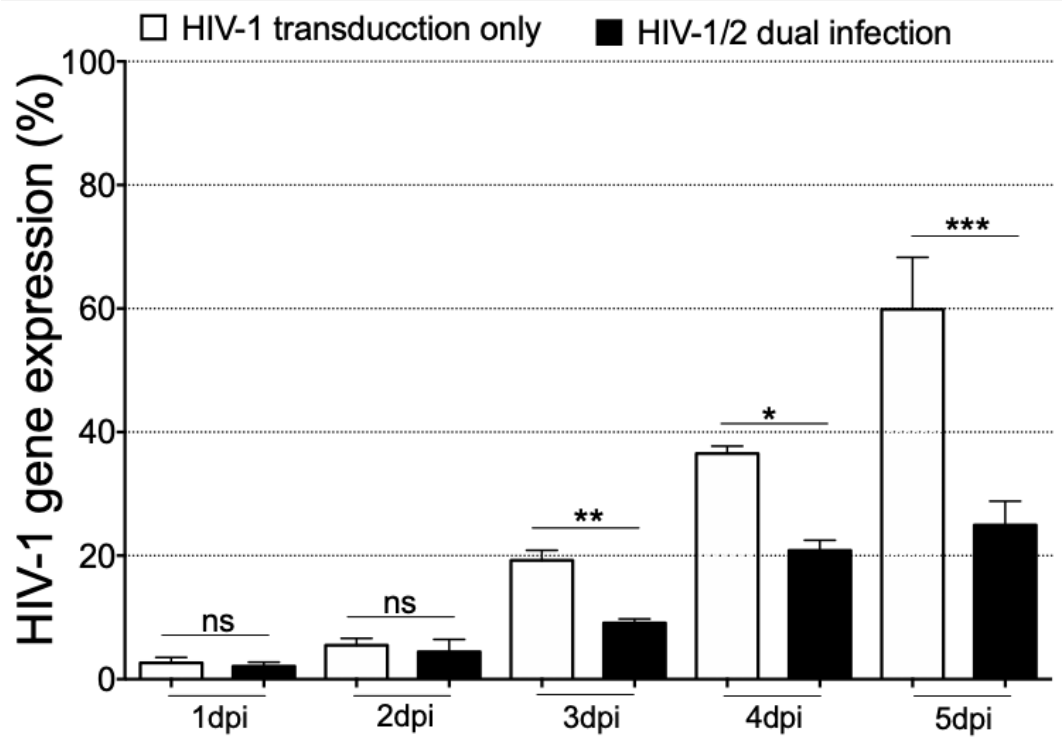
HIV-1 transducction only
HIV-1/2 dual infection
HIV-1 gene expression (%)
100
80
60
40
20
0
ns
ns
**
*
***
1dpi
2dpi
3dpi
4dpi
5dpi

HIV-1 LTR-driven transcription is inhibited by the TAR-2 element.

The TAR-2 (or HIV-2 TAR) has been reported to inhibit transcription from the HIV-1 LTR (*169*). We therefore hypothesized that the TAR-2 element could be responsible for inhibition of the HIV-1 gene expression observed in our experiments. To test that hypothesis, replication competent HIV-2 and a TAR-2-expressing construct were used respectively in an infection assay and in a transfection assay for 48 hours. TAR-2 expression levels in these experiments were compared using RT-qPCR with pTZU6 plasmid (containing U6 rather than TAR-2) used as a control. We found that overexpression yielded significantly higher amounts of TAR-2 than HIV-2 infection in TZM-GFP cells, both measured at 48 hours post-infection and post-transfection (fig. III-12). A transfection strategy was devised in which TAR-2 was transfected at a ratio of 40:1 relative to pNL4.3 in different cell lines (fig. III-13). TZM-GFP cells, HEK 293 FT cells, and Vero cells were transfected with the plasmids as described above, with a td-tomato expressing plasmid as an additional control for transfection efficiency. ELISA for HIV-1 p24 capsid was performed on the culture supernatants from these transfections and showed that HIV-1 viral particle release was drastically reduced (90% decrease compared to the controls) in the presence of TAR-2 (fig. III-14). We also found that inhibition of HIV-1 was not dependent on the cell-type used (fig. III-14).

To explore the significant drop in HIV-1 virion release in the presence of TAR-2 element, intracellular HIV-1 DNA and RNA were quantified with qPCR and RT-qPCR respectively. The results indicated that HIV-1 Gag mRNA significantly decreased (> 100-fold relative to the vector control) in the presence of TAR-2 element (fig. III-15). This points to a block in HIV-1 LTR-driven transcription. Such a block could occur at the

initiation step or at the elongation step of RNA Polymerase II transcription. Short viral transcripts are a hallmark of an abortive transcription as opposed to long polyadenylated transcripts that indicate a complete transcription process. The short viral transcripts which result from RNA polymerase early transcription complexes inability to clear the LTR promoter and proceed downstream of the transcriptional start site (TSS), were quantified with RT-qPCR. The data showed that HIV-1 LTR-driven transcription in the presence of TAR-2 produced short transcripts, even though the levels of longer HIV-1 transcripts were greatly reduced (fig. III-15, III-16).

Figure III-12: HIV-2 TAR RNA expression levels

FL pTAR-2 was transfected into TZM-GFP cells at 2 μg for 48 hours. Another set of TZM-GFP cells were concurrently infected with HIV-2 at a MOI of 0.8 for 48 hours. Transfected and infected cells were harvested, and intra-cellular HIV-2 TAR RNAs were quantified with RT-qPCR using specific primers.

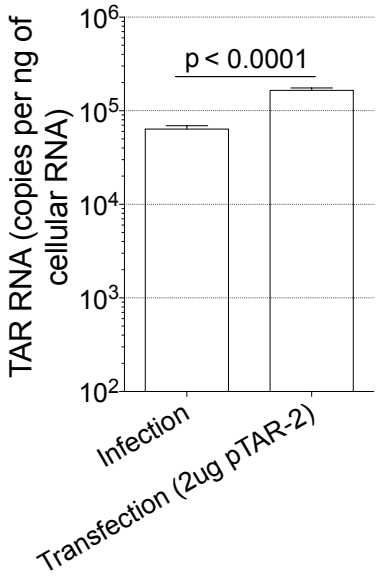
TAR RNA (copies per ng of cellular RNA)
10^6
10^5
10^4
10^3
10^2
p < 0.0001
Infection
Transfection (2ug pTAR-2)

Figure III-13: Strategy for transfection

1 x 10^6 TZM-bl cells or HEK 293 FT cells or Vero cells were plated into 6-well plates (2 plates/cell type/experiment), and let to attach overnight. Each plate was transfected with replication competent pNL4.3 (50 ng), pCMV-td tomato (10 ng) to control for transfection efficiency, and pZTU6 or full-length pTAR-2 (2,000 ng) for 48 hours. Supernatants from the two plates were collected to perform ELISA (duplicate samples per experiment). The first batch of transfected cells was fixed with 4% PFA for 30 minutes, and counterstained with DAPI. Stained plates were imaged with the Citation 5 automated epifluorescence microscope. The second batch was trypsinized and the transfected cells were collected in two aliquots for viral DNA analysis and viral RNA analysis. Three independent experiments were performed.

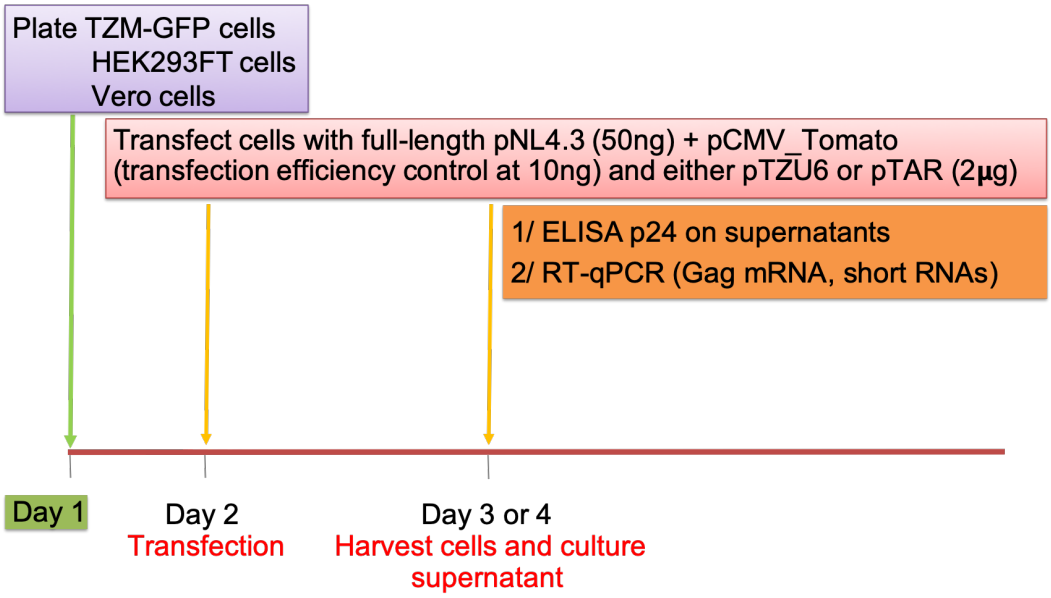
Plate TZM-GFP cells
HEK293FT cells
Vero cells
Transfect cells with full-length pNL4.3 (50ng) + pCMV_Tomato
(transfection efficiency control at 10ng) and either pTZU6 or pTAR (2µg)
1/ ELISA p24 on supernatants
2/ RT-qPCR (Gag mRNA, short RNAs)
Day 1
Day 2
Transfection
Day 3 or 4
Harvest cells and culture
supernatant

Figure III-14: Virus release analysis with ELISA p24

Culture supernatants were analyzed with an in-house ELISA p24 technique. Quantifications were performed using a p24 standard curve. For each cell line, the pTZU6 control was set at 100%. FL pTAR-2 was normalized to it (n = 3 independent runs).

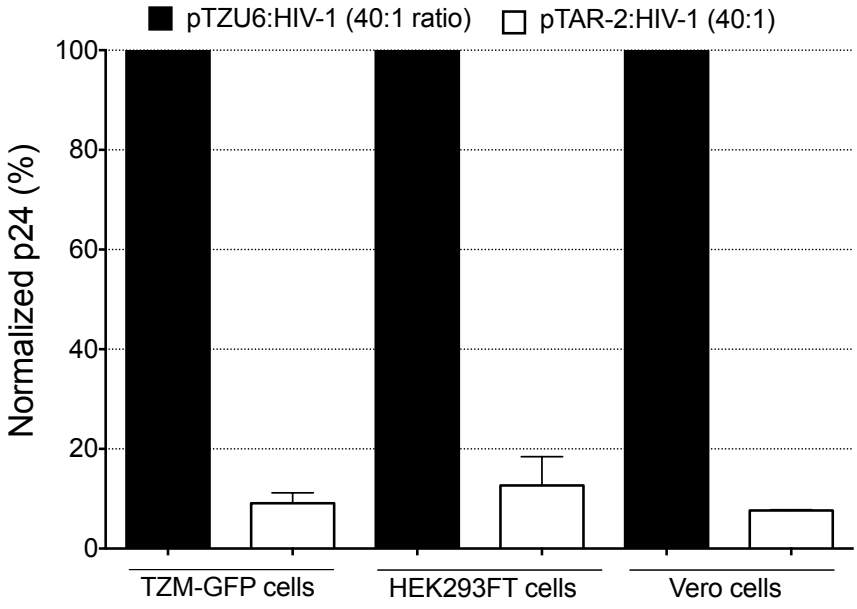
pTZU6:HIV-1 (40:1 ratio)
pTAR-2:HIV-1 (40:1)
Normalized p24 (%)
100
80
60
40
20
0
TZM-GFP cells
HEK293FT cells
Vero cells

Figure III-15: HIV-1 Gag RNA levels in transfected cells

Transcription from transfected pNL4.3 plasmid was measured with RT-qPCR using the primers described in table 1. The quantity of Gag RNA was divided by the number of viral DNA templates to get the ratio of viral Gag RNA to viral DNA templates.

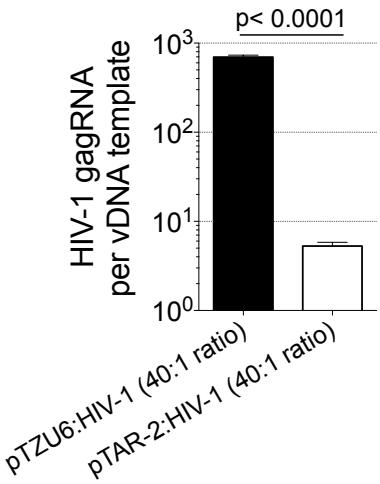
p< 0.0001
HIV-1 gagRNA per vDNA template
10^3
10^2
10^1
10^0
pTZU6:HIV-1 (40:1 ratio)
pTAR-2:HIV-1 (40:1 ratio)

Figure III-16: HIV-1 short transcription analysis during transfection

HIV-1 short RNA transcripts (first 200 nucleotides from the 5' end of the virus) were quantified using specific primers. The unpaired t test was used in figure III-10, figure III-13 and figure III-14

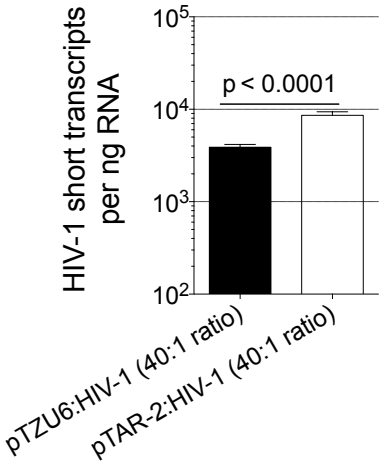
HIV-1 short transcripts per ng RNA
10^5
10^4
10^3
10^2
p < 0.0001
pTZU6:HIV-1 (40:1 ratio)
pTAR-2:HIV-1 (40:1 ratio)

TAR-2-mediated transcription inhibition is specific to HIV-1 LTR.

To rule out a potential design artifact or toxicity, the TAR-2 construct was tested against two other retroviruses, murine leukemia virus or MLV (gamma-retrovirus) and Rous sarcoma virus or RSV (alpha-retrovirus). First, HIV-1 and MLV reporter viruses were produced in the presence or absence of TAR-2 and used to infect HEK 293 FT cells (fig. III-17). The proportion of transduced cells (green for HIV-1, red for MLV) obtained with reporter virus preparations made in the presence of FL pTAR-2 was compared to that of the reporter virus preparations made in the presence of the pTZU6 control plasmid (fig. III-18 and III-19). There was a decrease in the proportion of HIV-1 positive cells in the TAR-2 samples relative to control, whereas the proportions of MLV positive cells remained similar under both conditions (fig. III-18 and III-19). These data indicated that TAR-2 targeted HIV-1 LTR promoter, but not the MLV LTR promoter.

Next, a co-transfection of the dual reporter eGFP/E2-Crimson RSV plasmid or the dual reporter eGFP/E2-Crimson pNL4.3 was performed with either the control pTZU6 or the FL pTAR-2 for 24 hours (fig. III-20). The mean fluorescence intensity (MFI) of the eGFP signals from the specific viral promoters (HIV-1 LTR or RSV LTR promoters) were normalized to the MFI of the CMV-driven E2-Crimson signal in the successfully transfected cells (fig. III-21 and III-22). The co-transfection assay also showed that unlike HIV-1 LTR promoter, RSV promoter was not targeted by TAR-2 (fig. III-21 and III-22). Collectively, these data support a selective inhibition of the HIV-1 LTR promoter by TAR-2, rather than a general suppression of LTR mediated transcription.

Figure III-17: Strategy outline for HIV-1/MLV reporter virus experiments

1 x 10^5 HEK 293 FT cells were plates into 12-well plates, and let to attach overnight. Attached cells were transfected with eGFP expressing pNL4.3 (20 ng), td-tomato expressing MLV (100 ng), pCMV-VSV(G) to pseudotyped the viruses, and either pTZU6 or pTAR-2 or one of its mutants (800 ng). The next day, the culture medium was changed and transfected were incubated for a total of 48 hours before supernatant were collected and frozen at -80 C. A new batch of HEK 293 FT cells were plated into 12-well plates, and let to attach overnight. The next day, virus supernatants containing the VSV(G)-pseudotyped viruses were thawed at room temperature, and used to infect the seeded cells for 48 hours. Infected cells were trypsinized, collected into 1.5 mL sterile microtubes, and fixed with 4% PFA for 30 minutes. Fixed cells were analyzed with the Accuri flow cytometer to identify HIV1-infected cells and MLV-infected cells. The ratios of HIV1-infected cells were normalized to MLV-infected cells. The ratios obtained from viruses made in the presence of pTAR-2 and its mutants were compared to those of viruses made in the presence of the control pTZU6. Three independent experiments were performed.

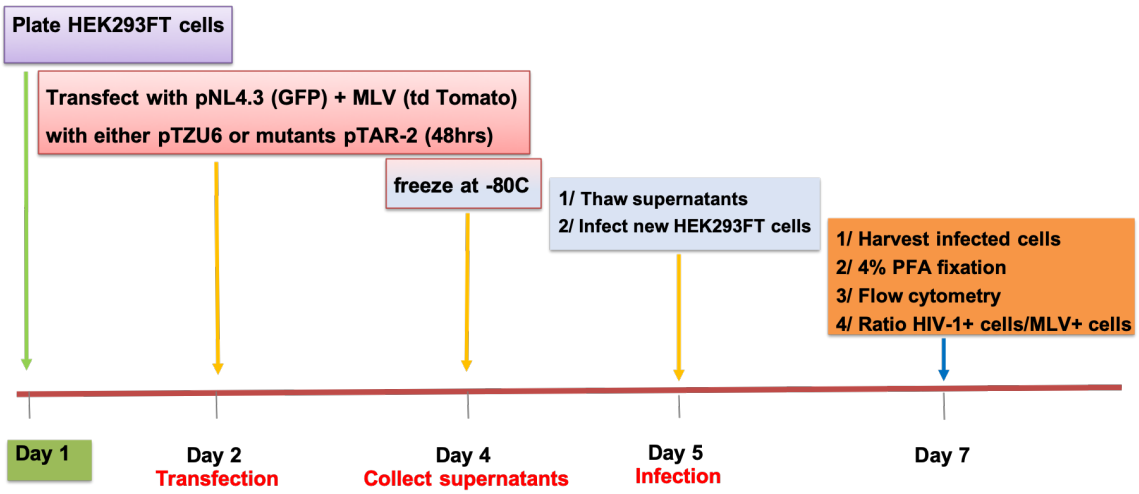
Plate HEK293FT cells
Transfect with pNL4.3 (GFP) + MLV (td Tomato)
with either pTZU6 or mutants pTAR-2 (48hrs)
freeze at -80C
1/ Thaw supernatants
2/ Infect new HEK293FT cells
1/ Harvest infected cells
2/ 4% PFA fixation
3/ Flow cytometry
4/ Ratio HIV-1+ cells/MLV+ cells
Day 1
Day 2
Transfection
Day 4
Collect supernatants
Day 5
Infection
Day 7

Figure III-18: Assessment of HIV-2 TAR effects on MLV

In the presence of FL pTAR-2 or pTZU6 control, VSV(G)-pseudotyped eGFP expressing HIV-1 and tomato-expressing MLV reporter viruses were produced and used to transduce HEK 293 FT cells. Transduced cells were analyzed with flow cytometry, representative plots are shown.

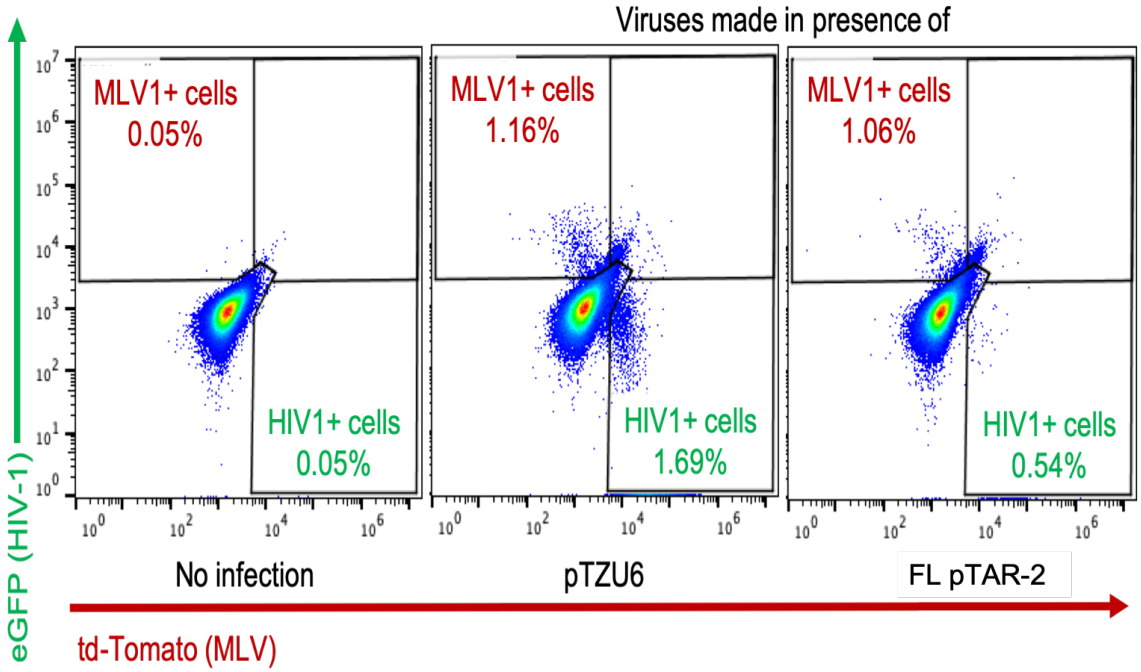
Viruses made in presence of
MLV1+ cells
0.05%
HIV1+ cells
0.05%
MLV1+ cells
1.16%
HIV1+ cells
1.69%
MLV1+ cells
1.06%
HIV1+ cells
0.54%
No infection
pTZU6
FL pTAR-2
eGFP (HIV-1)
td-Tomato (MLV)

Figure III-19: TAR-2 effects on MLV versus HIV-1

The percentage of HIV-1-transduced cells and MLV-transduced cells with reporter viruses made in the presence of the control pTZU6 or the FL pTAR-2 vectors are plotted.

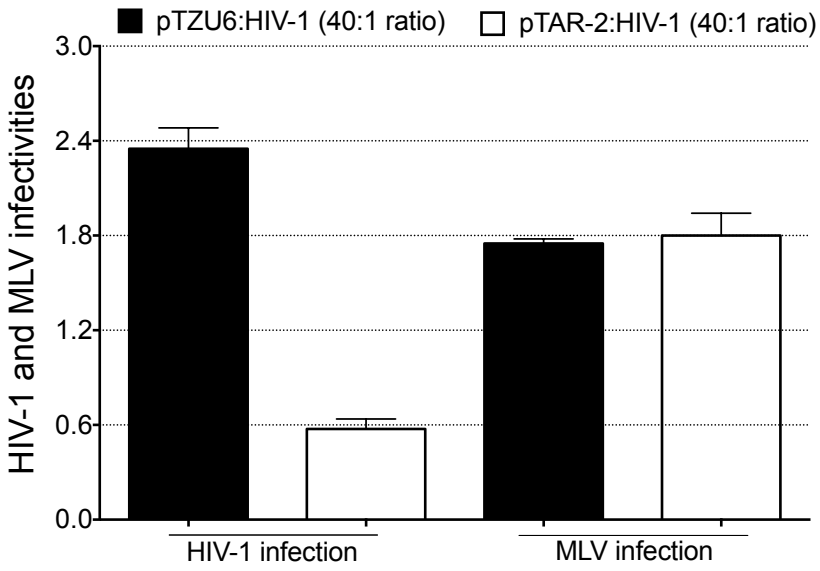
pTZU6:HIV-1 (40:1 ratio)
pTAR-2:HIV-1 (40:1 ratio)
HIV-1 and MLV infectivities
3.0
2.4
1.8
1.2
0.6
0.0
HIV-1 infection
MLV infection

Figure III-20: Strategy outline for HIV-1/RSV reporter virus experiments

1 x 10^5 HEK 293 FT cells were plates into 12-well plates, and let to attach overnight. Attached cells were transfected with dual reporters eGFP/E2-Crimson expressing pNL4.3 or RSV (20 ng), and either pTZU6 or pTAR-2 or one of its mutants (800 ng). The eGFP expression was driven by the HIV-1 LTR promoter or the RSV LTR promoter. The E2-Crimson expression was driven by a CMV early intermediate promoter. The next day, the culture medium was changed and transfected were incubated for a total of 48 hours. Transfected cells were trypsinized, collected into 1.5 mL sterile microtubes, and fixed with 4% PFA for 30 minutes. Fixed cells were analyzed with the Accuri flow cytometer to identify HIV1-transfected cells and RSV-transfected cells. The mean fluorescence intensity of the eGFP signal was normalized to that of the E2-Crimson signal. The ratios MFI eGFP/td-tomato of HIV-1 and RSV in the presence of pTAR-2 were compared to those made in the presence of the control pTZU6. Three independent experiments were performed.

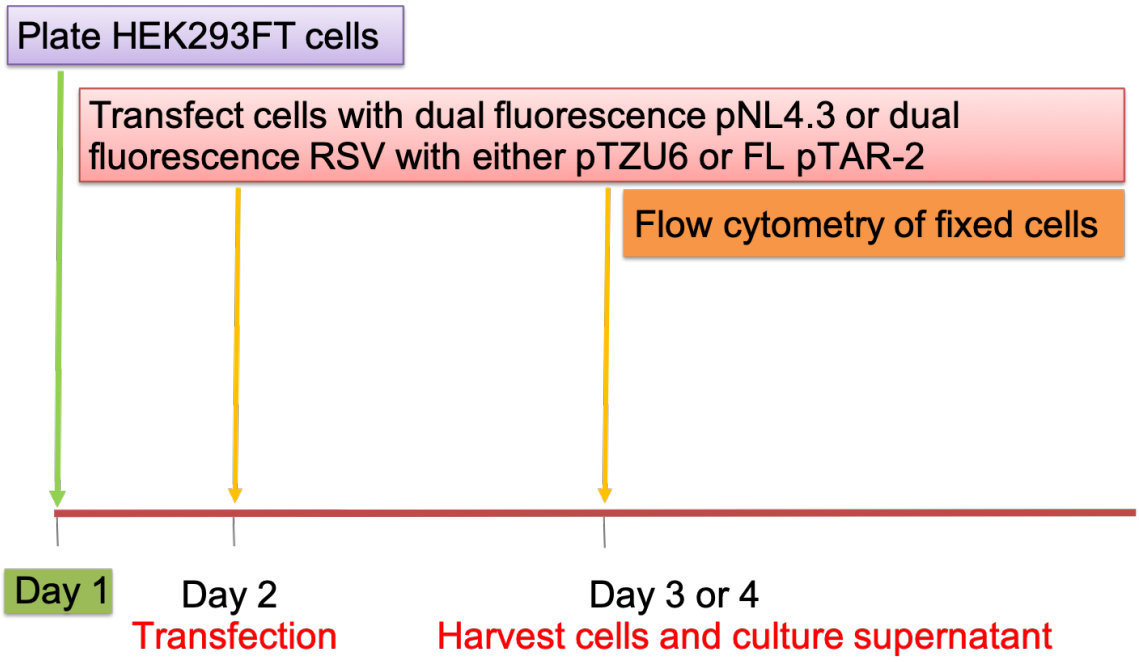
Plate HEK293FT cells
Transfect cells with dual fluorescence pNL4.3 or dual fluorescence RSV with either pTZU6 or FL pTAR-2
Flow cytometry of fixed cells
Day 1
Day 2
Transfection
Day 3 or 4
Harvest cells and culture supernatant

Figure III-21: TAR-2 effects on RSV versus HIV-1 (flow chart)

Representative plots of flow charts from transfection experiments performed with a dual reporter eGFP/E2-Crimson RSV vector for 24 hours in HEK 293 FT cells.

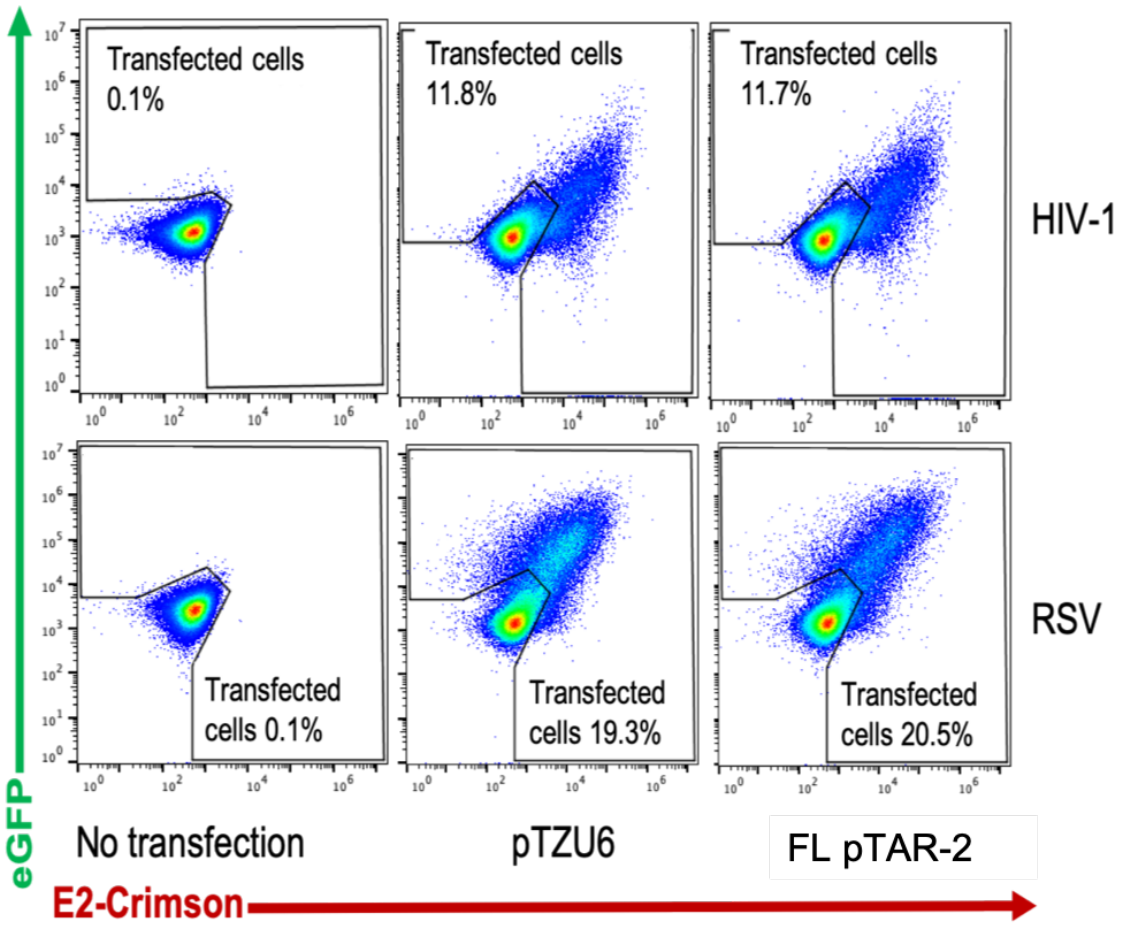
Transfected cells
0.1%
Transfected cells
11.8%
Transfected cells
11.7%
HIV-1
Transfected
cells 0.1%
Transfected
cells 19.3%
Transfected
cells 20.5%
RSV
eGFP
No transfection
pTZU6
FL pTAR-2
E2-Crimson

Figure III-22: TAR-2 effects on RSV versus HIV-1 (MFI quantitation)

The ratio of the mean fluorescence intensity (MFI) of the eGFP signal to the MFI of the E2-Crimson was calculated. The ratio eGFP MFI to E2-Crimson MFI in the control pTZU6-transfected cells was set at 100%, those of the FL pTAR2-transfected cells were normalized to the pTZU6 control.

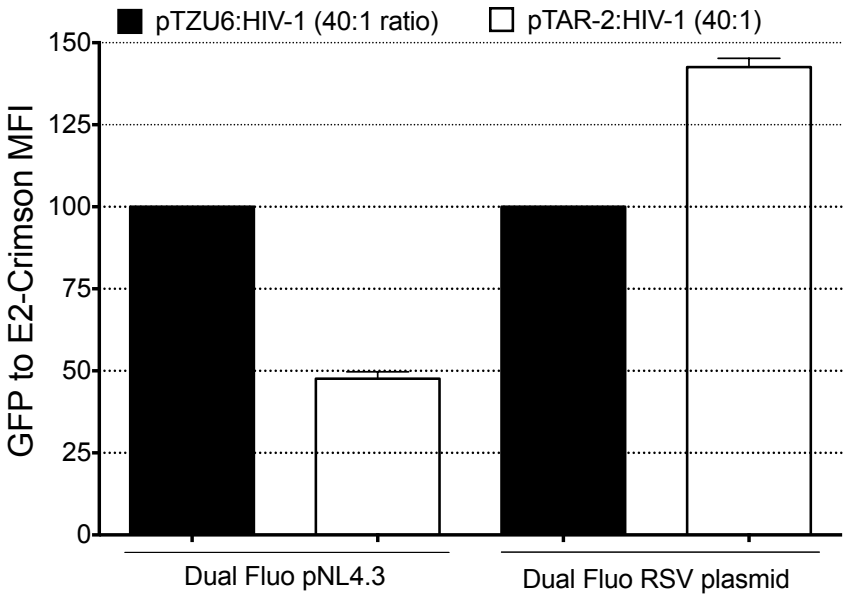
pTZU6:HIV-1 (40:1 ratio)
pTAR-2:HIV-1 (40:1)
GFP to E2-Crimson MFI
150
125
100
75
50
25
0
Dual Fluo pNL4.3
Dual Fluo RSV plasmid

Deletion mutagenesis of TAR-2 to identify the minimal region capable of inhibiting HIV-1 transcription.

We set out to map the specific regions within the 160 nucleotide FL TAR-2 that are responsible for inhibition of HIV-1 transcription. FL TAR-2 was predicted to form a four-stem loop RNA structure using UNAFOLD (IDT) (fig. III-23). We performed deletion mutagenesis of FL TAR-2 (primer sets and PCR conditions are described in tables 1 and 2). Hence, based on the predicted TAR-2 structure (fig. III-23), we generated TAR-2 mutants with only a single stem loop (SL_1, SL_2, or SL_3), two stem loops ($SL_{1,2}$, $SL_{1,3}$, or $SL_{2,3}$), or three stem loops but without the polyA stem loop ($SL_{1,2,3}$) (fig. III-23). We also constructed a TAR-2 variant that was only missing the stem loop 1 ($SL_{2,3,polyA}$). All constructs were cloned into the pTZU6 backbone. The full-length FL pTAR-2 contained loops 1,2,3, and polyA.

These constructs were tested by measuring their effect on the ratio of single reporter eGFP HIV-1 over td-tomato MLV viruses that were produced as described in fig. III-17. The number of HIV-1-transduced cells (green cells) was normalized to the number of MLV-transduced cells (red cells) for each TAR-2 mutant and the control pTZU6 (fig. III-24). All infectivity ratios (HIV+ cells/MLV+ cells) were expressed relative to reporter virus preparations made in the presence of the pTZU6 control. As both the full-length FL pTAR-2 and the polyA-deleted $SL_{1,2,3}$ reduced HIV-1 reporter virus production by approximately 65-70%, we concluded that the polyA stem loop is not required for suppression of HIV-1 gene expression. Removing further loops revealed that a combination of SL_2 with either SL_1 or SL_3 was sufficient to induce partial inhibition of HIV-1. The polyA stem loop did not appear to play a role, as $SL_{2,3}$ and $SL_{2,3,polyA}$ exhibited

similar anti-HIV-1 potency. Notably, individual TAR-2 stem loops by themselves were unable to downmodulate HIV-1. Hence, the data suggest that HIV-1 inhibition requires of a minimum of two stem loops, one of which should be SL_2, and the second either SL_1 or SL_3 (fig. III-24).

Figure III-23: TAR-2 mutants RNA sequences were uploaded on the UNAFOLD prediction software (IDT).

The software predicted for each mutant, several secondary structures and classified them from the most favorable to the least favorable structure in terms of thermodynamics. The structures shown above were either the first or the second most favorable secondary structures for the mutants. The top two represent the FL TAR-2 and its mutant without the poly A sequence, which was cloned into the $SL_{1,2,3}$ TAR-2 construct. The following two correspond to the FL TAR-2 without the first stem loop that was cloned into the $SL_{2,3,polyA}$ TAR-2 construct, and the FL TAR-2 with two deletions (minus SL2 and polyA), it was cloned into the $SL_{1,3}$ TAR-2 construct. The next two right below the previous are the FL TAR-2 without SL1 and poly A that was cloned into $SL_{2,3}$ TAR-2 construct, and the FL TAR-2 without the SL3 and the poly A that was cloned into the SL1,2 TAR-2 construct. The last three represent single stem loop structures of respectively SL1, SL2, and SL3 that were cloned into SL_1 pTAR-2, SL_2 TAR-2, and SL_3 TAR-2 constructs.

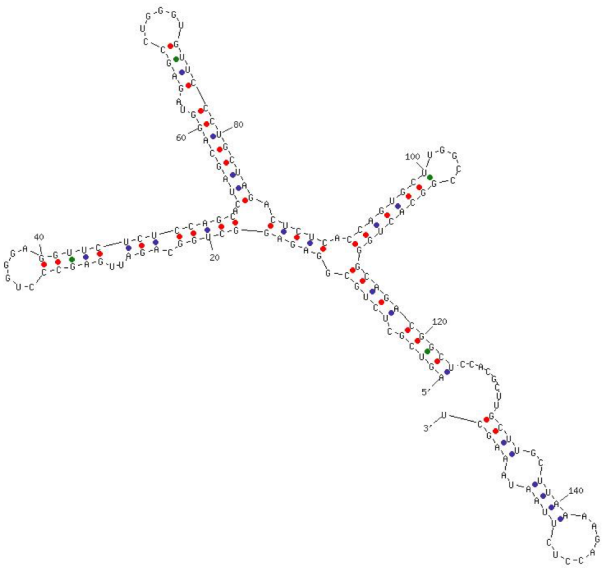

$SL_{1,2,3,poly\ A}$ TAR-2 (Full-length)

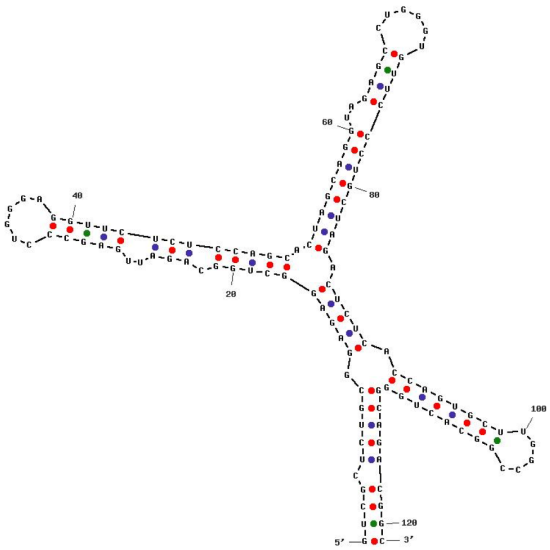

$SL_{1,2,3}$ TAR-2

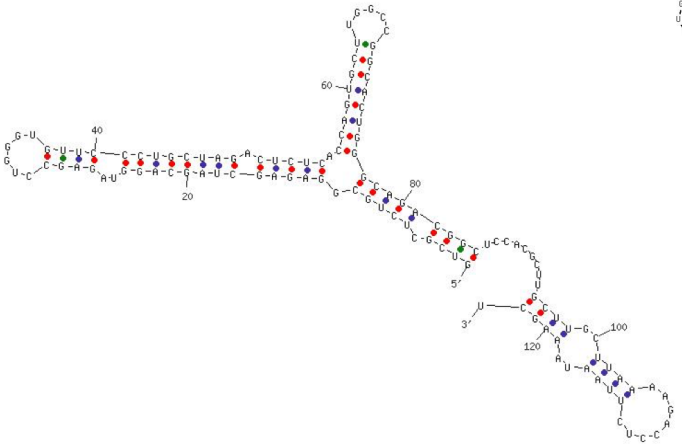

$SL_{2,3,polyA}$ TAR-2

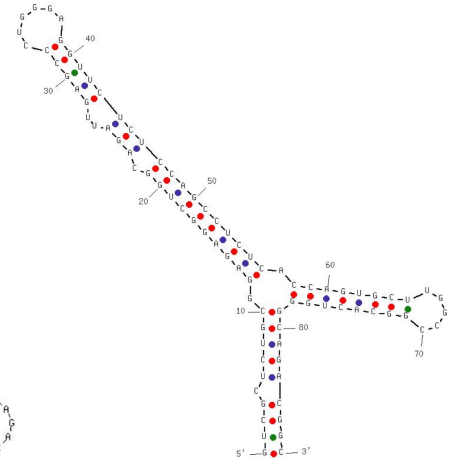

$SL_{1,3}$ TAR-2

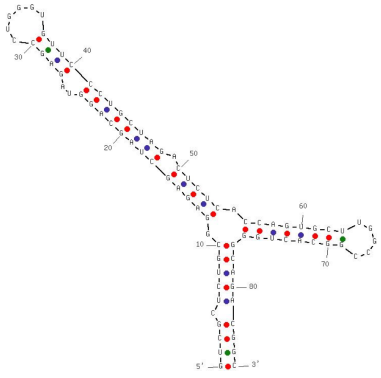

$SL_{2,3}$ TAR-2

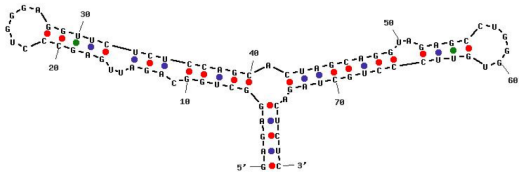

$SL_{1,2}$ TAR-2

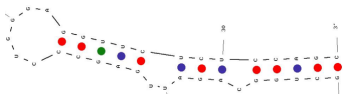

SL_1 TAR-2

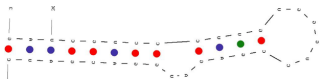

SL_2 TAR-2

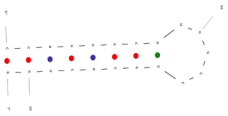

SL_3 TAR-2

Figure III-24: Differential effects of TAR-2 constructs on HIV-1 and MLV transduction

The proportions of HIV1-infected cells (green cells) and MLV-infected cells (red cells) achieved with the viruses made in the presence of the control pTZU6 or the FL pTAR-2 constructs were plotted in the graph. The Dunnett's (corrected one-way-ANOVA test) multiple comparison test was used.

B

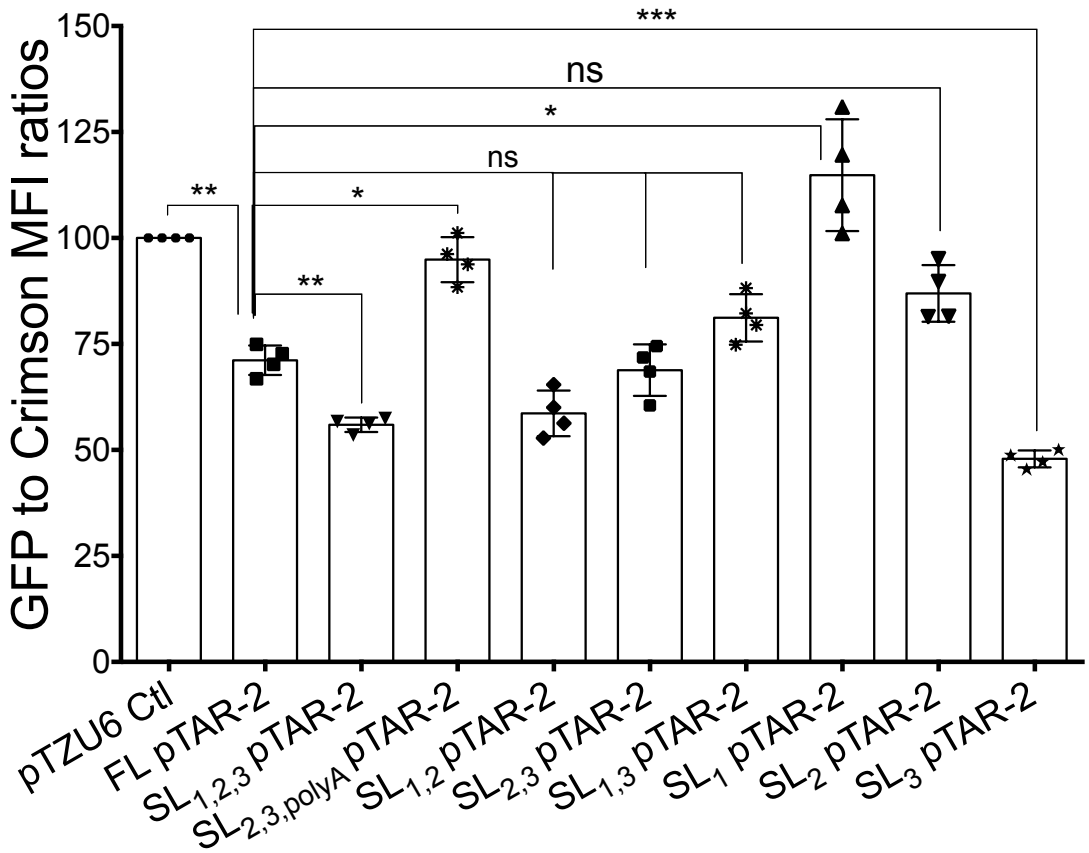
GFP to Crimson MFI ratios
150
125
100
75
50
25
0
***
ns
*
ns
**
*
**
pTZU6 Ctl
FL pTAR-2
SL1,2,3 pTAR-2
SL2,3,polyA pTAR-2
SL1,2 pTAR-2
SL2,3 pTAR-2
SL1,3 pTAR-2
SL1 pTAR-2
SL2 pTAR-2
SL3 pTAR-2

TAR blocks HIV-1 transcription in the context of infection.

TAR-2-mediated blockade of HIV-1 transcription occurred in the context of HIV-2 co-infection. To understand the delay in inhibition of HIV-1 by the TAR-2 during infection (72 hpi *vs.* 48 hpi for type I IFN responses), the kinetics of TAR-2 RNA expression during HIV-2 infection in TZM-bl cells was assessed with RT-qPCR. The data showed that TAR-2 RNA transcription reached its peak between 48 hpi and 72 hpi (fig. III-25). This suggest that TAR-2 would likely affect measurements of HIV-1 transcription by 72 hpi, which is consistent with our microscopy data (fig III-7). Then total HIV-1 viral DNA in infected cells was quantified using qPCR and appeared similar in both HIV-1 single infection and HIV-1/HIV-2 dual infection at all time points (fig. III-26). This suggests that HIV-1 cell entry and reverse transcription steps were not affected by HIV-2 infection. To explore the effects of the TAR-2 on HIV-1 LTR-driven transcription, cell-associated HIV-1 Gag RNA and exon 1-containing viral RNAs were quantified by RT-qPCR. All species of HIV-1 viral RNAs including the Gag RNA contain exons 1 (*73*). The results indicated that whereas HIV-1 Gag RNA increased more than 10-fold between 24 hpi and 72 hpi during single infection, in the presence of TAR-2 it significantly decreased (> 6-fold) from 48 to 72 hpi (fig. III-27). There were no significant differences at early time points of infection. This suggests either a failure to complete full-length transcripts or a block at transcription initiation by 72 hpi. To tease apart the two possibilities, HIV-1 short transcripts, a hallmark of abortive transcription in which transcription is initiated but fails to extend, were quantified and showed similar levels at 24 hpi and 48 hpi in single and dual infections (fig. III-28). During co-infection, viral short transcripts significantly

increased at 72 hpi (fig. III-28), while long transcripts decreased significantly at the same time point (fig. III-27), indicating a block in transcription elongation.

Figure IV-25: HIV-2 TAR RNA expression during HIV-2 infection

TZM-bl cells were infected with replication competent HIV-2 for 24hpi, 48hpi and 72hpi prior to harvesting. Infected cells were harvested and processed for RT-qPCR to quantify genomic RNA and total transcripts during infection.

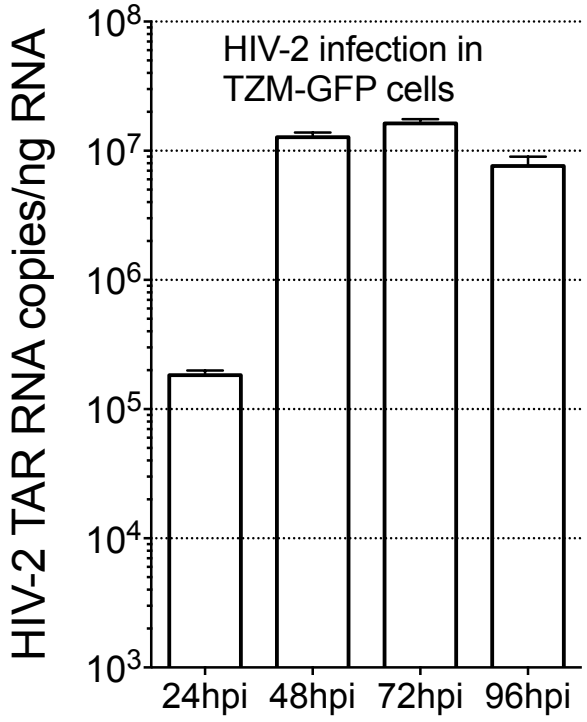
HIV-2 infection in
TZM-GFP cells
HIV-2 TAR RNA copies/ng RNA
10^8
10^7
10^6
10^5
10^4
10^3
24hpi
48hpi
72hpi
96hpi

Figure IV-26: HIV-1 total DNA in HIV-infected TZM-bl cells

Infection was performed as described in the methods section, total viral DNA levels were determined by qPCR.

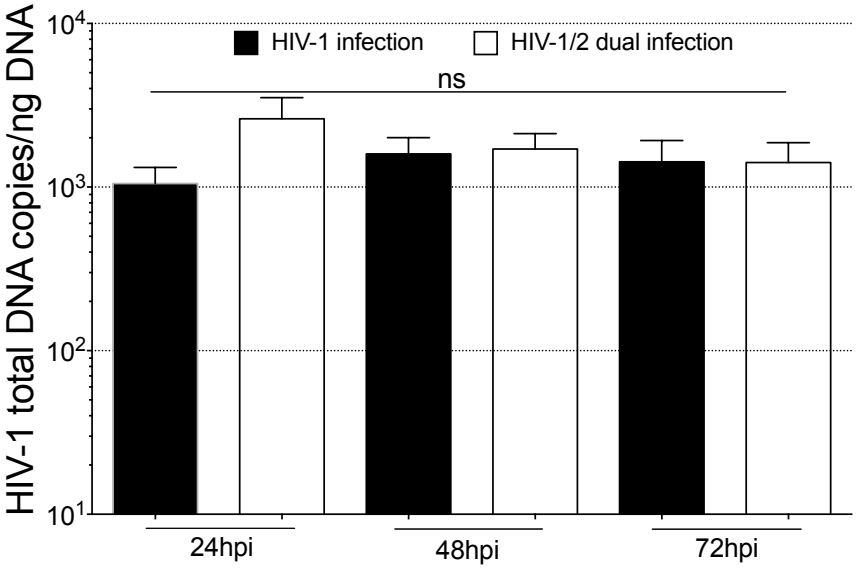
HIV-1 total DNA copies/ng DNA
10^4
10^3
10^2
10^1
HIV-1 infection
HIV-1/2 dual infection
ns
24hpi
48hpi
72hpi

Figure IV-27: Quantification of HIV-1 Gag RNA levels in HIV1-infected TZM-bl cells

Long transcript levels were quantified by RT-qPCR. Averages from three independent experiments are shown with SEM indicated.

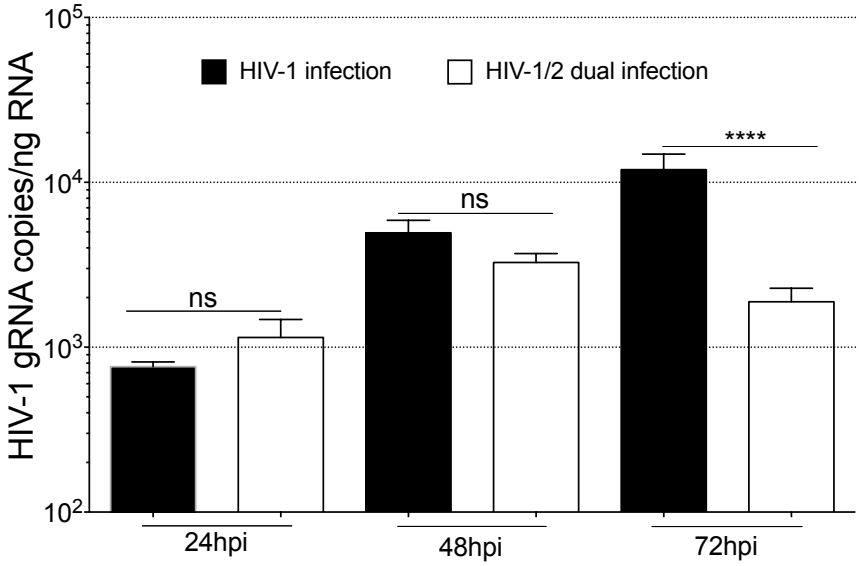
HIV-1 infection
HIV-1/2 dual infection
HIV-1 gRNA copies/ng RNA
10^5
10^4
10^3
10^2
ns
ns
****
24hpi
48hpi
72hpi

Figure IV-28: Quantification of HIV-1 short transcript levels in HIV1-infected TZM-bl cells

Short/abortive (D) transcript levels were quantified by RT-qPCR. Averages from three independent experiments are shown with SEM indicated. The Tukey's multiple comparison test was used in figure III-23, figure III-25, and figure III-26.

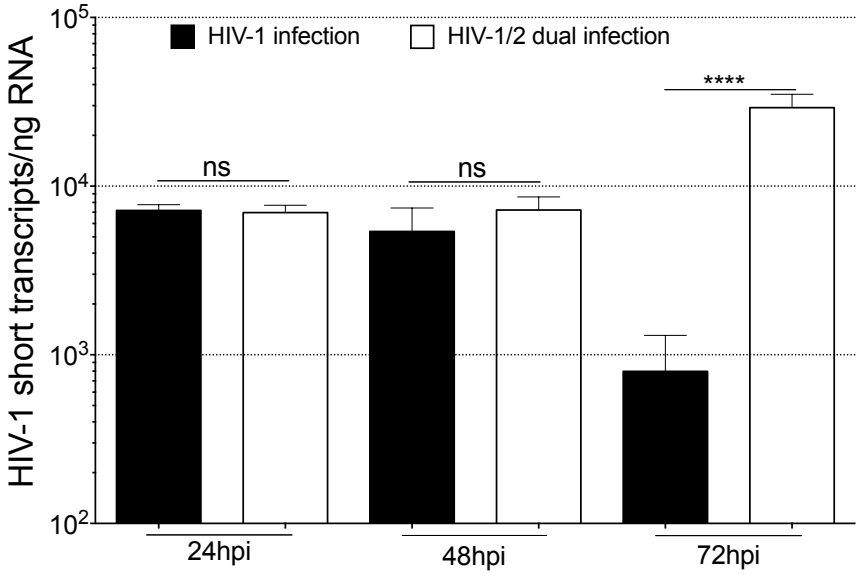
HIV-1 short transcripts/ng RNA
10^5
10^4
10^3
10^2
HIV-1 infection
HIV-1/2 dual infection
ns
ns
****
24hpi
48hpi
72hpi

TAR-2 prevents HIV-1 transcripts completion.

In the absence of Tat, the majority of RNA polymerase II (RNAPII) elongating complexes stall near the promoter region (*73*). Within that region, the C-terminal domain of RNAPII is heavily phosphorylated on its serine residues in position 5 (serine 5), and less phosphorylated on its serine 2 residues. Therefore, stalled RNAPII elongating complexes are serine 5 phosphorylated whereas non-stalled complexes are serine 2-phosphorylated (*55-75*). To overcome the stalling, HIV-1 hijacks the ubiquitous positive acting transcription elongation factor b (p-TEFb) using its TAR RNA and its Tat protein (*55-75*). Therefore, assessment of the occupancy of active p-TEFb at the HIV-1 TSS is an indirect measure of its association with RNAPII initiating complexes as they transition to elongating complexes upon binding to active p-TEFb. To confirm that HIV-1 LTR-driven transcription was restricted to abortive transcripts, Ser2-P RNAP II occupancy 1 kilobase pair (kbp) downstream of the HIV-1 TSS (TSS + 1 kbp) was assessed using ChIP assays. Active P-TEFb occupancy downstream HIV-1 promoter region showed that while it increased over time during HIV-1 single infection, it decreased during coinfections in TZM-bl cells (fig. III-29). Additionally, the occupancy of Ser2-P RNAP II was low at 24 hpi in both singly and dually infected cells. At 72 hpi the occupancy had significantly increased during HIV-1 single infection but remained low in dual infection (fig. III-30). This agrees with the quantification of HIV-1 Gag RNA (fig. III-27). To further establish that HIV-1 LTR-driven transcription is inhibited during transcription elongation, occupancy of Ser5-P RNAPII was assessed at the same location. The data indicate that there were almost no stalled RNAPII complexes downstream of the HIV-1 TSS at 24 hpi (fig. III-31). Curiously, there was significantly more stalling of RNAPII complexes during

HIV-1 single infection at 72 hpi. However, the ratio stalling complexes to elongating complexes remained below 1 unlike the ratio in coinfections (data not shown).

To confirm that TAR2-mediated blockade of HIV-1 transcription occur during transcription elongation as suggested by the data on transcription elongation, RNAPII occupancy at the HIV-1 transcriptional start site (TSS) was assessed as a marker for initiation at 24 hpi (no changes expected) and 72 hpi (differences expected). The data indicate that during single infection, active p-TEFb similarly occupied the HIV-1 TSS at all time points (fig. III-32). In contrast, active p-TEFb occupancy during coinfection seemed to decrease to levels similar to those of the DRB-treated samples from 24 hpi to 72 hpi. This suggest that TAR-2-mediated inhibition of HIV-1 transcription targets RNAPII transitioning from initiating complexes to elongating complexes by countering their interaction with active P-TEFb. The occupancy of Ser2-P RNAPII was similar in both HIV-1 single infection DRB-treated or not, and in coinfection at all time points (fig. III-33). This shows that there were no significant differences in the initiation of HIV-1 transcription between HIV-1 single infection and HIV-1/HIV-2 coinfections. The occupancy of Ser5-P RNAPII was higher in HIV1-infected samples treated with DRB and in coinfection whereas it was close to nothing in HIV-1 single infection at 24 hpi and 72 hpi (fig. III-34). This indicates that RNAP II initiating complexes tend to stall around the promoter region during coinfection and DRB treatment.

Figure IV-29: Active P-TEFb occupancy at 1 kbp downstream of HIV-1 TSS during HIV infection

Single HIV1-infected treated or not with DRB (P-TEFb inhibitor), and dual-infected TZM-bl cells were processed with ChIP using antibody against the threonine 176-phosphorylated P-TEFb form (active form), followed with qPCRs using specific primers (table 1) spanning a region of the HIV-1 genome located 1kbp downstream of the transcription start sites of HIV-1.

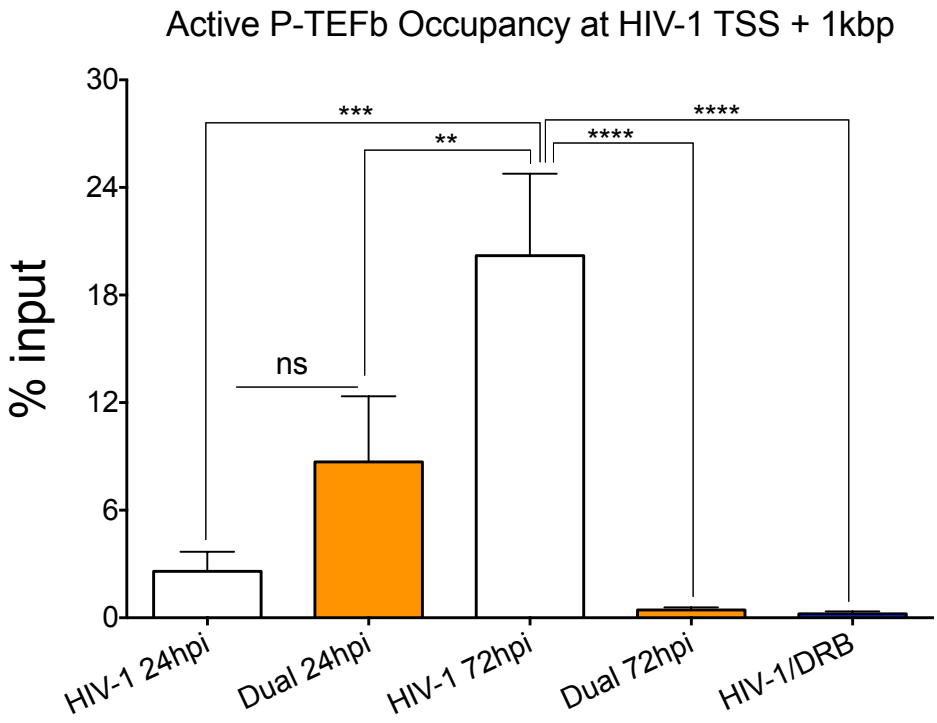
Active P-TEFb Occupancy at HIV-1 TSS + 1kbp
% input
30
24
18
12
6
0
***
**
****
****
ns
HIV-1 24hpi
Dual 24hpi
HIV-1 72hpi
Dual 72hpi
HIV-1/DRB

Figure IV-30: Ser2-P RNAPII occupancy at 1 kbp downstream of HIV-1 TSS during HIV infection

Single HIV1-infected treated or not with DRB (P-TEFb inhibitor), and dual-infected TZM-bl cells were processed with chromatin immunoprecipitation using antibody against the serine 2-phosphorylated form of RNAP II, followed with qPCRs using specific primers (table 1) spanning the location 1kbp downstream of the transcription start sites of HIV-1.

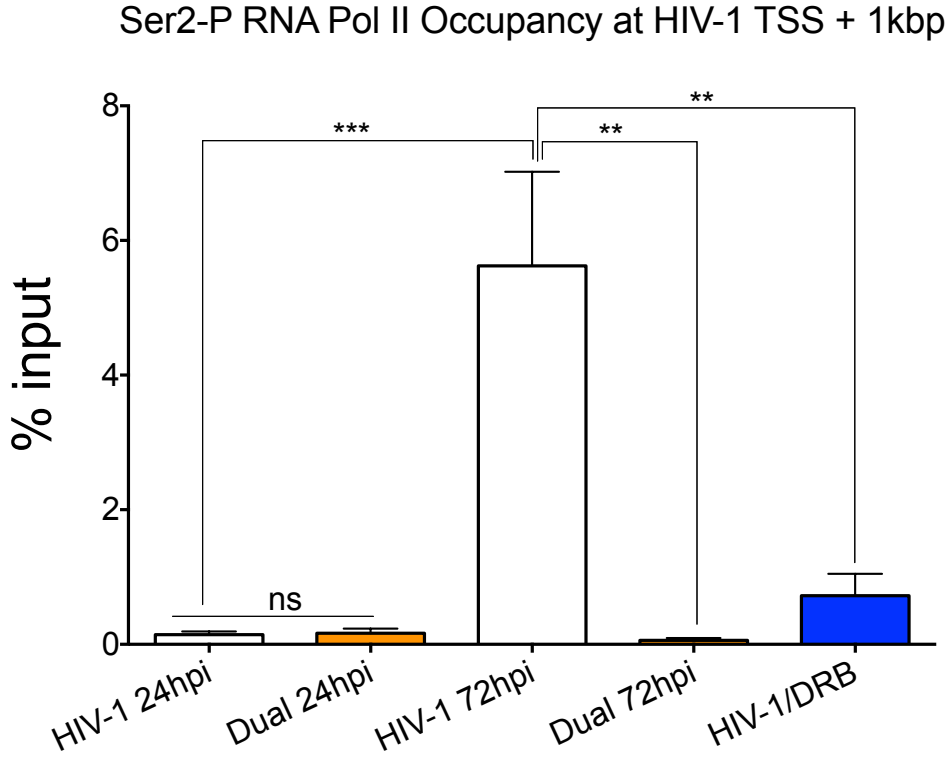
Ser2-P RNA Pol II Occupancy at HIV-1 TSS + 1kbp
% input
8
6
4
2
0
***
**
**
ns
HIV-1 24hpi
Dual 24hpi
HIV-1 72hpi
Dual 72hpi
HIV-1/DRB

Figure IV-31: Ser5-P RNAPII occupancy at 1 kbp downstream of HIV-1 TSS during HIV infection

Same as previously, except for the antibody used in the immunoprecipitation reaction. Antibody against the serine 5-phosporylated RNAP II (stalled form) was used. The same primers used in above were used here.

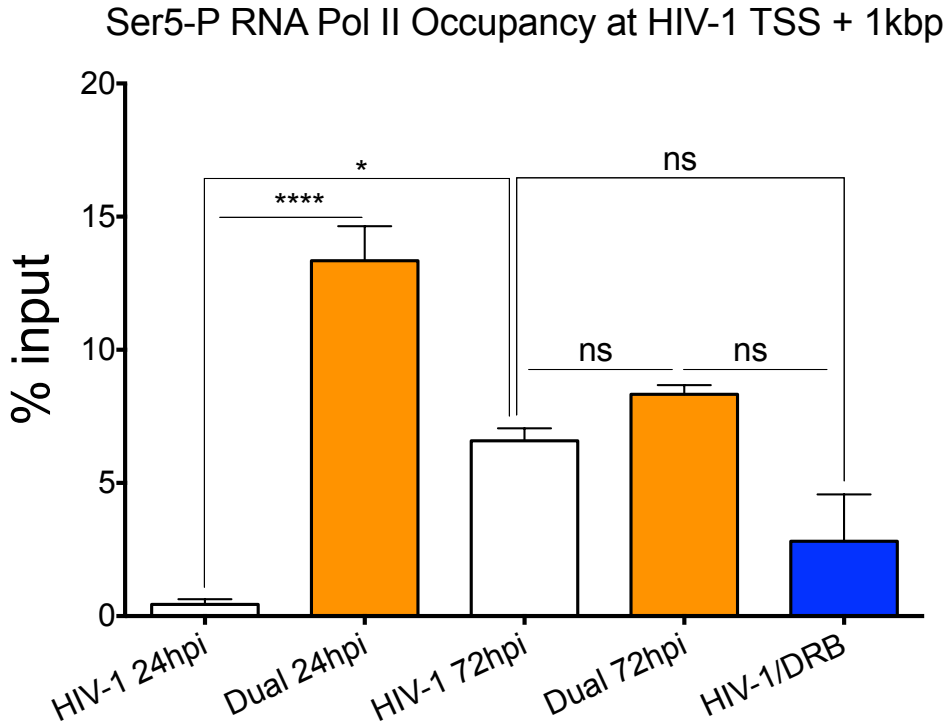
Ser5-P RNA Pol II Occupancy at HIV-1 TSS + 1kbp
% input
20
15
10
5
0
*
****
ns
ns
ns
HIV-1 24hpi
Dual 24hpi
HIV-1 72hpi
Dual 72hpi
HIV-1/DRB

Figure IV-32: Active P-TEFb occupancy at the HIV-1 TSS during HIV infection.

Single HIV1-infected treated or not with DRB (P-TEFb inhibitor), and dual-infected TZM-bl cells were processed with chromatin immunoprecipitation using antibody against the threonine 176-phosphorylated P-TEFb form (active form), followed with qPCRs using specific primers (table 1) spanning a region encompassing the HIV-1 TSS in the LTR.

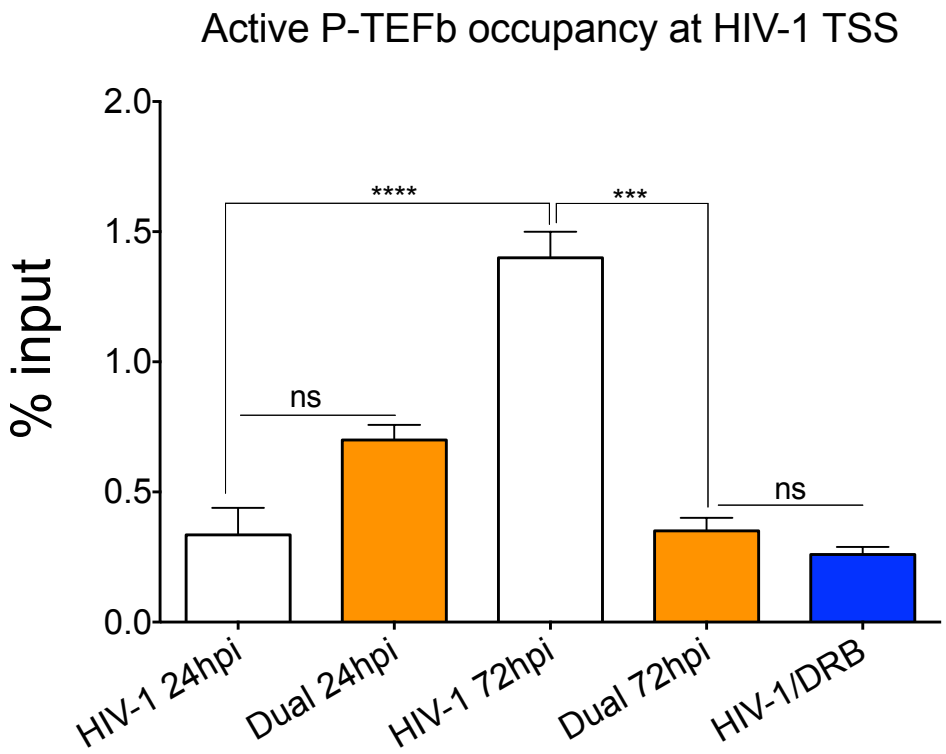
Active P-TEFb occupancy at HIV-1 TSS
% input
2.0
1.5
1.0
0.5
0.0
****
***
ns
ns
HIV-1 24hpi
Dual 24hpi
HIV-1 72hpi
Dual 72hpi
HIV-1/DRB

Figure IV-33: Ser2-P RNAPII occupancy at the HIV-1 TSS during HIV infection

Single HIV1-infected treated or not with DRB (P-TEFb inhibitor), and dual-infected TZM-bl cells were processed with chromatin immunoprecipitation using antibody against the serine 2-phosphorylated form of RNAP II, followed with qPCRs using specific primers (table 1) spanning a region encompassing the HIV-1 TSS in the LTR.

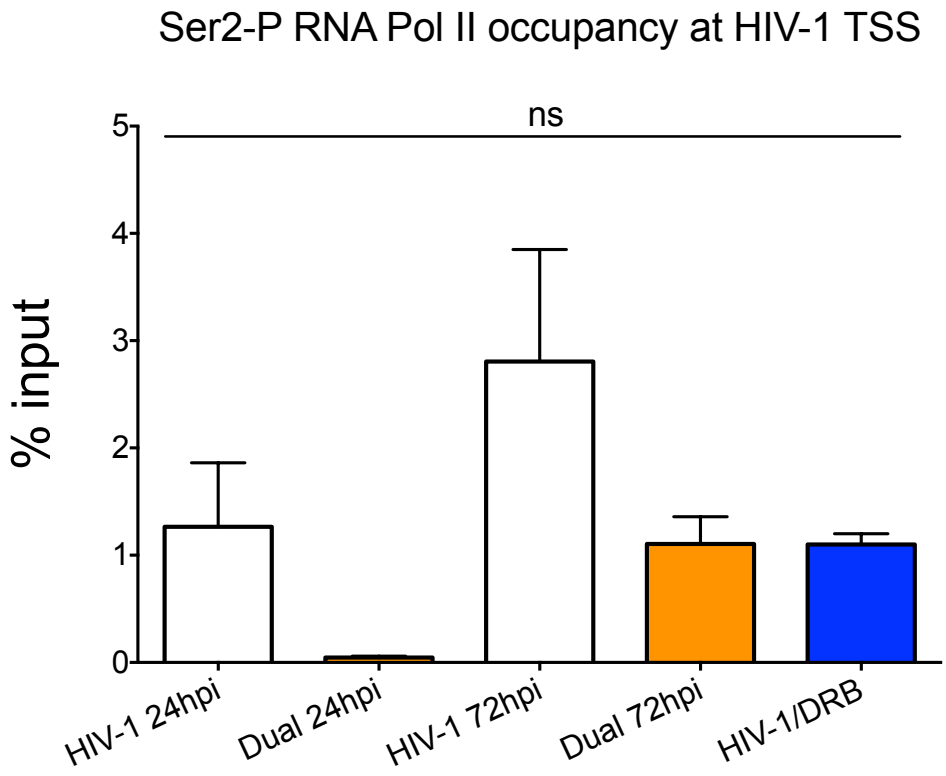
Ser2-P RNA Pol II occupancy at HIV-1 TSS
ns
% input
5
4
3
2
1
0
HIV-1 24hpi
Dual 24hpi
HIV-1 72hpi
Dual 72hpi
HIV-1/DRB

Figure IV-34: Ser5-P RNAPII occupancy at the HIV-1 TSS during HIV infection

Single HIV1-infected treated or not with DRB (P-TEFb inhibitor), and dual-infected TZM-bl cells were processed with chromatin immunoprecipitation using antibody against the serine 5-phosphorylated form of RNAP II, followed with qPCRs using specific primers (table 1) spanning a region encompassing the HIV-1 TSS in the LTR.

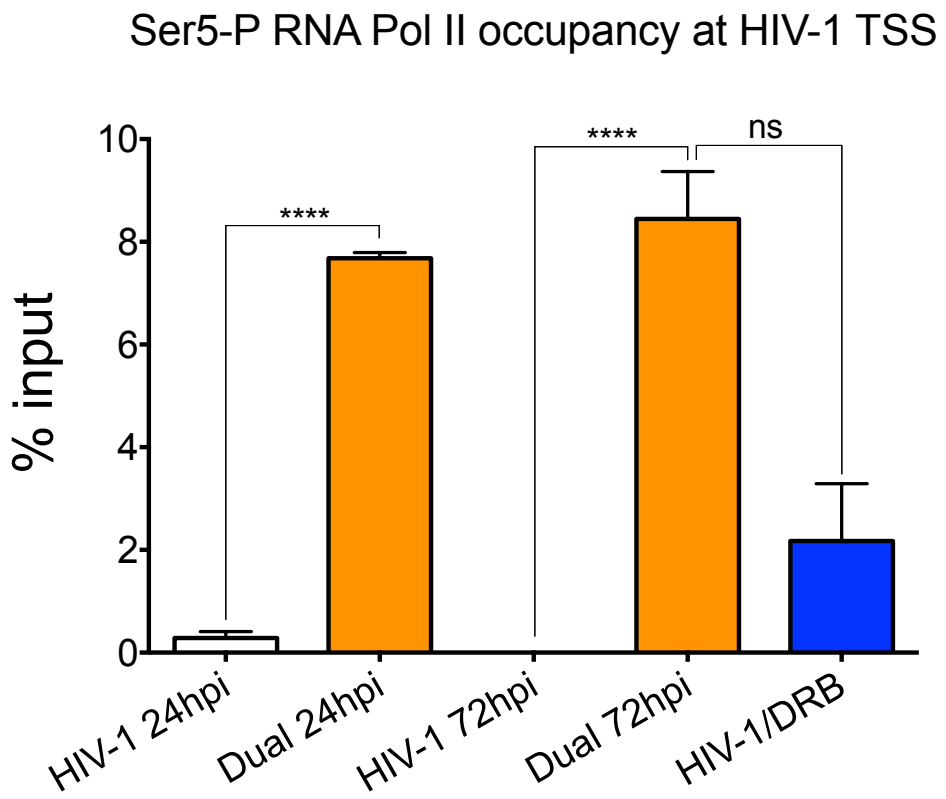
Ser5-P RNA Pol II occupancy at HIV-1 TSS
% input
10
8
6
4
2
0
****
****
ns
HIV-1 24hpi
Dual 24hpi
HIV-1 72hpi
Dual 72hpi
HIV-1/DRB

III. 3. Discussion

In this report, individual cells infected with both HIV-1 and HIV-2 were directly imaged, setting the stage to study the interactions between the two viruses under co-infection conditions. In all cases of HIV-2 protection against HIV-1 reported in the literature, HIV-2 infection preceded HIV-1 infection or was at least concurrent to it (*162-165*). There have been few reports of cases of HIV-2 superinfection in HIV-1-infected individuals conferring protection (*51*). That suggests that the order of infection might be important to the protective effects exerted by HIV-2. Our data support these prior observations (*51,162-165*), as HIV-2 potently suppressed HIV-1 infection when added prior to or simultaneously with HIV-1, but had far less impact once HIV-1 infection was established.

HIV-2 infection inhibited simultaneous HIV-1 infection through two main mechanisms that were not mutually exclusive: 1) induction of type I IFN responses, and 2) HIV-2 TAR-mediated inhibition of HIV-1 transcription. Both mechanisms have been reported previously (*98-99,127-132,153-160,166-172,189-192*), however, these studies did not clearly delineate their relative contributions in terms of timing of effect, targets of the inhibition, and specificity of the inhibition. Moreover, the previous reports did not map the direct inhibition mechanism to any specific sequences within the HIV-2 genome. Consistent with these reports (*98-99,153-160,189-192*), we showed that type I IFN responses were induced by HIV-2 around 48 hours post-infection. In our hands, these responses were not specific to the HIV-1 LTR and additionally downmodulated the expression of a reporter gene under control of an eIF1α promoter. Importantly, in the Vero cell line, which is deficient for type I IFN production, HIV-2 no longer inhibited expression

of eIF1α-dependent gene expression but still inhibited HIV-1 infection. These data clearly indicated that induction of type I IFN responses was responsible for the broad suppression of transcription, but a second more direct inhibition mechanism was able to inhibit transcription from the HIV-1 LTR promoter.

Other viral factors have been proposed to be involved in direct HIV-2 inhibition of HIV-1 infection (*166-172*). They are viral proteins (HIV-2 Rev and Vpx) that require overexpression in order to exert anti-HIV-1 effects (*166-167,171*). The report on HIV-2 Rev-mediated inhibition of HIV-1 infection claims that HIV-2 Rev protein acts as a dominant negative of HIV-1 Rev protein (*166*). Two other research groups reported independently that Vpx-mediated inhibition of HIV-1 occurs during reverse transcription (*167*) and nuclear entry of HIV-1 preintegration complexes (*171*). Neither HIV-2 Rev nor Vpx was reported to be involved in HIV-1 LTR activity downmodulation in the previous studies (*166-167,171*). Therefore, it was unlikely that the direct mechanism at hand could be due to any of these factors. The direct mechanism was discernable around 72 hours post-infection. And previous reports have shown that HIV-1 LTR can be targeted by HIV-2 TAR in transfection and infection settings, therefore, HIV-2 TAR might be the culprit (*168-170*). In such a scenario, the 72 hours delay to the inhibition could be the time needed for HIV-2 TAR to reach significant levels in HIV-2-infected TZM-bl cells. In contrast, transcription of the HIV-2 TAR RNA from a U6 promoter drove high expression of HIV-2 TAR RNA at early time points and was associated with rapid inhibition of HIV-1 transcription.

Moreover, some reports have claimed that HIV-2 provirus is unable to express its viral proteins at high levels comparable to HIV-1 (*41,145-150*). That inability is due to a

strong post-transcriptional control of HIV-2 gene expression exerted by its highly structured 5' untranslated region (UTR) present in all its viral transcripts (*145-146*). Unlike HIV-1 5'UTR, HIV-2 5'UTR is unable to recruit cellular factors required for the translation initiation complexes to read through its structure RNAs during translation of viral proteins (*41,145-150*). Therefore, it is unlikely that Vpx and Rev could be highly expressed in vivo to exert the reported effects. Accordingly, they should not have prominence for they would not be overexpressed from the integrated HIV-2 provirus. Additionally, data from the mutational analysis of HIV-2 that removed almost all its genome to the exception of the first 321 nucleotides provides further evidence that HIV-2 accessory genes would rather play a minor role in HIV-1 inhibition (*169*).

Here, we showed that HIV-2 TAR directly inhibited HIV-1 LTR activity by limiting its ability to promote full-length transcript synthesis. Transcription was initiated but RNA polymerase II was mainly restricted to short transcripts production. This agrees with three other reports (*166-167,171*). Indeed, anti-HIV-1 gene therapy attempts showed that HIV-1 and HIV-2 TAR elements can be used as decoy against HIV-1 Tat protein to block HIV-1 infection at the transcriptional level (*168,171*). Of all the HIV-1 Tat protein decoys tested, full-length TAR-2 is the most potent (*168*). We also showed that the direct inhibition mechanism reported here appeared to be HIV-1 specific and did not affect other retroviruses such as MLV and RSV. Hence, it appears that HIV-2 seems able to specifically target HIV-1 LTR-driven transcription.

In their report, Browning et al. showed that direct inhibition required a 160 nucleotides long RNA oligo (*169*). The construct they referred to as full-length TAR-2 includes the polyadenylation signal at the 5'LTR of HIV-2 (*169*). We showed that the

presence of that sequence was dispensable to HIV-1 inhibition as the full-length TAR-2 deleted of the polyadenylation signal was as inhibitory as the full-length construct. We also demonstrated that, although the most potent inhibition requires three predicted stem loops, direct inhibition could be observed with a combination of TAR-2 stem loop 2 in combination with stem loop 1 or stem loop 2. A shorter oligo would facilitate further investigations of the interface between HIV-2 TAR and HIV-1 Tat.

With regard to the second stem loop, Fenrick et al. have reported it to be an independent TAR element in the context of HIV-2 LTR transactivation (*193*). Of note, their overall predicted structure of TAR-2 was similar to ours to the exception of the missing poly A sequence in theirs. They showed that stem loop 2 alone could mediate HIV-2 LTR transactivation through its interaction with HIV-1 or HIV-2 Tat protein when stem loop 1 was deleted. But it had a lesser transactivation potential (four to eight-fold weaker) than the first stem loop. Moreover, they demonstrated that the reduced activity of stem loop 2 was primarily a function of its distance from the 5' cap, rather than an inability to bind Tat (*193*). Our data on the effects of HIV-2 TAR element on HIV-1 LTR activity suggest that no single HIV-2 TAR stem loop provided in trans was able to sequester HIV-1 Tat and consequently they had no inhibitory effects on HIV-1 LTR. We found that at least two TAR-2 stem loops were required to inhibit HIV-1 LTR activity, and all three were required for the maximum inhibition. This finding is contrary to the prior observation that deleting a single stem loop can be tolerated with little loss of transcriptional activity (*193*). As proximity to the 5' cap is strongly associated with improved transcriptional activation, our uncapped TAR-2 RNAs may require a more complete structure, and a high level of over expression, to effectively compete with the HIV-1 TAR sequence.

CHAPTER IV: COMPARATIVE STUDY OF THE KINETICS OF INFECTION OF HIV-1 AND HIV-2

IV. 1. Introduction

Efforts have been made over the years to decipher the mechanisms that underlie HIV-2 lower pathogenicity in the hope of learning cues from the retroviral biology that might help in addressing the challenges in HIV-1 cure, in HIV vaccine strategies, and in the design of safe and effective lentiviral delivery vectors for gene therapy. It has been reported that HIV-2 low pathogenicity could be related to lower transcription rates in vivo (*37*) which in turn could explain the lower plasma viral load measured in HIV-2-infected individuals (*195-196*). Transcriptional interferences have been described to be often associated with HIV-2 infection in vivo due to its propensity to integrate in the opposite direction of the host cell gene (*37*). Moreover HIV-2 unlike HIV-1 was subject to a stronger immunological control with potent type I interferon responses, HIV-2 specific antibody responses, and HIV-2 specific CD8+ T cell responses (*191*). Determinants of these observations were proposed to be related to events during the initial HIV-2 infection. Unlike HIV-1, early events in HIV-2 infection are not well understood.

Previous studies of the kinetics of HIV-1 and HIV-2 infection have shown differences in human monocytes-derived macrophages (MDM) and dendritic cells which HIV-1 was unable to efficiently infected. The restriction of infection in those cells was attributed to SAMHD1, a restriction factor that is counteracted by the viral factor Vpx only present in HIV-2 particles (*197-198*). Successful HIV-2 infection of macrophages led to

type I interferon responses which in turn primed HIV-2 specific adaptive immunity (*98*). In CD4+ T lymphocytes in which infection kinetics seemed similar, differences in replication rates, and in integration sites selection clearly point to deeper trafficking differences. Attempts at understanding those trafficking differences have proposed that HIV-1 recruits CPSF6 and CypA as key factors for trafficking upon cell entry (*99*). Unlike HIV-1, HIV-2 was unable to recruit CypA due to differences in its capsid protein.

We hypothesized that besides SAMDH1 and Vpx, they are likely other differences in the kinetics of the HIV-1 and HIV-2 that could explain the various outcomes to their respective infection. To test that hypothesis, we followed the kinetics of HIV-1 and HIV-2 infection with *fluorescent in situ hybridization* (*FISH*), and qPCR over the first 24 hours of infection in TZM-bl cells. We showed that HIV-1 infection in TZM-bl cells proceeded quickly upon viral entry. Relative to HIV-2, HIV-1exhibited faster integration into the host cell genome, and higher rates of transcription with transcriptional bursts. On the other hand, HIV-2 was slower with a roughly two hours delay (relative to HIV-1) in reverse transcription completion and integration. Analysis the state of the chromatin around HIV-1 and HIV-2 LTR promoters at 24 hpi showed that both LTRs had similar active chromatin marker H3K9me2 levels, and should be equally accessible to transcription factors. Host RNA polymerase II occupancy analysis at each LTR promoter start sites showed less occupancy in the case of HIV-2 LTR.

IV. 2. Results

To identify differences in the kinetics of vRNA and vDNA during the early stages of HIV-1 and HIV-2 life cycle, *FISH* probes specific for each virus (table IV-1) were used

to follow them from 4 hpi up to 12 hpi during infection in TZM-bl cells. These probes were tested for cross-reactivity against the non-autologous HIV and did not show non-specific binding (*141*). The vRNA and vDNA probes were previously described (*141*) and are summarized in table IV-1.

Table IV-1: List of the FISH probes made by ACDBio used in this study

Several regions of HIV-1 and HIV-2 genome were selected for the design of the FISH ZZ probes. Z-shaped are small oligonucleotides of 20-40 nucleotides that bind side by side over the length of a specific targeted sequence in the viral genome. Their Z shape allows the bind of their base to the target complementary sequence, and the binding of their top part to an amplifier of fluorescent signal. For HIV-$1_{NL4.3}$, two regions were selected for the design of specific vRNA and vDNA probes. For HIV-2_{ST}, only one region was selected for the design of the vRNA and vDNA probes. The viral RNA probes target the genomic RNA from the incoming virus and the one transcribed from the proviral DNA. The viral DNA probes detect the complementary strand of the + sense viral DNA.

ID	Name	Catalog #	ZZ	Description
PS-1	Hs-HIV-1	311921-C1	10	Anti-sense vRNA probe targeting within 801-1393bp of HIV-1 genome (*Gag-Pol*) Accession # NC_001802.1
PS-2	HIV-1-gag-pol-C3	317691-C3	60	Sense vDNA probe targeting within 507-4601bp of HIV-1 genome (Gag-Pol) Accession # NC_001802.1
PS-3	V-HIV-2-gag-C3	446221-C3	20	Anti-sense probe targeting within 1379-2447bp of HIV-2 genome (Gag) Accession # L07625.1
PS-4	V-HIV-2-gag-C1	499981-C1	20	Sense probe targeting within 1379-2447bp of HIV-2 genome 9Gag) Accession # L07625.1

Reverse transcription completion appeared to be delayed in HIV-2-infected TZM-bl cells.

The number of vRNA foci decreased over time from 4 hpi to 10 hpi in HIV-1-infected TZM-bl cells and from 4 hpi to 12 hpi in HIV-2-infected TZM-bl cells (fig. IV-1, IV-2, IV-3). HIV-1 vRNA rapidly decreased between 4 hpi and 6 hpi, time point at which more than 90% of vRNA spots had disappeared ($p < 0.001$, fig. IV-1, IV-2). By 10 hpi, rare vRNA spots were still present as shown in fig. IV-1 (bottom panel). HIV-2 vRNA slowly decreased during two phases (fig. IV-1, IV-3). The number of spots of vRNA did not significantly drop between 4 hpi and 6 hpi, but quickly went down between 6 and 12 hpi. By that time point, HIV-2 reverse transcription was nearly completed with very few vRNA spots that were still accounted for in fig. IV-1 (top panel).

HIV-1 vDNA reached a peak at 4 hpi (fig. IV-4, IV-5, IV-6). Although it still increased until 8hpi, the differences were not significant with FISH. This suggests that most of HIV-1 reverse transcription in TZM-bl cells was completed by 6 hpi. Similar to HIV-1 infection, HIV-2 vDNA reached its peak at 4 hpi (fig. IV-4, IV-5, IV-7). This suggested that the bulk of reverse transcription in HIV-2 could occur within the same time frame as HIV-1. However, the delay in completion with HIV-2 was in contrast with that of HIV-1 (fig. IV-2, IV-3). Of note, vDNA seemed to drop for both viruses at 14 hpi concurrently with nuclear translocation and integration of proviruses into the host genome (fig. IV-5, IV-6, IV-7). And HIV-2 vDNA markedly increased between 20 hpi and 22 hpi (fig. IV-5, IV-7) before getting back to its previous level. To confirm the apparent two-hour delay in reverse transcription completion between HIV-1 and HIV-2 in TZM-bl cells, we performed a TOA assay with TDF at 2 μM (fig. IV-8). TDF-induced inhibition of HIV-1 replication in TZM-GFP cells at 72 hpi dropped to 50% between 8 hpi and 10 hpi. That

suggests that the majority of reverse transcription products during HIV-1 infection were completed approximately by 10 hpi, at which time point the drug lost about 50% of its efficacy in the TZM-bl cells. HIV-2 inhibition by TDF reached 50% between 10 and 12 hpi. TDF potency was essentially lost (inhibition ≤ 10%) by 12-14 and 14-16 post infection by HIV-1 and HIV-2, respectively.

Figure IV-1: Staining of HIV-1 and HIV-2 viral RNAs with the FISH probes

FISH stained samples were imaged at 63X with a confocal microscope Leica SP8 diode. 20 to 30 frames were randomly picked for each time point. Sample images (various zoom focus) from the first stages of the viral life cycle are shown (scale bar 10 μm).

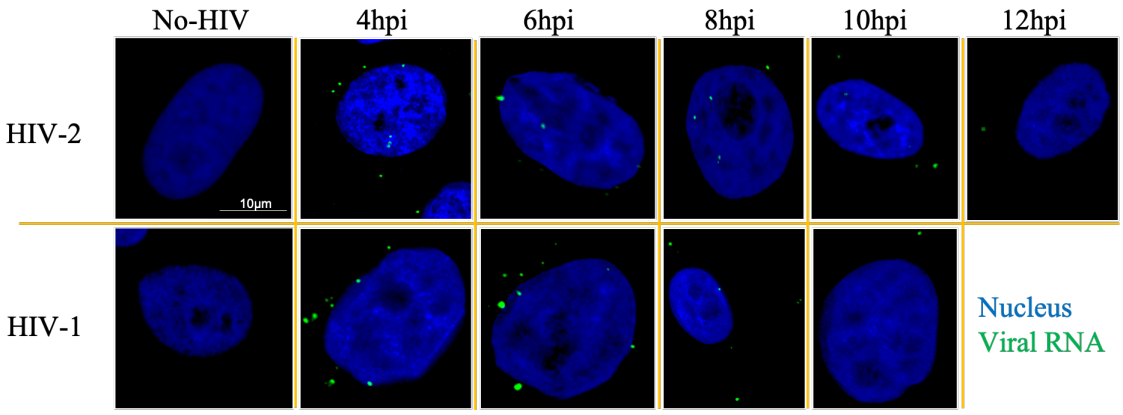
No-HIV
4hpi
6hpi
8hpi
10hpi
12hpi
HIV-2
HIV-1
10μm
Nucleus
Viral RNA

Figure IV-2: Quantification of HIV-1 RNAs spots.

Samples were processed as described in fig. IV-1. The number of HIV-1 RNA spots (green spots) and of nuclei (blue objects) were counted for each frame within each time point using the Cell Profiler software. Each nucleus accounted for a single cell. For each frame, the number of green spots was divided by the number of cells. The ratio of vRNA spots/cell per frame was averaged for the 20 to 30 frames taken in each time point for each independent experiment. The experiments were repeated at least twice. The averaged ratio of HIV-1 RNA spots/cell for each independent experiment were plotted. Data from at least two independent experiments were average in the graph. Tukey's multiple comparison test (one-way ANOVA test) was used to assess statistical differences.

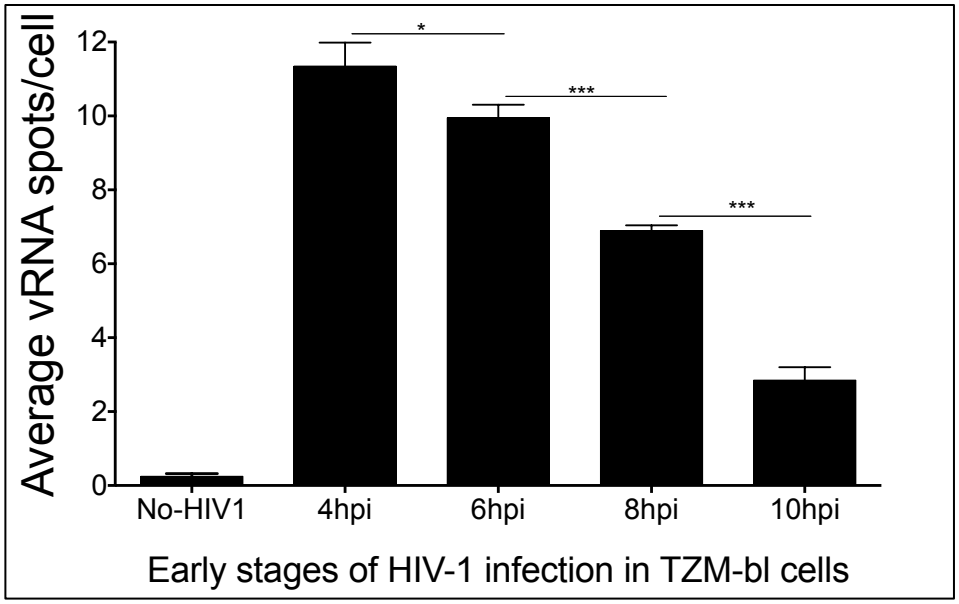
Average vRNA spots/cell
12
10
8
6
4
2
0
*
***
***
No-HIV1
4hpi
6hpi
8hpi
10hpi
Early stages of HIV-1 infection in TZM-bl cells

Figure IV-3: Quantification of HIV-2 RNAs spots

Samples were processed as described in fig. IV-1. The number of HIV-2 RNA spots (green spots) and of nuclei (blue objects) were counted for each frame within each time point using the Cell Profiler software. Each nucleus accounted for a single cell. For each frame, the number of green spots was divided by the number of cells. The ratio of vRNA spots/cell per frame was averaged for the 20 to 30 frames taken in each time point for each independent experiment. The experiments were repeated at least twice. The averaged ratio of HIV-2 RNA spots/cell for each independent experiment were plotted. Data from at least two independent experiments were average in the graph. Tukey's multiple comparison test (one-way ANOVA test) was used to assess statistical differences.

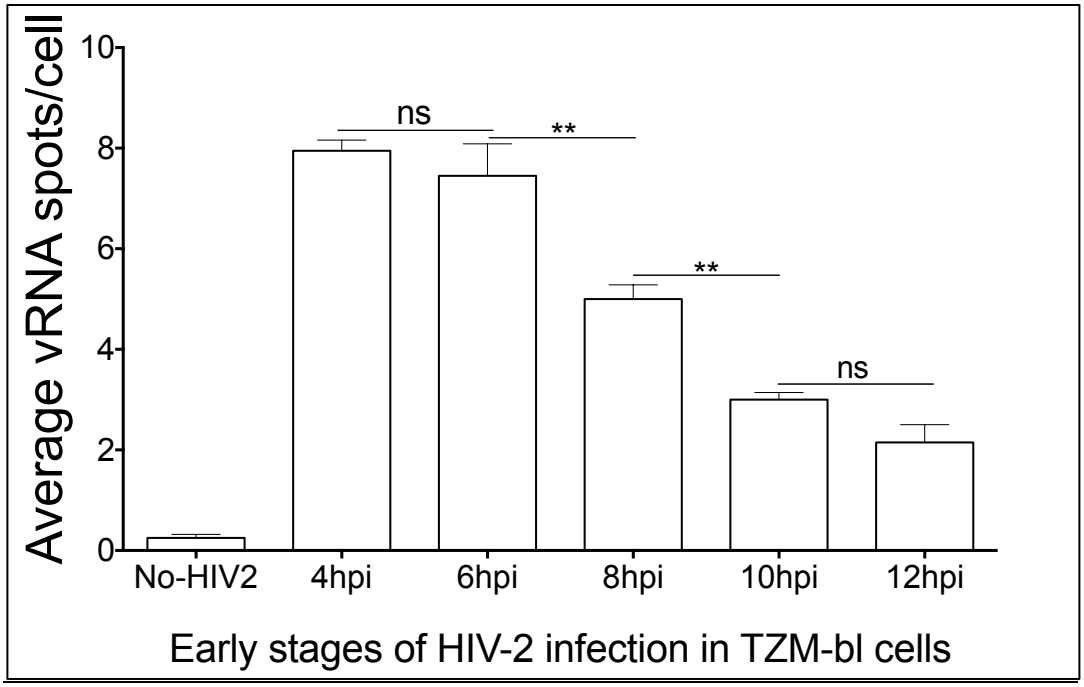
Average vRNA spots/cell
10
8
6
4
2
0
ns
**
**
ns
No-HIV2
4hpi
6hpi
8hpi
10hpi
12hpi
Early stages of HIV-2 infection in TZM-bl cells

Figure IV-4: Staining of HIV-1 and HIV-2 viral DNAs during early phases

TZM-bl cells were infected, incubated between 4 hrs. and 10 hrs for HIV-1 and between 4 hrs and 12 hrs. for HIV-2. Infected samples were fixed, and processed for *FISH* with the corresponding DNA probes as described in the method section. FISH stained samples were imaged at 63X with a confocal microscope Leica SP8. 20 to 30 frames were randomly collected and processed for each time point. Sample images (various zoom focus) from the first stages of the viral life cycle are shown (scale bar 10 μm).

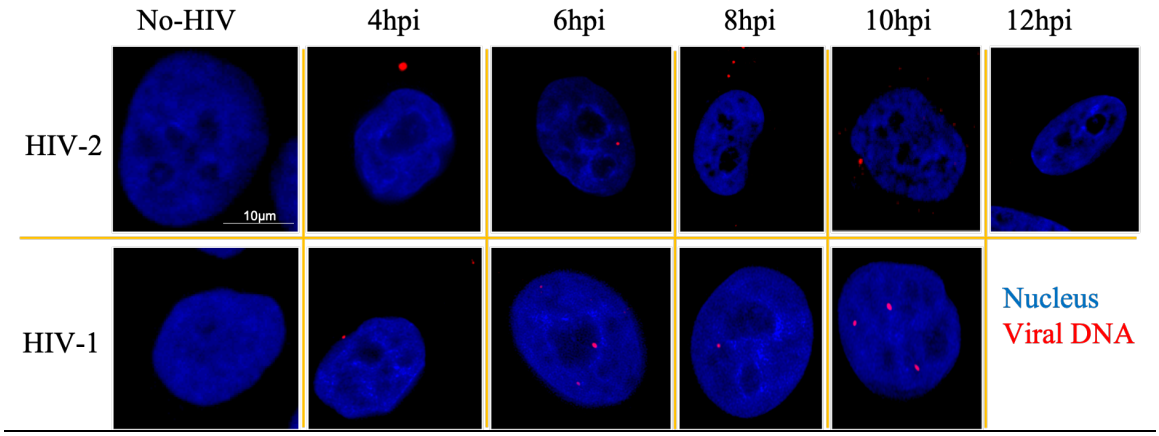
No-HIV
4hpi
6hpi
8hpi
10hpi
12hpi
HIV-2
HIV-1
10μm
Nucleus
Viral DNA

Figure IV-5: Staining of HIV-1 and HIV-2 viral DNAs during late phases.

TZM-bl cells were infected, incubated between 12 hrs. and 24 hrs for HIV-1 and between 12 hrs and 24 hrs. for HIV-2. Infected samples were fixed, and processed for *FISH* with the corresponding DNA probes as described in the method section. FISH stained samples were imaged at 63X with a confocal microscope Leica SP8. 20 to 30 frames were randomly collected and processed for each time point. Sample images (various zoom focus) from the second stages of the viral life cycle are shown (scale bar 10 μm).

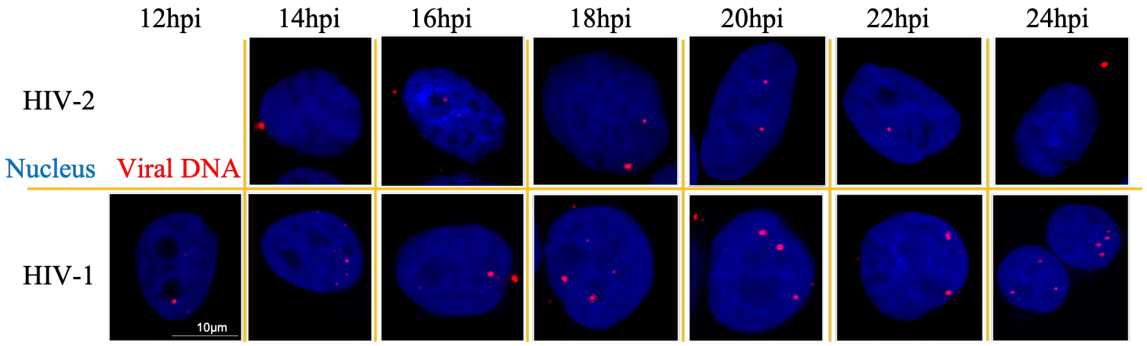
12hpi
14hpi
16hpi
18hpi
20hpi
22hpi
24hpi
HIV-2
Nucleus
Viral DNA
HIV-1
10μm

Figure IV-6: Quantification of HIV-1 DNAs spots at all time points

The number of HIV-1 DNA spots (red spots) and of nuclei (blue objects – equated to cell number) were counted for each frame within each time point using the Cell Profiler software. For each frame, the total number of red spots was divided by the number of cells. The ratio of vDNA spots/cell per frame was averaged for the 20 to 30 frames taken at individual time points for each independent experiment. The averaged ratio of HIV-1 DNA spots/cell for each independent experiment were plotted as shown. Data from at least two independent experiments were averaged in the graph. Tukey's multiple comparison test (one-way ANOVA test) was used to assess statistical differences.

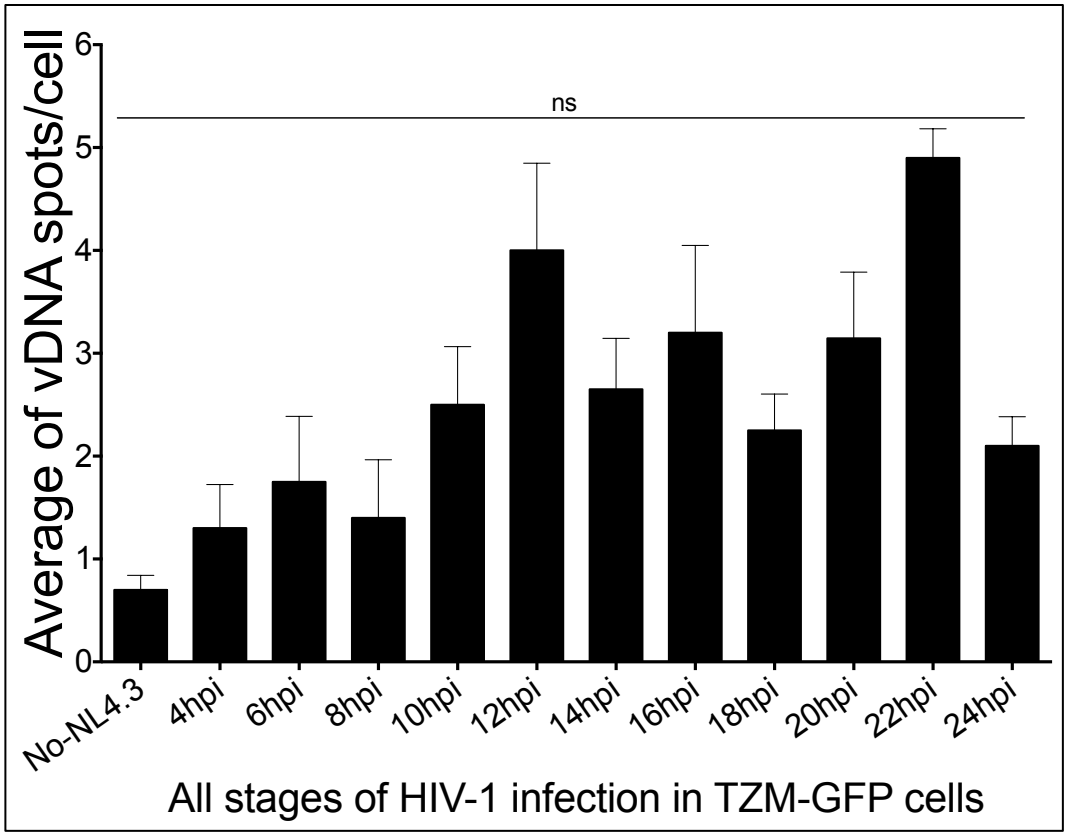
Average of vDNA spots/cell
0
1
2
3
4
5
6
ns
No-NL4.3
4hpi
6hpi
8hpi
10hpi
12hpi
14hpi
16hpi
18hpi
20hpi
22hpi
24hpi
All stages of HIV-1 infection in TZM-GFP cells

Figure IV-7: Quantification of HIV-2 DNAs spots at all time points

The number of HIV-2 DNA spots (red spots) and of nuclei (blue objects – equated to cell number) were counted for each frame within each time point using the Cell Profiler software. For each frame, the total number of red spots was divided by the number of cells. The ratio of vDNA spots/cell per frame was averaged for the 20 to 30 frames taken at individual time points for each independent experiment. The averaged ratio of HIV-2 DNA spots/cell for each independent experiment were plotted as shown. Data from at least two independent experiments were averaged in the graph. Tukey's multiple comparison test (one-way ANOVA test) was used to assess statistical differences.

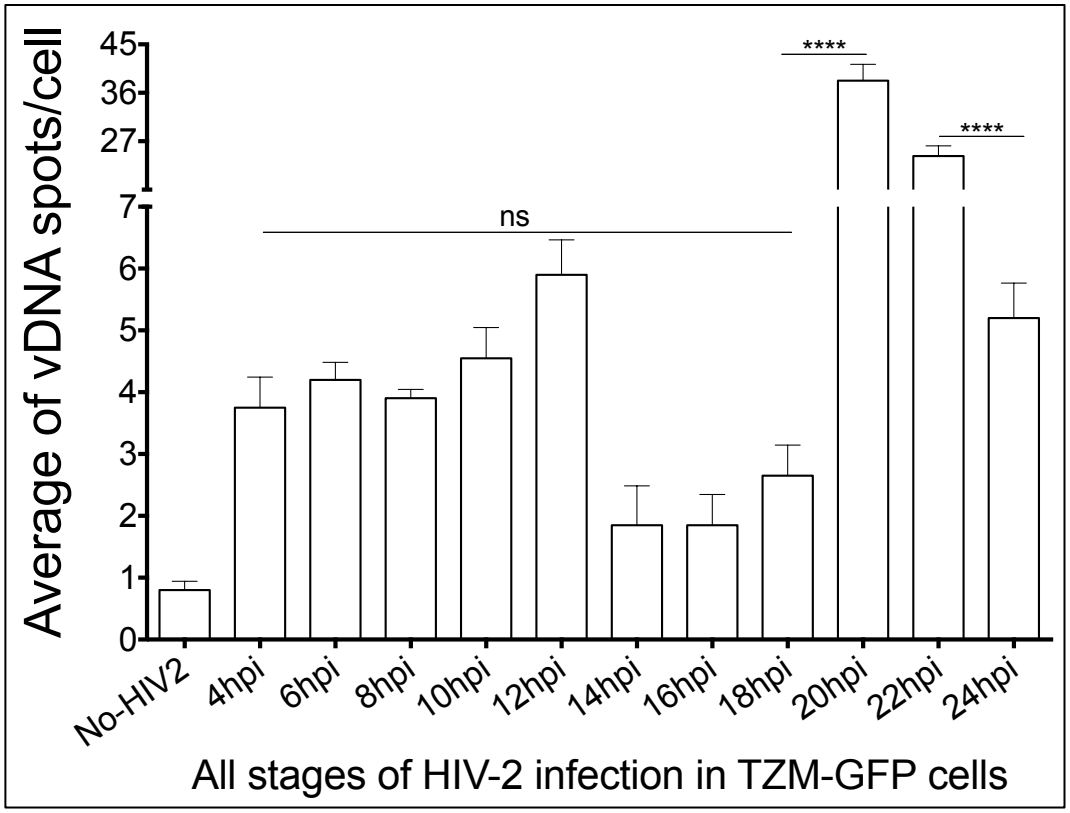
Average of vDNA spots/cell
45
36
27
7
6
5
4
3
2
1
0
ns
****
****
No-HIV2
4hpi
6hpi
8hpi
10hpi
12hpi
14hpi
16hpi
18hpi
20hpi
22hpi
24hpi
All stages of HIV-2 infection in TZM-GFP cells

Figure IV-8: Tenofovir time-of-addition (TOA) assay.

HIV-1 and HIV-2 infections were separately performed at 0.3 MOI for 72 hrs of incubation after addition of the virus (72 hpi). Tenofovir was added to the HIV-infected TZM-GFP cells at different time points post infection (0 hrs, 4 hrs, 8 hrs, 10 hrs, 12 hrs, 16 hrs, 20 hrs, 22 hrs, and 24 hrs). At 72 hpi, the cells were fixed with 4% paraformaldehyde (PFA), and counterstained with DAPI. Several frames were randomly imaged in order to analyze approximately a total of $1x10^5$ cells. The total number of cells as well as the number of HIV-infected cells GFP positive cells) were automatically determined with the automated epifluorescence microscope Cytation 5 as described in the methods section. The number of HIV-infected TZM-GFP cells was divided by the total number of cells to calculate a ratio of infected cells for each time-point of addition. The DMSO control-treated cells for each experiment was set to 100%, and the per cent inhibition was determined relative to them. The data set was fit with the GraphPad software. Three independent experiments were performed, and the average per cent inhibition of each experiment for the specific time of addition point was plotted. EC_{50} was determined by the intersection of the 50% efficiency line (dotted line) and the TOA curve.

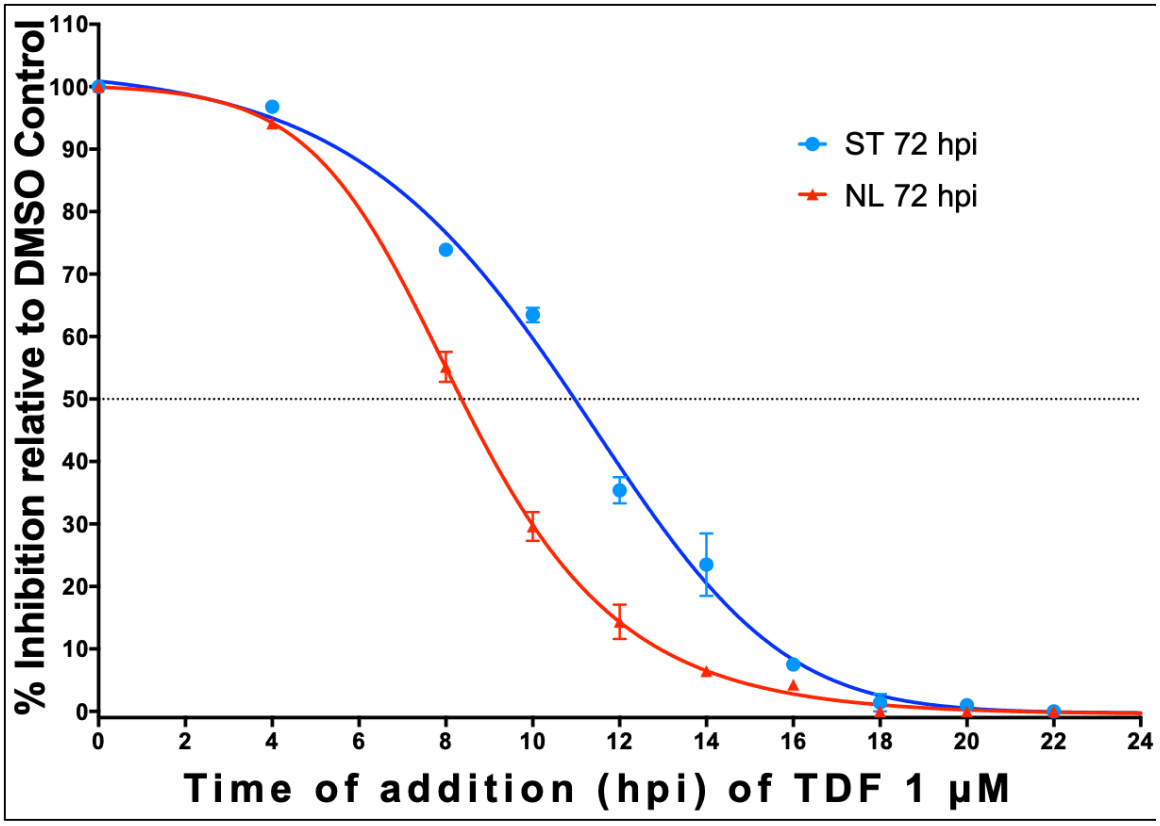
% Inhibition relative to DMSO Control
110
100
90
80
70
60
50
40
30
20
10
0
0
2
4
6
8
10
12
14
16
18
20
22
24
Time of addition (hpi) of TDF 1 µM
ST 72 hpi
NL 72 hpi

HIV-2 vDNAs nuclear translocation appeared to be slower in TZM-bl cells.

It appears that the nuclear translocation of HIV-2 pre-integration complexes (PICs) and their integration into host cell genome would also be delayed compared to HIV-1. The average ratio of nuclear HIV-1 vDNA spots to total cellular spots for each frame showed that nuclear translocation occurred alongside reverse transcription (fig. IV-9). It started as early as 6 hpi, and was nearly completed between 10 hpi and 12 hpi when roughly 80% of HIV-1 vDNA spots colocalized with the nuclei. At 16 hpi, the nuclear vDNA spots represented at least 90% of the total cellular vDNA. In contrast, HIV-2 vDNA spots seemed mainly cytoplasmic until 18 hpi, suggesting a possible delay in the nuclear translocation (fig. IV-10). The average ratio of nuclear to total vDNA spots showed that to the exception of 6 hpi, more than half of the spots were cytoplasmic until 16 hpi. At 18 hpi, nuclear localization of HIV-2 vDNA spots reached its peak at 70%. Then it slowly dropped to 35% at 24 hpi (fig. IV-10). This observation could indicate differences in nuclear translocation of HIV-1 and HIV-2 PICs and/or integration. To confirm the delay in HIV-2 nuclear translocation and/or integration into host cell genome of the TZM-bl cells, we performed a TOA assay with RAL at 1 μM (fig. IV-11). RAL-induced inhibition of HIV-1 replication in TZM-GFP cells at 72 hpi dropped to 50% between 10 hpi and 12 hpi, and HIV-2 inhibition by RAL reached 50% between 12 hpi and 14 hpi. RAL potency against HIV-1 and HIV-2 replication was completely lost (inhibition ≤ 10%) respectively between 16 and 18 hpi, *versus* 18 and 20 hpi.

Figure IV-9: HIV-1 DNA spots localization

Experiments were done as described in figures IV-4 and IV-5. Each dot on the plot corresponds to the nuclear HIV-1 DNA spots divided by total HIV-1 DNA spots in each frame. Nuclear translocation was defined as the association of HIV-1 DNA spots with the DAPI mask defined in the Cell Profiler pipeline created to analyze the images. The ratio nuclear HIV-1 DNA to total HIV-1 DNA was compared to 0.5 corresponding to a 50% nuclear localization cut off for the viral DNA (dotted line). Each individual ratio was determined for the 20 to 30 frames taken per time point in each independent experiment. Time points were repeated at least twice for HIV-1. The individual ratios for each experiment were matched to ratios from repeated experiments, and plotted. Ratios for frames that had no vDNA spots were set to zero.

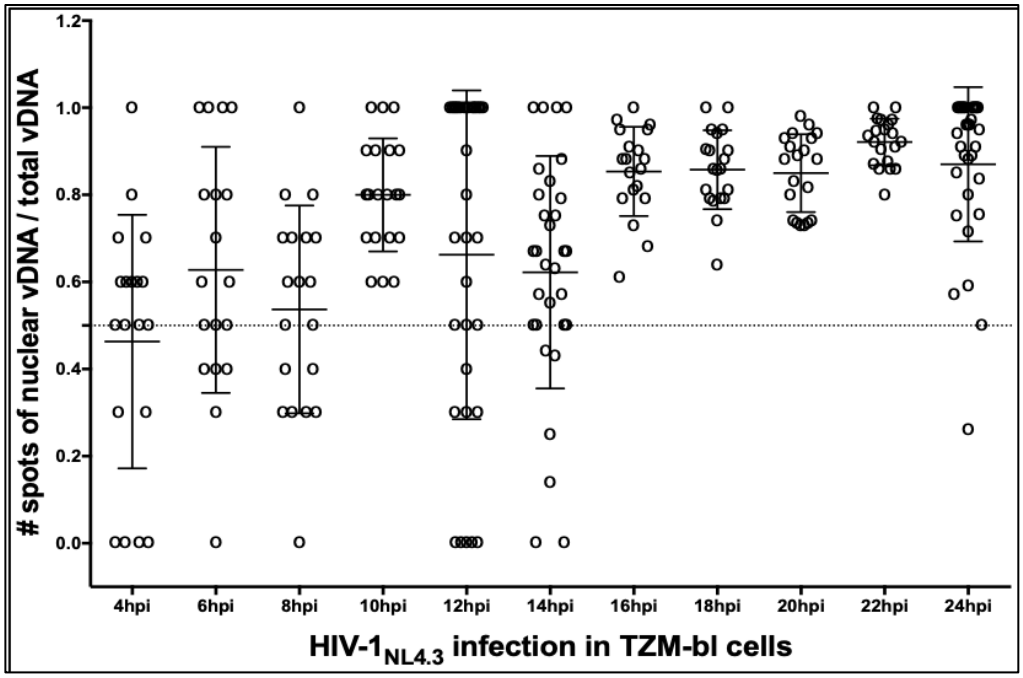
spots of nuclear vDNA / total vDNA
1.2
1.0
0.8
0.6
0.4
0.2
0.0
4hpi
6hpi
8hpi
10hpi
12hpi
14hpi
16hpi
18hpi
20hpi
22hpi
24hpi
HIV-1NL4.3 infection in TZM-bl cells

Fig. IV-10: HIV-2 DNA localization

Experiments were done as described in figures IV-4 and IV-5. Each dot on the plot corresponds to the nuclear HIV-2 DNA spots divided by total HIV-2 DNA spots in each frame. Nuclear translocation was defined as the association of HIV-2 DNA spots with the DAPI mask defined in the Cell Profiler pipeline created to analyze the images. The ratio nuclear HIV-2 DNA to total HIV-2 DNA was compared to 0.5 corresponding to a 50% nuclear localization cut off for the viral DNA (dotted line). Each individual ratio was determined for the 20 to 30 frames taken per time point in each independent experiment. Time points were repeated at least twice for HIV-2. The individual ratios for each experiment were matched to ratios from repeated experiments, and plotted. Ratios for frames that had no vDNA spots were set to zero.

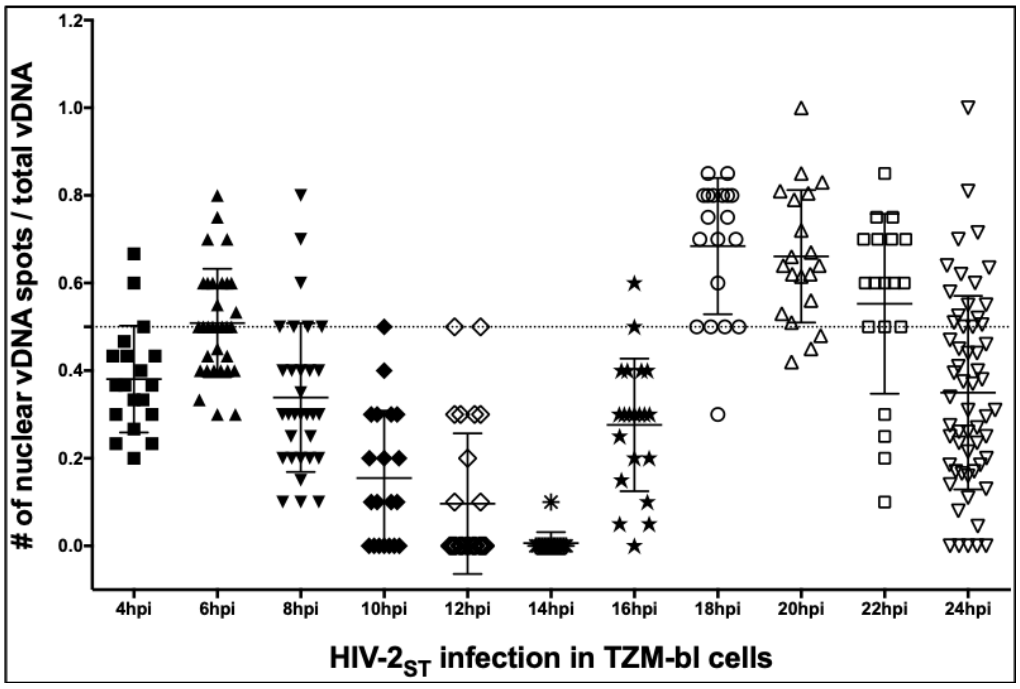
# of nuclear vDNA spots / total vDNA
1.2
1.0
0.8
0.6
0.4
0.2
0.0
4hpi
6hpi
8hpi
10hpi
12hpi
14hpi
16hpi
18hpi
20hpi
22hpi
24hpi
HIV-2ST infection in TZM-bl cells

Figure IV-11: Raltegravir TOA assay

HIV-1 and HIV-2 infections were separately performed at 0.3 MOI for 72 hrs. raltegravir (RAL) was added to TZM-GFP cells at the time points as indicated in the TDF TOA experiments. The cells were processed as described in fig. IV-8. Percent inhibition and EC_{50} were determined relative to DMSO control-treated cells, and plotted for 3 independent experiments.

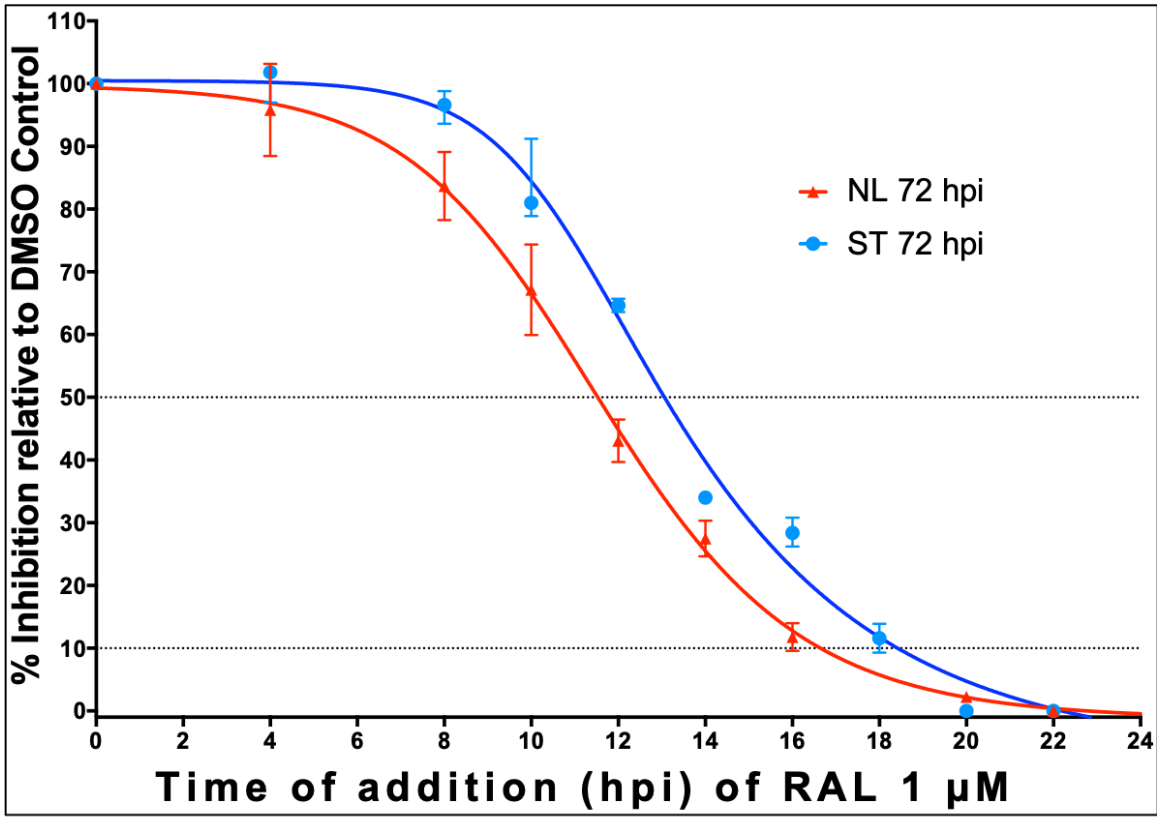
% Inhibition relative to DMSO Control
110
100
90
80
70
60
50
40
30
20
10
0
0
2
4
6
8
10
12
14
16
18
20
22
24
Time of addition (hpi) of RAL 1 µM
NL 72 hpi
ST 72 hpi

HIV-2 appeared to produce negative sense vRNA transcripts during infection in TZM-bl cells.

Another intriguing observation with the HIV-2 infection in the HeLa-based TZM-bl cells was the significantly higher vDNA levels between 20 hpi and 22 hpi compared to those measured between 4 hpi and 12 hpi during the early stages (fig. IV-5, IV-7). Such peculiar finding could suggest that the anti-sense vDNA probe used in this study was detecting another species of nucleic acid different from the intended HIV-2 vDNA. A possible explanation could be that the HIV-2 vDNA probe was binding to an anti-sense vRNA species produced by HIV-2 under the infection conditions used here. That transcript artificially increased the vDNA spots counted between 20 hpi and 22 hpi. And when favorable conditions for viral replication were met, the promoter for that transcription was turned off to allow the regular HIV-2 5'LTR promoter-driven transcription. The significant decrease of vDNA spots between 22 hpi and 24 hpi seems compatible with such explanation. That increase led us to hypothesize that HIV-2 might be producing negative sense RNA transcripts during that time frame. To test that hypothesis, HIV-2-infected samples were treated with Rnase A prior to the FISH procedure to remove all RNA species. and stained samples were compared to matched samples from the same experiments without Rnase A treatment (fig. IV-12).

Figure IV-12: Quantification of Rnase treatment on HIV-2 DNA spots

HIV-2-infected TZM-bl cells were incubated for 20 hpi and 22 hpi. Corresponding samples were divided in two batches. The first batch of 20 hpi and 22 hpi samples were not treated with Rnase before the FISH procedure. The second batch was treated with Rnase A as described in the method section. Both batches were imaged using the Leica sp8 confocal microscope as described before. Samples images are shown. The total number of HIV-2 DNA spots were divided by the number of cells in each frame for each time point (20 hpi and 22 hpi), and for each Rnase treatment conditions (treated or non-treated). The ratios of all frames for the same experiment were averaged. Averaged ratios for the same time point and the same Rnase treatment conditions (treated or non-treated) were plotted.

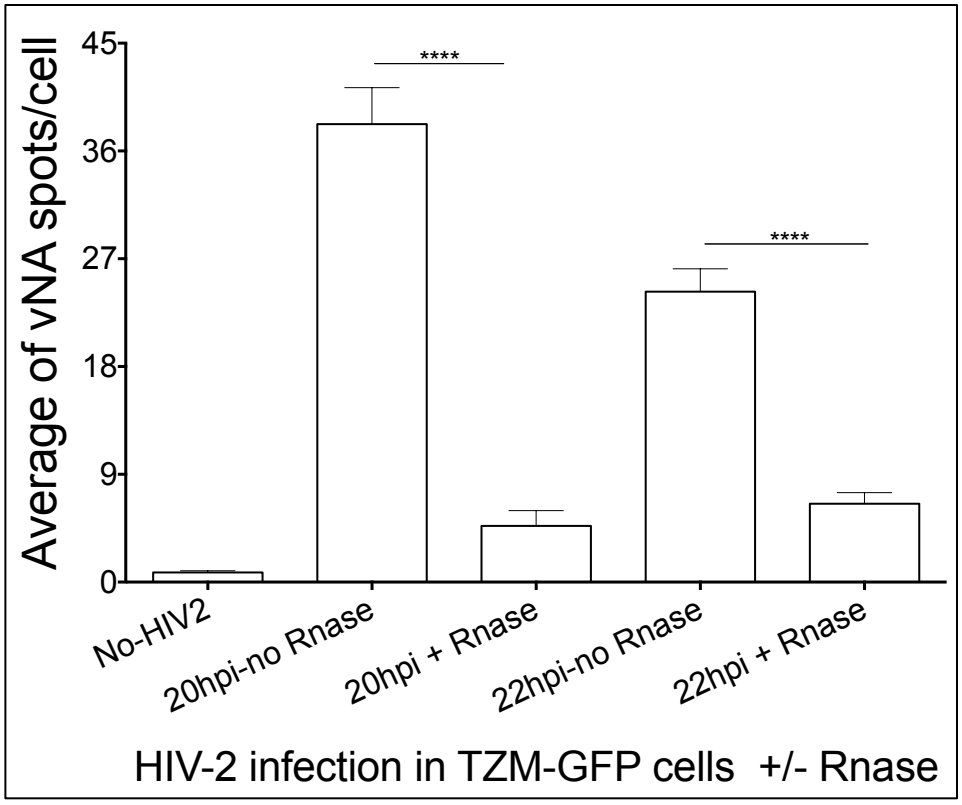
Average of vNA spots/cell
45
36
27
18
9
0
****
****
No-HIV2
20hpi-no Rnase
20hpi + Rnase
22hpi-no Rnase
22hpi + Rnase
HIV-2 infection in TZM-GFP cells +/- Rnase

With similar H3K4me2 level, HIV-1 LTR had more RNA Polymerase II occupancy than HIV-2 LTR.

During the late stages of infection in TZM-bl cells, it appeared on the imaging data that HIV-1 transcribed more vRNA than HIV-2 (fig. IV-13). To assess the difference in transcription between HIV-1 and HIV-2, accessibility of the LTR promoter region to transcription factors was analyzed using an antibody against the active chromatin marker H3K4me2 in a chromatin immunoprecipitation (ChIP) assay (fig. IV-14). Both HIV-1 and HIV-2 yield similar levels of viral DNA in the input sample, which represented 10% of the harvested cells (no IP) as shown in table IV-2. An independent marker, the human glyceraldehyde 3-phosphate dehydrogenase (GAPDH) gene promoter, a highly expressed gene that has the active chromatin marker H3K4me2 was used to control for the efficiency of the antibody used in the immunoprecipitation step. The results showed that there was more GAPDH promoter pulled down from samples infected by HIV-2 than by HIV-1 (table IV-1). That result could be due to slight differences in the number of TZM-bl cells actually processed during the ChIP assay. To account for these differences, HIV LTR data obtained with H3K4me2 antibody were normalized to data from the GAPDH promoter. Their LTR promoter regions had high level of H3K4me2 representing 80% of the Input (fig. IV-14). And there was no significant difference between the two HIVs. This suggested that both HIV-1 and HIV-2 promoter region were equally accessible to RNAP II and other transcription factors required for transcription.

Next, the occupancy of RNAP II was assessed at the HIV LTRs. The expectation was that with similar accessibility, differences in LTR-driven transcription could originate from differences in RNAP II presence at these LTR promoters. To test this hypothesis, an

antibody against the processive serine 2-phosphorylated form of RNA polymerase II was used to access occupancy at the transcription start site. As with the antibody against H3K4me2, qPCR with primers targeting GAPDH promoter start site were used to control for the efficiency of the pull-down. The HIV-1 and HIV-2 LTRs data were normalized to the GAPDH promoter data. RNAP II occupied less the HIV-2 LTR promoter start site (fig. IV-15).

Figure IV-13: Transcription of nascent vRNA

FISH stained samples were imaged at 63X with a confocal microscope Leica SP8. 20 to 30 frames were randomly picked for each time point. Sample images (various zoom focus) from the second stages of the viral life cycle are shown (scale bar 10 μm).

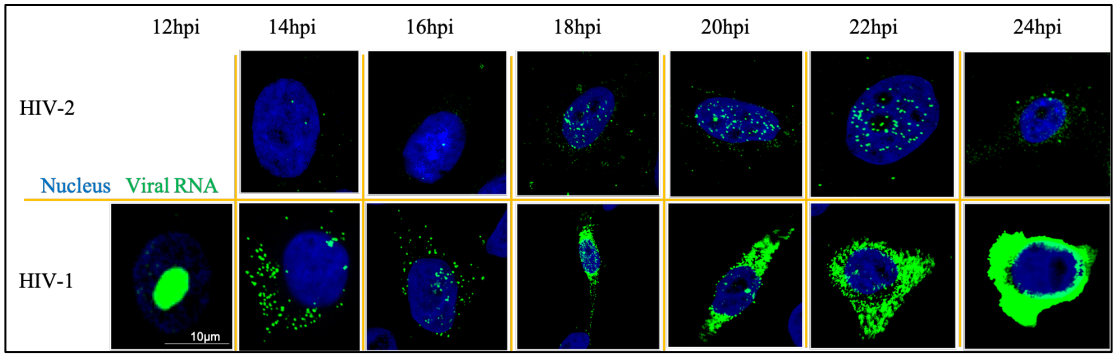
12hpi
14hpi
16hpi
18hpi
20hpi
22hpi
24hpi
HIV-2
Nucleus
Viral RNA
HIV-1
10μm

Table IV-1: HIV-2 and in HIV-1 LTR copies quantification in ChIP input samples

TZM-bl cells were infected at similar level with HIV-1 and HIV-2 for 24 hrs. Infected cells were processed according to the ChIP assay coupled to the Taqman-based qPCR assay protocols described in the Method section. Immunoprecipitation was performed with ChIP grade anti-human H3K4me2 antibodies, anti-RNAP II (serine 2-phosphorylated form). Each experimented was independently repeated 2 to 3 times.

Antibody against	Samples	Log_{10} copies of DNA/PCR		
		Input	IgG control	IP sample
H3K4me2	HIV-1 infection	4.26	0	3.54
	HIV-2 infection	4.91	0	1.17
Ser2-P RNAPII	HIV-1 infection	5.25	0	3.90
	HIV-2 infection	4.65	0	1.21

Figure III-14: H3K4me2 active chromatin marker at HIV LTR promoters (normalized data)

TZM-bl cells were infected at similar level with HIV-1 and HIV-2 for 24 hrs. Infected cells were processed according to the ChIP assay coupled to the Taqman-based qPCR assay protocols described in the Method section. Immunoprecipitation was performed with ChIP grade anti-human H3K4me2 antibody. The occupancy of H3K4me2 at the LTRs was normalized to the GAPDH promoter data. Each experimented was repeated 2 to 3 times.

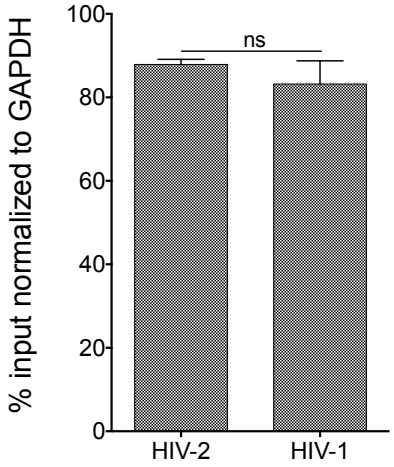

H3K4me2 at HIV LTRs (TZM-bl cells at 24 hpi)

Figure III-15: RNAPII occupancy at HIV LTR promoters (normalized data)

TZM-bl cells were infected at similar level with HIV-1 and HIV-2 for 24 hrs. Infected cells were processed according to the ChIP assay coupled to the Taqman-based qPCR assay protocols described in the Method section. Immunoprecipitation was performed with ChIP grade anti-human serine 2 RNAP II antibody. The occupancy of serine 2 RNAP II at the LTRs was normalized to the GAPDH promoter data. Each experimented was repeated 2 to 3 times.

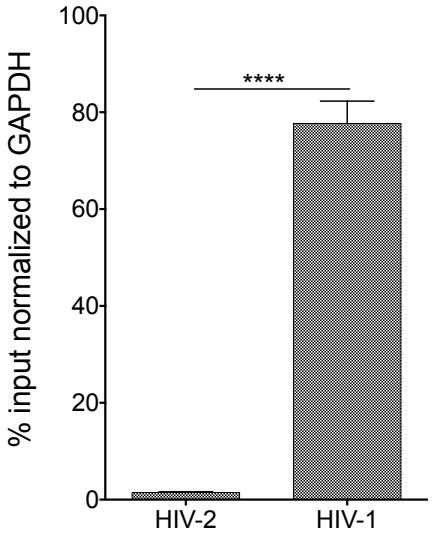

RNAPII at HIV LTRs (TZM-bl cells at 24 hpi)

HIV-2 seemed less efficient at transcribing its provirus during infection in TZM-bl cells.

Imaging and ChIP data indicate that HIV-1 could be more efficient at transcribing its genes than HIV-2 (fig. IV-13). To confirm that these observations reflect a genuine feature of HIV-2 and not some technical artifacts a chimeric HIV-1 construct was prepared that has an HIV-2 Nef c-terminus insert (table II-1, fig. IV-16). That construct allowed the design of one set of primers and probe targeting within the HIV-2 Nef c-terminal region present in both viruses (table II-1). Chimeric Nef HIV-1 and HIV-2 infections were performed in TZM-bl cells at 0.5 MOI. Infected-TZM-GFP cells were harvested at 24 hpi, 48 hpi, and 72 hpi and divided into two batches to assess cell-associated vRNA and vDNA. The qPCR data indicated that at all three time points, both infections reached similar level of total viral DNA (fig. IV-17) which includes all forms of vDNA (linear DNA, 1LTRs, 2LTRs, integrated provirus, and auto-integrants). Unlike the imaging data, the RT-qPCR data indicated that HIV-2 transcribed as much vRNA transcripts as HIV-1 per infected cell (fig. IV-18) and per DNA template (fig. IV-19).

Figure IV-16: Chimeric Nef HIV-1

Generation of an HIV-1 pNL4.3 with a chimeric Nef gene that encodes for the N-terminus of HIV-1NL4.3 Nef and the C-terminus of HIV-2ST Nef protein. The resulting plasmid is referred to as pNL4.3 chimeric Nef.

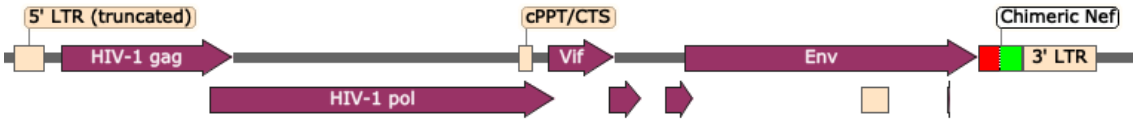

Chimeric Nef pNL4.3
14,281 bp

Figure IV-17: Viral DNA load per infected cells

TZM-GFP cells were infected with HIV-1 or HIV-2 at 0.03 MOI in the presence of Nelfinavir to prevent spread (secondary infection). Infected cells were harvested at 24 hpi, 48 hpi and 72 hpi. Viral DNA was extracted and amplified with primers and probes specific to HIV-2ST Nef C-terminus sequence. Intracellular viral DNA loads were divided by the numbers of infected cells (GFP+ cells) determined by fluorescence microscopy. Experiments were repeated 2 to 3 times. Tukey's multiple comparison test (one-way ANOVA test) was used to assess the statistical differences.

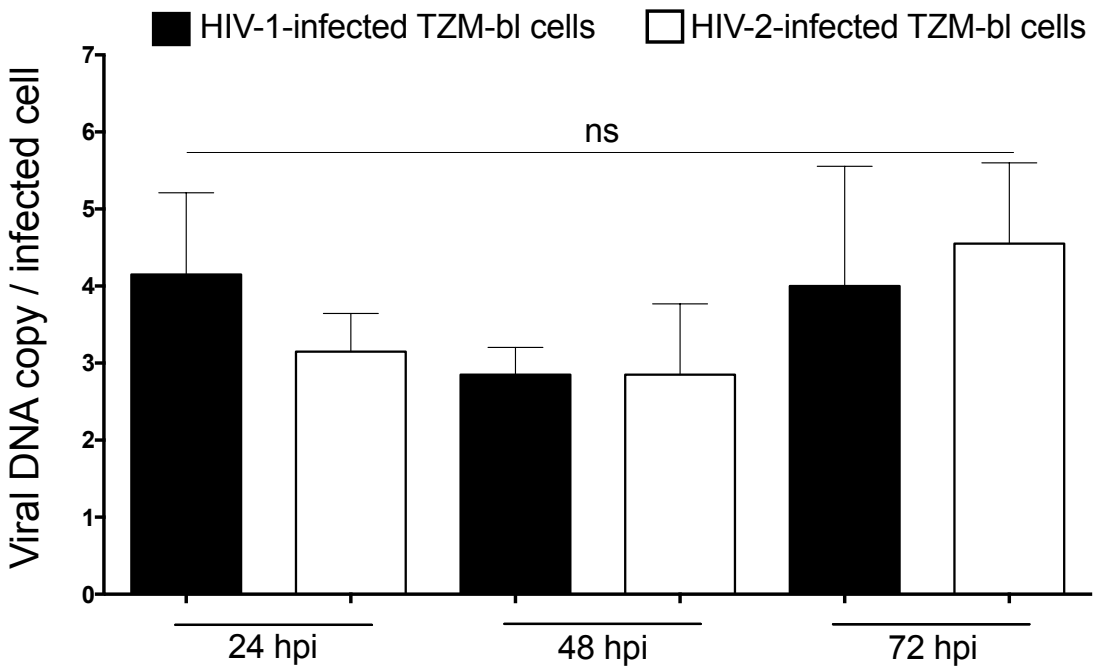
HIV-1-infected TZM-bl cells
HIV-2-infected TZM-bl cells
Viral DNA copy / infected cell
0
1
2
3
4
5
6
7
ns
24 hpi
48 hpi
72 hpi

Figure IV-18: Viral RNA load per infected cells

TZM-GFP cells were infected with HIV-1 or HIV-2 at 0.03 MOI in the presence of Nelfinavir to prevent spread (secondary infection). Infected cells were harvested at 24 hpi, 48 hpi and 72 hpi. Viral RNA was extracted and amplified with primers and probes specific to HIV-2ST Nef C-terminus sequence. Cell-associated viral RNA loads were divided by the numbers of infected cells (GFP+ cells) determined by fluorescence microscopy. Experiments were repeated 2 to 3 times. Tukey's multiple comparison test (one-way ANOVA test) was used to assess the statistical differences.

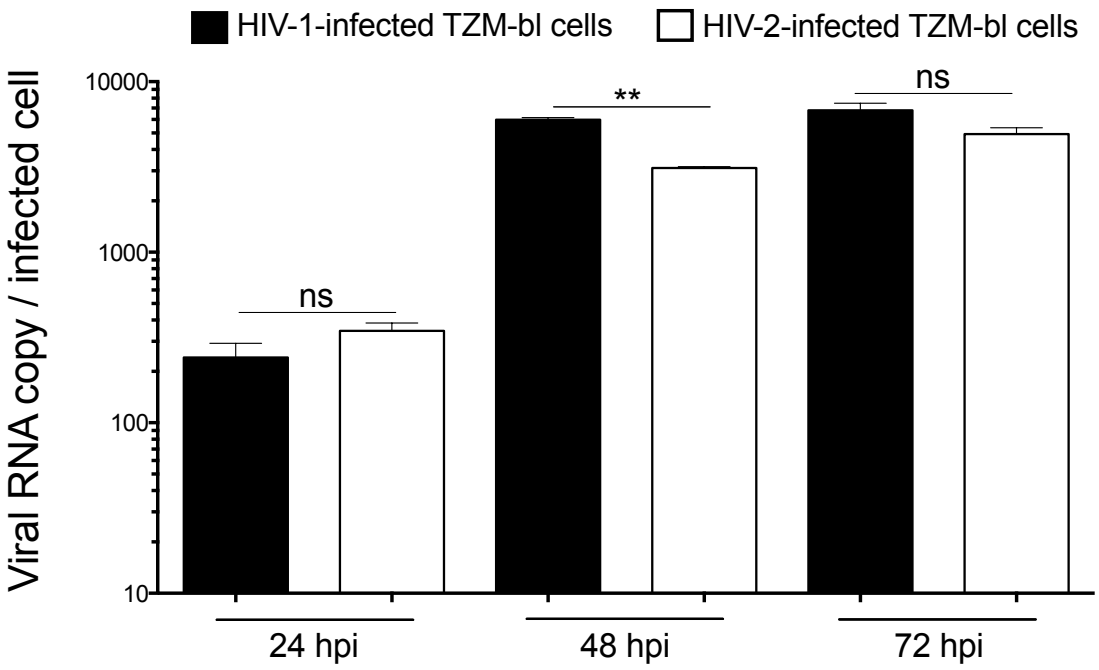
HIV-1-infected TZM-bl cells
HIV-2-infected TZM-bl cells
Viral RNA copy / infected cell
10000
1000
100
10
ns
**
ns
24 hpi
48 hpi
72 hpi

Figure IV-19: Viral RNA transcripts per viral DNA template

TZM-GFP cells were infected with HIV-1 or HIV-2 at 0.03 MOI in the presence of Nelfinavir to prevent spread (secondary infection). Infected cells were harvested at 24 hpi, 48 hpi and 72 hpi. Viral RNA and vDNA were extracted and amplified with primers and probes specific to HIV-2ST Nef C-terminus sequence. The cell-associated vRNA copy number was divided by intracellular vDNA copy number. Experiments were repeated 2 to 3 times. Tukey's multiple comparison test (one-way ANOVA test) was used to assess the statistical differences.

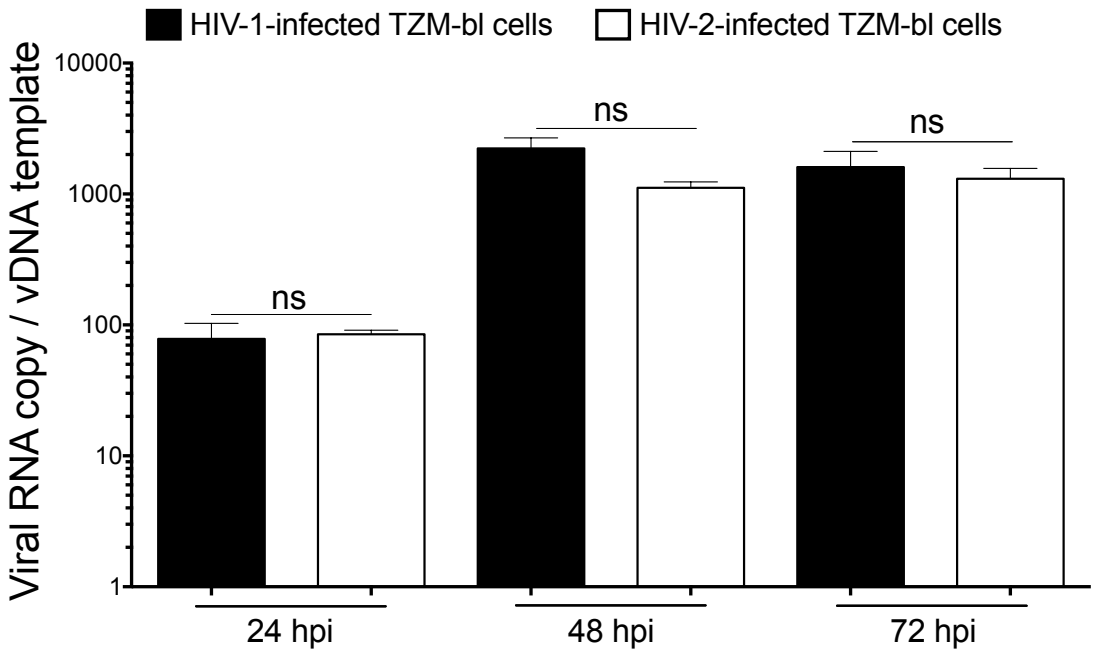
HIV-1-infected TZM-bl cells
HIV-2-infected TZM-bl cells
Viral RNA copy / vDNA template
10000
1000
100
10
1
ns
ns
ns
24 hpi
48 hpi
72 hpi

IV. 3. Discussion

In this study, we compared side by side the kinetics of HIV-1 and HIV-2 infections in order to identify specific time points at which there may be differences between infection by these two viruses. We designed probes to specifically interrogate the fate of the viral nucleic acids in HeLa-based TZM-bl cells. These probes allowed for the detection (qualitative analysis) and the counting of individual vRNA or vDNA spots (quantitative analysis). The data collected showed that HIV-2 reverse transcription was slower than HIV-1's with a roughly 2 hrs delay in completion. The delay in reverse transcription completion was characterized by a slower decrease in the number of viral RNA spots over time compared to HIV-1. The delay was confirmed by a TOA of TDF that showed that TDF was still 50% active up to 11 hpi in the case of HIV-2 infection versus 8 hpi in the case of HIV-1. The slower reverse transcription dynamics impacted the vDNA synthesis, its nuclear translocation, and its integration into the host cell genome as these later steps also showed a roughly 2 hrs. delay confirmed with a TOA of RAL. This is the first study to look into the dynamics of HIV-1 and HIV-2 viral RNA and DNA during the early stages from cell entry to integration into the genome of the target cells.

This observation of a delay in the completion of the reverse transcription of HIV-2 could be due to the reverse transcription step itself as both HIV-1 and HIV-2 have been reported to have the same binding affinity to cellular dNTPs (*199*), but different efficiencies of dNTPs incorporation (3 to 5-fold higher for HIV-1) (*200*). The dNTPs incorporation is a 2-step process involving a conformational change followed with the dNTP incorporation into the nascent DNA chain (*200-201*). And the rate-limiting step is the conformational change step. It seems possible that HIV-1 RT is better at this step than

HIV-2 RT. The delay in the completion of reverse transcription could also be related to a slower target cell entry of HIV-2 than HIV-1. Indeed, the bimodal kinetics of HIV-2 vRNA spots during the first 12 hrs with a slow decrease between 4 hpi and 6 hpi and a faster decrease between 6 and 12 hpi, could indicate that cell entry is also a rate-limiting step. In this case, the viral particles slowly enter the target cell, and the pool of vRNA spots gets replenished up to the point where the majority of viral particles have gained access to the cytoplasm (first phase of reverse transcription – 4 hpi to 6hpi). From there on, reverse transcription would proceed on the remaining pool without replenishment making it appear fast during the second phase (6 hpi to 12 hpi). A previous report (*202*) has shown that for X4-tropic HIVs, HIV-1 isolates were faster at entering the target cells than X4-tropic HIV-2, which both HIV-2_{ST} and HIV-$1_{NL4.3}$ are.

We also noted that the number of vDNA spots significantly increases during the late stages of the virus life cycle between 20 hpi and 22 hpi. They decreased back to their level prior to 20 hpi by 24 hpi indicating a transient event that would probably be missed by other conventional non-microscopic techniques such as qPCR and RT-qPCR. These vDNA spots were curiously different in shape and size from the viral DNA spots observed during the early stages, and early on during the late stages of the virus life cycle. Interestingly, these spots were also sensitive to Rnase digestion suggesting that some of these vDNA spots were rather spots of negative strand RNA also called anti-sense RNA. The significance of such an observation is still unclear. However, based on previous reports on cellular (*203-208*) and HIV-1 (*208-212*) negative strand RNA transcription, we could infer that the production of a negative strand RNA species could be a common feature of HIV-1 and HIV-2 infection. It has been reported to occur under certain circumstances in

which HIV Tat protein production was unable to drive efficient 5'LTR transactivation. The negative sense RNA transcripts were proposed to originate from a cryptic promoter located at the 3'LTR promoter or between the Nef gene and the 3' LTR promoter. The activity of that promoter is suppressed upon sufficient Tat production and efficient 5'LTR transactivation (*208-212*). Whether the anti-sense RNA transcripts produced in cell culture systems infected with HIV-1 are translated into viral proteins is still debated (*208-212*). There are conflicting reports on the existence of viral antisense proteins. The controversy around them is fueled by a lack of specific antibodies to detect them, and by questions about their relevance in vivo (*208-212*).

At first, HIV-2 seemed less efficient at transcribing its genome. And the few transcripts produced by HIV-2 looked almost exclusively nuclear suggesting an export default. This observation can be a genuine transcription issue with the HIV-2 LTR promoter or due to a faulty HIV-2 vRNA probe. Therefore, we looked into histone markers of active chromatin to assess the accessibility of the viral LTR promoters of HIV-1 and HIV-2 to RNAP II and other host transcription factors. The presence of the active histone marker H3K4me2 at these LTRs showed that both LTRs were equally accessible to transcription factors as shown by their similar H3K4me2 occupancy. Although it has been reported that HIV-2 tends to integrate more often into the heterochromatin than HIV-1 (*37*), we did not notice any difference between HIV-1 and HIV-2. As both viruses' LTRs were accessible to RNAP II, we assessed RNAP II occupancy in HIV-infected TZM-bl cells at 24 hpi. Our data showed that occupancy was higher at the HIV-1 LTR than in HIV-2's. Reduced occupancy of RNAP II at HIV-2 LTR was consistent with the decreased transcription from the HIV-2 LTR indicated by the microscopy data. Previous reports have

compared the transcription of HIV-1 to HIV-2 in a wide variety of HIV-infected cells (*37,41,147*). Most of the studies reported that there was little to no difference in terms of transcription efficiency between the two viruses, with the exception of the report by *MacNeil et al* (*37*). This report showed that HIV-1 was very efficient at producing high levels of its transcripts whereas HIV-2 was not. That feature was attributed to transcriptional interferences in which HIV-2 integrates in an inverted position with the regard to the cellular gene it has integrated into.

To strengthen the claim that HIV-2 produces less viral transcripts than HIV-1, we measure cell-associated vRNA and vDNA in HIV-infected TZM-bl cells. A chimeric Nef HIV-1 was made to allow for the use of the same PCR primers and probe to quantify viral nucleic acids, and to eliminate the possibility that differences in the PCR efficiency of our HIV-1 and HIV-2 primers/probe sets was contributing to the apparent differences in viral replication kinetics. The data showed that although there were some differences in transcription between HIV-1 and HIV-2, those differences were not significant in TZM-bl cells as suggested by the imaging and the ChIP data. This observation points to sensitivity issues with the HIV-2 probe used in this work or to the fact that the qPCRs picked up sense and antisense RNA species given that the RT-qPCR performed in this study were not strand specific RT-qPCR assay but rather used random hexamer primers for cDNA synthesis. Moreover, comparing HIV-1 and HIV-2 transcription is also complicated by the facts that the FISH probe detects a sequence within the *Gag* region whereas the qPCR primers and probe target a sequence within the *Nef* region. At any rates, it either appears that some RNA species were not properly detected by the FISH technique, leading to an underestimation of the total number of vRNA spots counted or the RT-qPCR quantified both HIV-2 sense

and antisense RNA species, resulting in an overestimation. Of note, HIV-1 does not produce as much as antisense RNA under the same condition as shown before (*141*). As a consequence, the phenotype of low transcription could be an artifact related to the probe issue. In which case, it is not surprising that the technique missed the transcriptional bursts that were seen with HIV-1 infection (*141*) but not in HIV-2-infected TZM-bl cell images. It could also be a genuine feature of the HIV-2 infection in TZM-bl cells that we could not properly explore and that could be further studied with proper qPCR techniques.

REFERENCE

1. World Health Organization (WHO). WHO global HIV & AIDS statistics 2019 fact sheet. Geneva, Switzerland, **2019**. Available from https://www.unaids.org/sites/default/files/media_asset/2019-UNAIDS-data_en.pdf (Accessed on 10-12-2019).
2. Roser, M.; Ritchie, H. HIV AIDS. Our World in Data. April **2018**. Available from https://ourworldindata.org/grapher/share-of-population-infected-with-hiv-ihme (accessed on 10-12-2019).
3. Barré-Sinoussi, F.; Chermann, J.; Rey, F.; Nugeyre, M.; Chamaret, S.; Gruest, J.; Dauguet, C.; Axler-Blin, C.; Vezinet-Brun, F.; Rouzioux, C.; *et al*. Isolation of a T-lymphotropic retrovirus from a patient at risk for acquired immune deficiency syndrome (AIDS). *Science* **1983**, *220* (4599), 868–871. https://doi.org/10.1126/science.6189183.
4. Robertson, D. L.; Sharp, P. M.; McCutchan, F. E.; Hahn, B. H. Recombination in HIV-1. *Nature* **1995**; *374*:124– 6. [PubMed: 7877682]
5. Robertson, D. L.; Anderson, J. P.; Bradac, J. A.; Carr, J. K.; Foley, B.; Funkhouser, R. K.; Gao, F.; Hahn, B. H.; Kalish, ML, Kuiken C, *et al*. HIV-1 nomenclature proposal. *Science* **2000** April 7; 288:55–56.
6. Blackard, J. T.; Cohen, D. E.; Mayer, K. H. Human immunodeficiency virus superinfection and recombination: current state of knowledge and potential clinical consequences. *Clin. Infect. Dis.* **2002**; *34*:1108–14. [PubMed: 11915000]

7. Taylor, B. S.; Sobieszczyk, M. E.; McCutchan, F. E.; Hammer, S. M. The challenge of HIV-1 subtype diversity. *N. Engl. J. Med.* **2008**, *358* (15), 1590–1602. https://doi.org/10.1056/NEJMra0706737.
8. Clavel, F.; Guyader, M.; Guétard, D.; Sallé, M.; Montagnier, L.; Alizon, M. Molecular cloning and polymorphism of the human immune deficiency virus type 2. *Nature* **1986** Dec 18-31; *324*(6098):691-5.
9. Kanki, P. J.; M'Boup, S.; Ricard, D.; Barin, Frnci.; Denis, O.; Boye, C.; Sangare, L.; Travers, K.; Albaum, M.; Marlink, R.; *et al*. Human T-lymphotropic virus type 4 and the Human immunodeficiency virus in West Africa. *Science* **1987**, *236* (4803), 827–30.
10. Simon, F.; Matheron, S.; Tamalet, C.; Loussert-Ajaka, I.; Bartczak, S.; Pepin, J. M.; Dhiver, C.; Gamba, E.; Elbim, C.; Gastaut, J. A.; *et al*. Cellular and plasma viral load in patients infected with HIV-2. *AIDS* **1993**, *7*, 1411–7.
11. Popper, S. J.; Sarr, A. D.; Travers, K. U.; Guèye-Ndiaye, A.; Mboup, S.; Essex, M. E.; Kanki, P. J. Lower human immunodeficiency virus (HIV) type 2 viral load reflects the difference in pathogenicity of HIV-1 and HIV-2. *J. Infect. Dis.* **1999**, *180* (4), 1116–1121. https://doi.org/10.1086/315010.
12. Reeves, J. D.; Doms, R. W. Human immunodeficiency virus type 2. *J. General Virol.* **2002**; *83*: 1253–1265.
13. Berry, N.; Jaffar, S.; Schim van der Loeff, M.; Ariyoshi, K.; Harding, E.; N'Gom, P. T.; Dias, F.; Wilkins, A.; Ricard, D.; Aaby, P.; *et al*. Low-level viremia and high CD4% predict normal survival in a cohort of HIV type-2-infected villagers. *AIDS Res. Hum. Retrovir.* **2002**; *18*: 1167–73.

14. Eholié, S.; Anglaret, X. Commentary: Decline of HIV-2 prevalence in West Africa: Good news or bad news? *International J. Epidemiol.* **2006**, *35* (5), 1329–1330. https://doi.org/10.1093/ije/dyl156.

15. Schim van der Loeff, M. F.; Larke, N.; Kaye, S.; Berry, N.; Ariyoshi, K.; Alabi, A.; Van Tienen, C.; Leligdowicz, A.; Sarge-Njie, R.; Da Silva, Z. J.; *et al*. Undetectable plasma viral load predicts normal survival in HIV-2-infected people in a West African village. *Retrovirology* **2010**, *7* (46).

16. de Silva, T.; Weiss, R. A. HIV-2 goes global: an unaddressed issue in Indian anti-retroviral programs. *Indian J. Med. Res*. **2010**; *132*: 660–662.

17. Ibe, S.; Yokomaku, Y.; Shiino, T.; Tanaka, R.; Hattori, J.; Fujisaki, S.; Iwatani, Y.; Mamiya, N.; Utsumi, M.; Kato, S.; *et al*. HIV-2 CRF01_AB: First circulating recombinant form of HIV-2. *JAIDS* **2010**, *54* (3), 241–247. https://doi.org/10.1097/QAI.0b013e3181dc98c1.

18. Campbell-Yesufu, O. T.; Gandhi, R. T. Update on human immunodeficiency virus (HIV)-2 infection. *Clin. Infect. Dis.* **2011**; *52*: 780–787.

19. Fryer, H. R.; Van Tienen, C.; Van Der Loeff, M. S.; Aaby, P.; Da Silva, Z. J.; Whittle, H.; Rowland-Jones, S. L.; de Silva, T. I. Predicting the extinction of HIV-2 in rural Guinea-Bissau. *AIDS* **2015**, *29* (18), 2479–86. https://doi.org/10.1097/QAD.0000000000000844.

20. Visseaux, B.; Damond, F.; Matheron, S.; Descamps, D.; Charpentier, C. HIV-2 molecular epidemiology. *Infection, Genetics and Evolution* **2016**, *46*, 233–240. https://doi.org/10.1016/j.meegid.2016.08.010.

21. Gao, F.; Bailes, E.; Robertson, D. L.; Chen, Y.; Rodenburg, C. M.; Michael, S. F.; Cummins, L. B.; Arthur, L. O.; Peeters, M.; Shaw, G. M.; *et al*. Origin of HIV-1 in the chimpanzee *Pan troglodytes troglodytes*. *Nature* **1999**; 397:436–41.

22. Bailes, E., Gao, F., Bibollet-Ruche, F., Courgnaud, V., Peeters, M., Marx, P. A., Hahn, B. H., Sharp, P. M. Hybrid origin of SIV in chimpanzees. Science **2003**, 300: 1713. doi:10.1126/science.1080657.

23. Barlow, K. L.; Ajao, A. O.; Clewley, J. P. Characterization of a novel simian immunodeficiency virus (SIVmonNG1) genome sequence from a Mona monkey (Cercopithecus Mona). *J. Virol.* **2003**, *77* (12), 6879–88. https://doi.org/10.1128/JVI.77.12.6879-6888.2003.

24. Courgnaud, V.; Abela, B.; Pourrut, X.; Mpoudi-Ngole, E.; Loul, S.; Delaporte, E.; Peeters, M. Identification of a new simian immunodeficiency virus lineage with a Vpu gene present among different Cercopithecus monkeys (C. Mona, C. Cephus, and C. Nictitans) from Cameroon. *J. Virol.* **2003**, *77* (23), 12523–34. https://doi.org/10.1128/JVI.77.23.12523-12534.2003.

25. Schindler, M.; Münch, J.; Kutsch, O.; Li, H.; Santiago, M. L.; Bibollet-Ruche, F.; Müller-Trutwin, M. C.; Novembre, F. J.; Peeters, M.; Courgnaud, V.; Bailes, E.; *et al*. Nef-mediated suppression of T cell activation was lost in a lentiviral lineage that gave rise to HIV-1. *Cell* **2006**, *125* (6), 1055–67. https://doi.org/10.1016/j.cell.2006.04.033.

26. Sharp, P. M.; Hahn, B. H. Origins of HIV and the AIDS pandemic. *Cold Spring Harbor Perspect. Med.* **2011**, *1* (1), a006841–a006841. https://doi.org/10.1101/cshperspect.a006841.

27. Etienne, L.; Hahn, B. H.; Sharp, P. M.; Matsen, F. A.; Emerman, M. Gene loss and adaptation to Hominids underlie the ancient origin of HIV-1. *Cell Host & Microbe* **2013**, *14* (1), 85–92. https://doi.org/10.1016/j.chom.2013.06.002.

28. Faria, N. R.; Rambaut, A.; Suchard, M. A.; Baele, G.; Bedford, T.; Ward, M. J.; Tatem, A. J.; Sousa, J. D.; Arinaminpathy, N.; Pépin, J.; *et al*. The early spread and epidemic ignition of HIV-1 in human populations. *Science* **2014**, *346* (6205), 56–61. https://doi.org/10.1126/science.1256739.

29. Luciw PA. Human immunodeficiency viruses and their replication; in Fields BN (ed): Virology, 3rd ed. Philadelphia, Lippincott-Raven, **1996**, pp 1881–1952.

30. Peeters, M.; Courgnaud, V. Overview of primate lentiviruses and their evolution in non-human primates in Africa. In HIV Sequence Compendium; HIV sequence compendium. Theoretical Biology and Biophysics Group, Los Alamos National Laboratory: *Los Alamos, NM, USA,* **2002**; 2–23.

31. Levy JA. HIV and the pathogenesis of AIDS, 3rd ed. Washington, ASM Press, **2007**.

32. Santos, A. F.; Soares, M. A. HIV Genetic diversity and drug resistance. *Viruses* **2010**, *2* (2), 503–531. https://doi.org/10.3390/v2020503.

33. German Advisory Committee Blood (Arbeitskreis Blut), Subgroup 'Assessment of pathogens transmissible by blood'. Human immunodeficiency virus (HIV). *Transfus. Med. Hemother.* **2016**, *43* (3), 203–222. https://doi.org/10.1159/000445852.

34. Kanki, P. J.; Travers, K. U.; MBoup, S.; Hsieh, C. C.; Marlink, R. G.; Gueye-NDiaye, A.; Siby, T.; Thior, I.; Hernandez-Avila, M.; Sankalé, J. L.; *et al*. Slower heterosexual spread of HIV-2 than HIV-1. *Lancet* **1994**; *343*, 943–6.

35. Marlink, R.; Kanki, P. J.; Thior, I.; Travers, K.; Eisen, G.; Siby, T.; Traore, I.; Hsieh, C.-C.; Dia, M. C.; Gueye, E.-H.; *et al*. Reduced rate of disease development after HIV-2 infection as compared to HIV-1. *Science* **1994**, *265* (5178), 1587–1590.

36. Jaffar, S.; Grant, A. D.; Whitworth, J.; Smith, P. G.; Whittle, H. The natural history of HIV-1 and HIV-2 infections in adults in Africa: A literature review. *Bull. WHO* **2004**, *82* (6), 462–9.

37. MacNeil, A.; Sankale, J.-L.; Meloni, S. T.; Sarr, A. D.; Mboup, S.; Kanki, P. Genomic sites of human immunodeficiency virus type 2 (HIV-2) integration: Similarities to HIV-1 in vitro and possible differences in vivo. *J. Virol.* **2006**, *80* (15), 7316–7321. https://doi.org/10.1128/JVI.00604-06.

38. Martinez-Steele, E.; Awasana, A. A.; Corrah, T.; Sabally, S.; van der Sande, M.; Jaye, A.; Togun, T.; Sarge-Njie, R.; McConkey, S. J.; Whittle, H.; *et al*. Is HIV-2-induced AIDS different from HIV-1-associated AIDS? Data from a West African clinic. *AIDS* **2007**, *21* (3), 317–24. https://doi.org/10.1097/QAD.0b013e328011d7ab.

39. Rowland-Jones, S. L.; Whittle, H. C. Out of Africa: What can we learn from HIV-2 about protective immunity to HIV-1? *Nat. Immunol.* **2007**, *8* (4), 329–331. https://doi.org/10.1038/ni0407-329.

40. Gueudin, M.; Damond, F.; Braun, J.; Taïeb, A.; Lemée, V.; Plantier, J.-C.; Chêne, G.; Matheron, S.; Brun-Vézinet, F.; Simon, F. Differences in proviral DNA load between HIV-1- and HIV-2-infected patients: *AIDS* **2008**, *22* (2), 211–215. https://doi.org/10.1097/QAD.0b013e3282f42429.

41. Soto-Rifo, R.; Limousin, T.; Rubilar, P. S.; Ricci, E. P.; Decimo, D.; Moncorge, O.; Trabaud, M.-A.; Andre, P.; Cimarelli, A.; Ohlmann, T. Different effects of the TAR

structure on HIV-1 and HIV-2 genomic RNA translation. *Nucleic Acids Res.* **2012**, *40* (6), 2653–2667. https://doi.org/10.1093/nar/gkr1093.

42. Nyamweya, S.; Hegedus, A.; Jaye, A.; Rowland-Jones, S.; Flanagan, K. L.; Macallan, D. C. Comparing HIV-1 and HIV-2 infection: lessons for viral immunopathogenesis. *Rev. Med. Virol.* **2013**, *23* (4), 221–240. https://doi.org/10.1002/rmv.1739.
43. Miyazaki, Y.; Miyake, A.; Doi, N.; Koma, T.; Uchiyama, T.; Adachi, A.; Nomaguchi, M. Comparison of biochemical properties of HIV-1 and HIV-2 capsid proteins. *Front. Microbiol.* **2017**, *8*, 1082. https://doi.org/10.3389/fmicb.2017.01082.
44. Saleh, S.; Vranckx, L.; Gijsbers, R.; Christ, F.; Debyser, Z. Insight into HIV-2 latency may disclose strategies for a cure for HIV-1 infection. *J. Virus Eradication* **2017**, *3*, 7–14.
45. Denis, F.; Barin, F.; Gershy-Damet, G.; Rey, J. L.; Lhuillier, M.; Mounier, M.; Leonard, G.; Sangare, A.; Goudeau, A.; M'Boup, S.; *et al*. Prevalence of human T-lymphotropic retroviruses type III (HIV) and type IV in Ivory Coast. *Lancet* **1987** Feb 21; *1* (8530), 408-11.
46. Evans, L. A.; Moreau, J.; Odehouri, K.; Seto, D.; Thomson-Honnebier, G.; Legg, H.; Barboza, A.; Cheng-Mayer, C.; Levy, J. A. Simultaneous isolation of HIV-1 and HIV-2 from an AIDS patient. *Lancet* **1988** Dec 17; 2 (8625): 1389-91.
47. Rayfield, M.; De Cock, K.; Heyward, W.; Goldstein, L.; Krebs, J.; Kwok, S.; Lee, S.; McCormick, J.; Moreau, J. M.; Odehouri, K.; *et al*. Mixed human immunodeficiency virus (HIV) infection in an individual: demonstration of both HIV type 1 and type 2 proviral sequences by using polymerase chain reaction. *J. Infect. Dis.* **1988** Dec; *158*(6): 1170-6.

48. Schim van der Loeff, M. F.; Jaffar, S.; Aveika, A. A.; Sabally, S.; Corrah, T.; Harding, E.; Alabi, A.; Bayang, A.; Ariyoshi, K.; Whittle, H. C. Mortality of HIV-1, HIV-2 and HIV-1/HIV-2 dually infected patients in a clinic-based cohort in the Gambia: *AIDS* **2002**, *16* (13), 1775–83. https://doi.org/10.1097/00002030-200209060-00010.

49. da Silva, Z. J.; Oliveira, I.; Andersen, A.; Dias, F.; Rodrigues, A.; Holmgren, B.; Andersson, S.; Aaby, P. Changes in prevalence and incidence of HIV-1, HIV-2 and dual infections in urban areas of Bissau, Guinea-Bissau: Is HIV-2 disappearing? *AIDS* **2008**, *22* (10), 1195–02. https://doi.org/10.1097/QAD.0b013e328300a33d.

50. Motomura, K.; Chen, J.; Hu, W.-S. Genetic recombination between human immunodeficiency virus type 1 (HIV-1) and HIV-2, two distinct human Lentiviruses. *J. Virol.* **2008**, *82* (4), 1923–1933. https://doi.org/10.1128/JVI.01937-07.

51. Günthard, H. F.; Huber, M.; Kuster, H.; Shah, C.; Schüpbach, J.; Trkola, A.; Böni, J. HIV-1 Superinfection in an HIV-2–Infected woman with subsequent control of HIV-1 plasma viremia. *Clin. Infect. Dis.* **2009**, *48* (11), e117–e120. https://doi.org/10.1086/598987.

52. de Silva, T. I.; van Tienen, C.; Rowland-Jones, S. L.; *et al*. Dual infection with HIV-1 and HIV-2: double trouble or destructive interference? *HIV Ther.* **2010** May 4; *3*(4) https://doi.org/10.2217/hiv.10.26.

53. Dilley, K. A.; Ni, N.; Nikolaitchik, O. A.; Chen, J.; Galli, A.; Hu, W.-S. Determining the frequency and mechanisms of HIV-1 and HIV-2 RNA copackaging by single-virion analysis. *J. Virol.* **2011**, *85* (20), 10499–10508. https://doi.org/10.1128/JVI.05147-11.

54. Prince, P. D.; Matser, A.; van Tienen, C.; Whittle, H. C.; Schim van der Loeff, M. F. Mortality rates in people dually infected with HIV-1/2 and those infected with either

HIV-1 or HIV-2: a systematic review and meta-analysis. *AIDS* **2014**, *28* (4), 549–558. https://doi.org/10.1097/01.SPC.0000432532.87841.78.

55. Yamazaki, S.; Kondo, M.; Sudo, K.; Ueda, T.; Fujiwara, H.; Hasegawa, N.; Kato, S. Qualitative real-time PCR assay for HIV-1 and HIV-2 RNA. *Japan J. Infect. Dis.* **2016**, *69* (5), 367–372. https://doi.org/10.7883/yoken.JJID.2015.309.
56. Kao, S.; Calman, A.; Luciw, P. *et al.* Anti-termination of transcription within the long terminal repeat of HIV-1 by *tat* gene product. *Nature* **1987**, *330***,** 489–93. https://doi.org/10.1038/330489a0
57. Roy, S.; Delling, U.; Chen, C.-H.; Rosen, C. A.; Sonenberg, N. A Bulge Structure in HIV-I TAR RNA Is Required for Tat Binding and Tat- Mediated Trans-Activation. *Genes & Development* **1990**, *4*, 1365–1373. https://doi.org/10.1101/gad.4.8.1365.
58. Herrmann, C.H., Rice, A.P. Lentivirus Tat proteins specifically associate with a cellular protein kinase, TAK, that hyperphosphorylates the carboxyl-terminal domain of the large subunit of RNA polymerase II: candidate for a Tat cofactor. *J. Virol.* **1995**, *69* (3),1612–20.
59. Marshall NF, Price DH. 1995. Purification of p-TEFb, a transcription factor required for the transition into productive elongation. *J. Biol. Chem.* **1995**, 270: 12335–8.
60. Marshall, N. F.; Peng, J.; Xie, Z.; Price, D. H. Control of RNA polymerase II elongation potential by a novel carboxyl-terminal domain kinase. *J. Biol. Chem.* **1996**, *271* (43), 27176–83. https://doi.org/10.1074/jbc.271.43.27176.
61. Herrmann, C. H.; Gold, M. O.; Rice, A. P. Viral transactivators specifically target distinct cellular protein kinases that phosphorylate the RNA polymerase II C-terminal

domain. *Nucleic Acids Research* **1996**, *24* (3), 501–8. https://doi.org/10.1093/nar/24.3.501.

62. Zhu, Y.; Pe'ery, T.; Peng, J.; Ramanathan, Y.; Marshall, N.; Marshall, T.; Amendt, B.; Mathews, M. B.; Price, D. H. Transcription elongation factor p-TEFb is required for HIV-1 Tat transactivation in vitro. *Genes & Development* **1997**, *11* (20), 2622–32. https://doi.org/10.1101/gad.11.20.2622.
63. Mancebo, H. S. Y.; Lee, G.; Flygare, J.; Tomassini, J.; Luu, P.; Zhu, Y.; Peng, J.; Blau, C.; Hazuda, D.; Price, D.; Flores, O. P-TEFb kinase is required for HIV Tat transcriptional activation in vivo and in vitro. *Genes & Development* **1997**, *11* (20), 2633–44. https://doi.org/10.1101/gad.11.20.2633.
64. Wei, P.; Garber, M. E.; Fang, S.-M.; Fischer, W. H.; Jones, K. A. A Novel CDK9-associated C-type cyclin interacts directly with HIV-1 Tat and mediates its high-affinity, loop-specific binding to TAR RNA. *Cell* **1998**, *92* (4), 451–462. https://doi.org/10.1016/S0092-8674(00)80939-3.
65. Bieniasz, P. D.; Grdina, T. A.; Bogerd, H. P.; Cullen, B. R. Recruitment of a protein complex containing Tat and cyclin T1 to TAR governs the species specificity of HIV-1 Tat. *EMBO J* **1998**, *17* (23), 7056–65. https://doi.org/10.1093/emboj/17.23.7056.
66. Fujinaga, K.; Cujec, T. P.; Peng, J.; Garriga, J.; Price, D. H.; Graña, X.; Peterlin, B. M. The ability of positive transcription elongation factor b to transactivate human immunodeficiency virus transcription depends on a functional kinase domain, Cyclin T1, and Tat. *J. Virol.* **1998**, *72* (9), 7154–9. https://doi.org/10.1128/JVI.72.9.7154-7159.1998.

67. Garber, M. E.; Wei, P.; KewalRamani, V. N.; Mayall, T. P.; Herrmann, C. H.; Rice, A. P.; Littman, D. R.; Jones, K. A. The interaction between HIV-1 Tat and human Cyclin T1 requires zinc and a critical cysteine residue that is not conserved in the murine CycT1 protein. *Genes & Development* **1998**, *12* (22), 3512–27. https://doi.org/10.1101/gad.12.22.3512.

68. Wada, T.; Takagi, T.; Yamaguchi, Y.; Ferdous, A.; Imai, T.; Hirose, S.; Sugimoto, S.; Yano, K.; Hartzog, G. A.; Winston, F.; *et al*. DSIF, a novel transcription elongation factor that regulates RNA polymerase II processivity, is composed of human Spt4 and Spt5 homologs. *Genes & Development* **1998**, *12* (3), 343–356. https://doi.org/10.1101/gad.12.3.343.

69. Kwak YT, Ivanov D, Guo J, Nee E, Gaynor RB. Role of the human and murine cyclin T proteins in regulating HIV-1 Tat-activation. *J. Mol. Biol.* **1999**, *288*: 57–69. https://doi.org/10.1006/jmbi.1999.2664

70. Yamaguchi, Y.; Takagi, T.; Wada, T.; Yano, K.; Furuya, A.; Sugimoto, S.; Hasegawa, J.; Handa, H. NELF, a multi-subunit complex containing RD, cooperates with DSIF to repress RNA polymerase II elongation. *Cell* **1999**, *97* (1), 41–51. https://doi.org/10.1016/S0092-8674(00)80713-8.

71. Ramanathan, Y.; Rajpara, S. M.; Reza, S. M.; Lees, E.; Shuman, S.; Mathews, M. B.; Pe'ery, T. Three RNA polymerase II carboxyl-terminal domain kinases display distinct substrate preferences. *J. Biol. Chem.* **2001**, *276* (14), 10913–20. https://doi.org/10.1074/jbc.M010975200.

72. Kim, Y. K.; Bourgeois, C. F.; Isel, C.; Churcher, M. J.; Karn, J. Phosphorylation of the RNA polymerase II carboxyl-terminal domain by CDK9 is directly responsible for

human immunodeficiency virus type 1 Tat-activated transcriptional elongation. *Mol. Cell. Biol.* **2002**, *22* (13), 4622–37. https://doi.org/10.1128/MCB.22.13.4622-4637.2002.

73. Tahirov, T. H.; Babayeva, N. D.; Varzavand, K.; Cooper, J. J.; Sedore, S. C.; Price, D. H. Crystal structure of HIV-1 Tat complexed with human p-TEFb. *Nature* **2010**, *465* (7299), 747–51. https://doi.org/10.1038/nature09131.
74. Karn, J.; Stoltzfus, C. M. Transcriptional and posttranscriptional regulation of HIV-1 gene expression. *Cold Spring Harbor Perspect. Med.* **2012**, *2* (2), a006916–a006916. https://doi.org/10.1101/cshperspect.a006916.
75. McNamara, R. P.; McCann, J. L.; Gudipaty, S. A.; D'Orso, I. Transcription factors mediate the enzymatic disassembly of promoter-bound 7SK snRNP to locally recruit P-TEFb for transcription elongation. *Cell Reports* **2013**, *5* (5), 1256–1268. https://doi.org/10.1016/j.celrep.2013.11.003.
76. Mbonye, U.; Wang, B.; Gokulrangan, G.; Shi, W.; Yang, S.; Karn, J. Cyclin-dependent kinase 7 (CDK7)-mediated phosphorylation of the CDK9 activation loop promotes P-TEFb assembly with Tat and proviral HIV reactivation. *J. Biol. Chem.* **2018**, *293* (26), 10009–10025. https://doi.org/10.1074/jbc.RA117.001347.
77. Schulze-Gahmen, U.; Hurley, J. H. Structural mechanism for HIV-1 TAR loop recognition by Tat and the super elongation complex. *Proc. Natl. Acad. Sci. USA* **2018**, *115* (51), 12973–12978. https://doi.org/10.1073/pnas.1806438115.
78. Stevenson, M.; Stanwick, T. L.; Dempsey, M. P.; Lamonica, C. A. HIV-1 replication is controlled at the level of T cell activation and proviral integration. *The EMBO J.* **1990**, *9* (5), 1551–1560. https://doi.org/10.1002/j.1460-2075.1990.tb08274.x.

79. Hill, C. M.; Deng, H.; Unutmaz, D.; *et al*. Envelope glycoproteins from human immunodeficiency virus types 1 and 2 and simian immunodeficiency virus can use human CCR5 as a coreceptor for viral entry and make direct CD4-dependent interactions with this chemokine receptor. *J. Virol.* **1997**, *71*: 6296-6304.

80. McDonald, D.; Vodicka, M. A.; Lucero, G.; Svitkina, T. M.; Borisy, G. G.; Emerman, M.; and Hope, T. J. Visualization of the intracellular behavior of HIV in living cells. *J. Cell Biol.* **2002** *159*, 441–452.

81. Fassati, A. HIV infection of non-dividing cells: a divisive problem. *Retrovirology* **2006**, *3*, 74.

82. Sloan, R. D.; Wainberg, M. A. The role of unintegrated DNA in HIV infection. *Retrovirology* **2011**, *8* (1), 52. https://doi.org/10.1186/1742-4690-8-52.

83. Miller, M. D.; Farnet, C. M.; Bushman, F. D. Human immunodeficiency virus type 1 preintegration complexes: Studies of organization and composition. *J. Virol.* **1997**, *71*, 9.

84. Hulme, A. E.; Perez, O.; Hope, T. J. Complementary assays reveal a relationship between HIV-1 uncoating and reverse transcription. *Proc. Natl. Acad. Sci. USA* **2011**, *108* (24), 9975–9980. https://doi.org/10.1073/pnas.1014522108.

85. Ruegsegger, U.; Beyer, K.; Keller, W. Purification and characterization of human cleavage factor Im involved in the 3' end processing of messenger RNA precursors. *J. Biol. Chem.* **1996**, *271* (11), 6107–6113.

86. Lee, K.; Ambrose, Z.; Martin, T. D.; Oztop, I.; Mulky, A.; Julias, J. G.; Vandegraaff, N.; Baumann, J. G.; Wang, R.; Yuen, W., *et al*. Flexible use of nuclear import pathways

by HIV-1. *Cell Host & Microbe* **2010**, *7* (3), 221–233. https://doi.org/10.1016/j.chom.2010.02.007.

87. Kataoka, N.; Bachorik, J. L.; Dreyfuss, G. Transportin-SR, a nuclear import receptor for SR proteins. *J. Cell Biol.* **1999**, *145* (6), 1145–1152. https://doi.org/10.1083/jcb.145.6.1145.
88. Christ, F.; Thys, W.; De Rijck, J.; Gijsbers, R.; Albanese, A.; Arosio, D.; Emiliani, S.; Rain, J. C.; Benarous, R.; Cereseto, A.; *et al*. Transportin-SR2 imports HIV into the nucleus. *Curr. Biol.* **2008**, *18*, 1192–1202.
89. Brass, A. L.; Dykxhoorn, D. M.; Benita, Y.; Yan, N.; Engelman, A.; Xavier, R. J.; Lieberman, J.; and Elledge, S. J. Identification of host proteins required for HIV infection through a functional genomic screen. *Science* **2008**, *319*, 921–926.
90. Konig, R.; Zhou, Y.; Elleder, D.; Diamond, T. L.; Bonamy, G. M.; Irelan, J. T.; Chiang, C. Y.; Tu, B. P.; De Jesus, P. D.; Lilley, C. E.; *et al*. Global analysis of host-pathogen interactions that regulate early-stage HIV-1 replication. *Cell* **2008**, *135*, 49–60.
91. Yamashita, M.; and Emerman, M. Cellular restriction targeting viral capsids perturbs human immunodeficiency virus type 1 infection of nondividing cells. *J. Virol.* **2009**, *83*, 9835–9843.
92. Stetson, D. B., Ko, J. S., Heidmann, T., and Medzhitov, R. Trex1 prevents cell-intrinsic initiation of autoimmunity. *Cell* **2008**, *134*, 587–598.
93. Yan, N.; Regalado-Magdos, A. D.; Stiggelbout, B.; Lee-Kirsch, M. A.; Lieberman, J. The cytosolic exonuclease TREX1 inhibits the innate immune response to human immunodeficiency virus type 1. *Nat. Immunol.* **2010**, *11* (11), 1005–1013. https://doi.org/10.1038/ni.1941.

94. Kranzusch, P. J.; Vance, R. E. cGAS dimerization entangles DNA recognition. *Immunity* **2013**, *39* (6), 992–994. https://doi.org/10.1016/j.immuni.2013.11.012.

95. Cox, A. L.; Siliciano, R. F. Making sense of HIV innate sensing. *Immunity* **2013**, *39* (6), 998–1000. https://doi.org/10.1016/j.immuni.2013.11.014.

96. Watson, R. O.; Bell, S. L.; MacDuff, D. A.; Kimmey, J. M.; Diner, E. J.; Olivas, J.; Vance, R. E.; Stallings, C. L.; Virgin, H. W.; Cox, J. S. The cytosolic sensor cGAS detects *Mycobacterium tuberculosis* DNA to induce type I interferons and activate autophagy. *Cell Host & Microbe* **2015**, *17* (6), 811–819. https://doi.org/10.1016/j.chom.2015.05.004.

97. Luban, J.; Bossolt, K. L.; Franke, E. K.; *et al*. Human immunodeficiency virus type 1 Gag protein binds to cyclophilins A and B. *Cell* **1993**; *73*: 1067-78.

98. Lahaye, X.; Satoh, T.; Gentili, M.; Cerboni, S.; Conrad, C.; Hurbain, I.; El Marjou, A.; Lacabaratz, C.; Lelièvre, J.-D.; Manel, N. The capsids of HIV-1 and HIV-2 determine immune detection of the viral cDNA by the innate sensor cGAS in dendritic cells. *Immunity* **2013**, *39* (6), 1132–1142. https://doi.org/10.1016/j.immuni.2013.11.002.

99. Rasaiyaah, J.; Tan, C. P.; Fletcher, A. J.; Price, A. J.; Blondeau, C.; Hilditch, L.; Jacques, D. A.; Selwood, D. L.; James, L. C.; Noursadeghi, M.; *et al*. HIV-1 evades innate immune recognition through specific cofactor recruitment. *Nature* **2013**, *503* (7476), 402–405. https://doi.org/10.1038/nature12769.

100. Bukrinsky, M. I.; Sharova, N.; Dempsey, M. P.; Stanwick, T. L.; Bukrinskaya, A. G.; Haggerty, S.; Stevenson, M. Active nuclear import of human immunodeficiency virus type 1 preintegration complexes. *Proc. Natl. Acad. Sci. USA* **1992**; 89: 6580-4.

101. Chen, H.; Engelman, A. Asymmetric processing of human immunodeficiency virus type 1 cDNA in vivo: Implications for functional end coupling during the chemical steps of DNA transposition. *Mol. Cell. Biol.* **2001**, *21* (20), 6758–67. https://doi.org/10.1128/MCB.21.20.6758-6767.2001.

102. Katz, R. A.; Greger, J. G.; Boimel, P.; Skalka, A. M. Human immunodeficiency virus type 1 DNA nuclear import and integration are mitosis independent in cycling cells. *J. Virol.* **2003**; 77: 13412-7

103. Arhel, N. J., Souquere-Besse, S., Munier, S., Souque, P., Guadagnini, S., Rutherford, S., Prevost, M. C., Allen, T. D., and Charneau, P. HIV-1 DNA flap formation promotes uncoating of the pre-integration complex at the nuclear pore. *EMBO J.* **2007** *26*, 3025–3037.

104. Laguette, N.; Sobhian, B.; Casartelli, N.; Ringeard, M.; Chable-Bessia, C.; Ségéral, E.; Yatim, A.; Emiliani, S.; Schwartz, O.; Benkirane, M. SAMHD1 is the dendritic- and myeloid-cell-specific HIV-1 restriction factor counteracted by Vpx. *Nature* **2011**, *474* (7353), 654–657. https://doi.org/10.1038/nature10117.

105. Hrecka, K.; Hao, C.; Gierszewska, M.; Swanson, S. K.; Kesik-Brodacka, M.; Srivastava, S.; Florens, L.; Washburn, M. P.; Skowronski, J. Vpx relieves inhibition of HIV-1 infection of macrophages mediated by the SAMHD1 protein. *Nature* **2011**, *474* (7353), 658–661. https://doi.org/10.1038/nature10195.

106. Mangeat, B., Turelli, P., Caron, G., Friedli, M., Perrin, L., Trono, D. Broad antiretroviral defense by human APOBEC3G through lethal editing of nascent reverse transcripts. *Nature* **2003**, *424*:99–103. http://dx.doi.org/10 .1038/nature01709.

107. Zhang, H., Yang, B., Pomerantz, R. J., Zhang, C. M., Arunachalam, S. C., Gao, L. The cytidine deaminase CEM15 induces hypermutation in newly synthesized HIV-1 DNA. *Nature* **2003**, *424*:94–8. http://dx.doi.org/10.1038 /nature01707.

108. Suspene, R., Sommer, P., Henry, M., Ferris, S., Guetard, D., Pochet, S., Chester, A., Navaratnam, N., Wain-Hobson, S., Vartanian, J. P. APOBEC3G is a single-stranded DNA cytidine deaminase and functions independently of HIV reverse transcriptase. *Nucleic Acids Res.* **2004** *32*:2421–9. http://dx .doi.org/10.1093/nar/gkh554.

109. Yu, Q., Konig, R., Pillai, S., Chiles, K., Kearney, M., Palmer, S., Richman, D., Coffin, J. M., Landau, N. R. Single-strand specificity of APOBEC3G accounts for minus-strand deamination of the HIV genome. *Nat. Struct. Mol. Biol.* **2004**, *11*:435–442. http://dx.doi.org/10.1038/nsmb758.

110. Malim, M. H. APOBEC proteins and intrinsic resistance to HIV-1 infection. *Phil. Trans. R. Soc. B* **2009**, *364* (1517), 675–687. https://doi.org/10.1098/rstb.2008.0185.

111. Krupp, A., McCarthy, K. R., Ooms, M., Letko, M., Morgan, J. S., Simon, V., Johnson, W. E. APOBEC3G polymorphism as a selective barrier to cross-species transmission and emergence of pathogenic SIV and AIDS in a primate host. *PLoS Pathog.* **2013**, *9*: e1003641. http://dx.doi.org/10.1371 /journal.ppat.1003641.

112. Lecossier, D., Bouchonnet, F., Clavel, F., Hance, A. J. Hypermutation of HIV-1 DNA in the absence of the Vif protein. *Science* **2003** *300*:1112. http://dx.doi.org/10.1126/science.1083338.

113. Marin, M., Rose, K. M., Kozak, S. L., Kabat, D. HIV-1 Vif protein binds the editing enzyme APOBEC3G and induces its degradation. *Nat. Med.* **2003**, *9*:1398 –1403. http://dx.doi.org/10.1038/nm946.

114. Yu, X. H., Yu, Y. K., Liu, B. D., Luo, K., Kong, W., Mao, P. Y., Yu, X. F. Induction of APOBEC3G ubiquitination and degradation by an HIV-1 Vif-Cul5-SCF complex. *Science* **2003**, *302*:1056–1060. http://dx.doi.org/10 .1126/science.1089591.

115. Sheehy, A. M., Gaddis, N. C., Malim, M. H. The antiretroviral enzyme APOBEC3G is degraded by the proteasome in response to HIV-1 Vif. *Nat. Med.* **2003**, *9*:1404 –1407. http://dx.doi.org/10.1038/nm945.

116. Kobayashi, M., Takaori-Kondo, A., Miyauchi, Y., Iwai, K., Uchiyama, T. Ubiquitination of APOBEC3G by an HIV-1 Vif-Cullin5-Elongin B-Elongin C complex is essential for Vif function. *J. Biol. Chem.* **2005**, *280*: 18573–18578. http://dx.doi.org/10.1074/jbc.C500082200.

117. Letko, M.; Silvestri, G.; Hahn, B. H.; Bibollet-Ruche, F.; Gokcumen, O.; Simon, V.; Ooms, M. Vif proteins from diverse primate lentiviral lineages use the same binding site in APOBEC3G. *J. Virol.* **2013**, *87*:11861–11871. http://dx.doi.org/10.1128/JVI.01944-13.

118. Smith, J. L.; Izumi, T.; Borbet, T. C.; Hagedorn, A. N.; Pathak, V. K. HIV-1 and HIV-2 Vif interact with human APOBEC3 proteins using completely different determinants. *J. Virol.* **2014**, *88* (17), 9893–9908. https://doi.org/10.1128/JVI.01318-14.

119. Takeuchi, J. S., Perche, B., Migraine, J. et al. High level of susceptibility to human TRIM5alpha conferred by HIV-2 capsid sequences. *Retrovirology* **2013**; *10*: 50.

120. Jimenez-Guardeño, J. M.; Apolonia, L.; Betancor, G.; Malim, M. H. Immunoproteasome activation enables human TRIM5α restriction of HIV-1. *Nat. Microbiol.* **2019**, *4* (6), 933–940. https://doi.org/10.1038/s41564-019-0402-0.

121. Monette, A.; Panté, N.; Mouland, A. J. HIV-1 remodels the nuclear pore complex. *J. Cell Biol.* **2011**, *193* (4), 619–631. https://doi.org/10.1083/jcb.201008064.

122. Ao, Z.; Jayappa, K. D.; Wang, B.; Zheng, Y.; Wang, X.; Peng, J.; Yao, X. Contribution of host nucleoporin 62 in HIV-1 integrase chromatin association and viral DNA integration. *J. Biol. Chem.* **2012**, *287* (13), 10544–10555. https://doi.org/10.1074/jbc.M111.317057.

123. Buseyne, F.; Le Gall, S.; Boccaccio, C; Abastado, J. P.; Lifson, J. D.; Arthur, L. O.; Rivière, Y.; Heard, J. M.; Schwartz, O. MHC-I-restricted presentation of HIV-1 virion antigens without viral replication. *Nat Med* **2001**; *7*:344-9.

124. Poon, B.; Chen, I. S. Y. Human immunodeficiency virus type 1 (HIV-1) Vpr enhances expression from unintegrated HIV-1 DNA. *Journal of Virology* **2003**, *77* (7), 3962–3972. https://doi.org/10.1128/JVI.77.7.3962-3972.2003.

125. Hrecka, K.; Hao, C.; Shun, M.-C.; Kaur, S.; Swanson, S. K.; Florens, L.; Washburn, M. P.; Skowronski, J. HIV-1 and HIV-2 exhibit divergent interactions with HLTF and UNG2 DNA repair proteins. *Proc Natl Acad Sci USA* **2016**, *113* (27), E3921–E3930. https://doi.org/10.1073/pnas.1605023113.

126. Coiras, M.; López-Huertas, M. R.; Pérez-Olmeda, M.; et al. Understanding HIV-1 latency provides clues for the eradication of long-term reservoirs. *Nat. Rev. Microbiol.* **2009** Nov; *7*(11):798-812. doi: 10.1038/nrmicro2223

127. Pinto, L. A.; Joao-Covas, M.; Victorino, R. M. M. T Helper crossreactivity to viral recombinant proteins in HIV2-infected patients. *AIDS* **1993**, *7* (10), 1389–91.

128. Bertoletti, A.; Cham, F.; Mcadam, S.; Rostron, T.; Rowland-Jones, S.; Sabally, S.; Corrah, T.; Ariyoshi, K.; Whittle, H. Cytotoxic T cells from human immunodeficiency virus type 2-infected patients frequently crossreact with different human immunodeficiency virus type 1 clades. *J. Virol.* **1998**, *72* (3), 2439–48.

129. Buseyne, F.; Rivière, Y. The flexibility of the TCR allows recognition of a large set of naturally occurring epitope variants by HIV-specific cytotoxic T lymphocytes. *Int. Immunol.* **2001**, *13* (7), 941–50. https://doi.org/10.1093/intimm/13.7.941.

130. Hanson, A.; Dieng-Sarr, A.; Shea, A.; Jones, N.; Mboup, S.; Kanki, P.; Cao, H. Distinct profile of T cell activation in HIV type 2 compared to HIV type 1 infection: differential mechanism for immunoprotection. *AIDS Res. Hum. Retroviruses* **2005**, *21* (9), 791–8. https://doi.org/10.1089/aid.2005.21.791.

131. Zheng, N. N.; McElrath, M. J.; Sow, P.-S.; Hawes, S. E.; Diallo-Agne, H.; Stern, J. E.; Li, F.; Mesher, A. L.; Robinson, A. D.; Gottlieb, G. S.; *et al.* Role of human immunodeficiency virus (HIV)-specific T-cell immunity in control of dual HIV-1 and HIV-2 infection. *J. Virol.* **2007**, *81* (17), 9061–9071. https://doi.org/10.1128/JVI.00117-07.

132. Pasternak, A. O.; Jurriaans, S.; Bakker, M.; Berkhout, B.; Lukashov, V. V. Steady increase in cellular HIV-1 load during the asymptomatic phase of untreated infection despite stable plasma viremia. *AIDS* **2010**, *24* (11), 1641–1649. https://doi.org/10.1097/QAD.0b013e32833b3171.

133. Schroder, A. R., Shinn, P., Chen, H., et al. HIV-1 integration in the human genome favors active genes and local hotspots. *Cell* **2002**, *110*:521-529.

134. Cherepanov, P.; Maertens, G.; Proost, P.; Devreese, B.; Van Beeumen, J.; Engelborghs, Y.; De Clercq, E.; Debyser, Z. HIV-1 integrase forms stable tetramers and associates with LEDGF/P75 protein in human cells. *J. Biol. Chem.* **2003**, *278* (1), 372–381. https://doi.org/10.1074/jbc.M209278200.

135. Turlure, F., Devroe, E., Silver, P. A., Engelman, A. Human cell proteins and human immunodeficiency virus DNA integration. *Front Biosci.* **2004** *9*: 3187–3208.

136. Dieudonné, M.; Maiuri, P.; Biancotto, C.; Knezevich, A.; Kula, A.; Lusic, M.; Marcello, A. Transcriptional competence of the integrated HIV-1 provirus at the nuclear periphery. *EMBO J* **2009**, *28* (15), 2231–2243. https://doi.org/10.1038/emboj.2009.141.

137. Marini, B.; Kertesz-Farkas, A.; Ali, H.; Lucic, B.; Lisek, K.; Manganaro, L.; Pongor, S.; Luzzati, R.; Recchia, A.; Mavilio, F.; Giacca, M.; Lusic, M. Nuclear architecture dictates HIV-1 integration site selection. *Nature* **2015**, *521* (7551), 227–231. https://doi.org/10.1038/nature14226.

138. Emiliani, S.; Mousnier, A.; Busschots, K.; Maroun, M.; Van Maele, B.; Tempé, D.; Vandekerckhove, L.; Moisant, F.; Ben-Slama, L.; Witvrouw, M.; *et al*. Integrase mutants defective for interaction with LEDGF/P75 are impaired in chromosome tethering and HIV-1 replication. *J. Biol. Chem.* **2005**, *280* (27), 25517–25523. https://doi.org/10.1074/jbc.M501378200.

139. Ciuffi A, Llano M, Poeschla E et al. A role for LEDGF/p75 in targeting HIV DNA integration. *Nat Med* **2005**, *11*: 1287–1289.

140. Llano M, Saenz DT, Meehan A et al. An essential role for LEDGF/p75 in HIV integration. *Science* **2006** Oct 20; *314*(5798): 461–4.

141. Puray-Chavez, M.; Tedbury, P. R.; Huber, A. D.; Ukah, O. B.; Yapo, V.; Liu, D.; Ji, J.; Wolf, J. J.; Engelman, A. N.; Sarafianos, S. G. Multiplex single-cell visualization of nucleic acids and protein during HIV infection. *Nat. Commun.* **2017**, *8* (1), 1882. https://doi.org/10.1038/s41467-017-01693-z.

142. Sauter, D.; Unterweger, D.; Vogl, M.; et al. Human tetherin exerts strong selection pressure on the HIV-1 group N Vpu protein. *PLoS Pathog* **2012**; *8*: e1003093.

143. Lewinski, M. K.; Jafari, M.; Zhang, H.; Opella, S. J.; Guatelli, J. Membrane Anchoring by a C-Terminal Tryptophan Enables HIV-1 Vpu to Displace Bone Marrow Stromal Antigen 2 (BST2) from Sites of Viral Assembly. *J. Biol. Chem.* **2015**, *290* (17), 10919–10933. https://doi.org/10.1074/jbc.M114.630095.

144. Pornillos, O.; Higginson, D. S.; Stray, K. M.; Fisher, R. D.; Garrus, J. E.; Payne, M.; He, G.-P.; Wang, H. E.; Morham, S. G.; Sundquist, W. I. HIV Gag Mimics the Tsg101-Recruiting Activity of the Human Hrs Protein. *J. Cell Biol.* **2003**, *162* (3), 425–434. https://doi.org/10.1083/jcb.200302138.

145. Becker, J. T.; Sherer, N. M. Subcellular localization of HIV-1 *Gag-Pol* mRNAs regulates sites of virion assembly. *J. Virol.* **2017**, *91* (6), e02315-16, /jvi/91/6/e02315-16.atom. https://doi.org/10.1128/JVI.02315-16.

146. Kozak, M. Influences of mRNA secondary structure on initiation by eukaryotic ribosomes. *Proc. Natl. Acad. Sci. USA* **1986**, *83* (9), 2850–2854. https://doi.org/10.1073/pnas.83.9.2850.

147. Kozak, M. Circumstances and mechanisms of inhibition of translation by secondary structure in eucaryotic mRNAs. *Mol. Cell. Biol.* **1989**, *9* (11), 5134–5142. https://doi.org/10.1128/MCB.9.11.5134.

148. Nunes-Cabaço, H.; Matoso, P.; Foxall, R. B.; Tendeiro, R.; Pires, A. R.; Carvalho, T.; Pinheiro, A. I.; Soares, R. S.; Sousa, A. E. Thymic HIV-2 infection uncovers posttranscriptional control of viral replication in Human thymocytes. *J. Virol.* **2015**, *89* (4), 2201–2208. https://doi.org/10.1128/JVI.03047-14.

149. Evans, V. A.; Khoury, G.; Saleh, S.; Cameron, P. U.; Lewin, S. R. HIV persistence: chemokines and their signaling pathways. *Cytokine & Growth Factor Reviews* **2012**, *23* (4–5), 151–157. https://doi.org/10.1016/j.cytogfr.2012.05.002.

150. Saayman, S.; Ackley, A.; Turner, A.-M. W.; Famiglietti, M.; Bosque, A.; Clemson, M.; Planelles, V.; Morris, K. V. An HIV-encoded antisense long noncoding RNA epigenetically regulates viral transcription. *Mol. Ther.* **2014**, *22* (6), 1164–1175. https://doi.org/10.1038/mt.2014.29.

151. Chavez, L.; Calvanese, V.; Verdin, E. HIV latency is established directly and early in both resting and activated primary CD4 T cells. *PLoS Pathog.* **2015**, *11* (6), e1004955. https://doi.org/10.1371/journal.ppat.1004955.

152. Sun, W.-W.; Jiao, S.; Sun, L.; Zhou, Z.; Jin, X.; Wang, J.-H. SUN2 modulates HIV-1 infection and latency through association with lamin A/C to maintain the repressive chromatin. *mBio* **2018**, *9* (3), e02408-17, /mbio/9/3/mBio.02408-17.atom. https://doi.org/10.1128/mBio.02408-17.

153. Lehner, T.; Wang, Y.; Pido-Lopez, J.; Whittall, T.; Bergmeier, L. A.; Babaahmady, K. The emerging role of innate immunity in protection against HIV-1 infection. *Vaccine* **2008**, *26* (24), 2997–3001. https://doi.org/10.1016/j.vaccine.2007.11.060.

154. Manel, N.; Hogstad, B.; Wang, Y.; Levy, D. E.; Unutmaz, D.; Littman, D. R. A cryptic sensor for HIV-1 activates antiviral innate immunity in dendritic cells. *Nature* **2010**, *467* (7312), 214–217. https://doi.org/10.1038/nature09337.

155. Manel, N.; Littman, D. R. Hiding in plain sight: how HIV evades innate immune responses. *Cell* **2011**, *147* (2), 271–274. https://doi.org/10.1016/j.cell.2011.09.010.

156. Levy, J. A.; Scott, I.; Mackewicz, C. Protection from HIV/AIDS: the importance of innate immunity. *Clin. Immunol.* **2003**, *108* (3), 167–174. https://doi.org/10.1016/S1521-6616(03)00178-5.

157. Kane, M.; Zang, T. M.; Rihn, S. J.; Zhang, F.; Kueck, T.; Alim, M.; Schoggins, J.; Rice, C. M.; Wilson, S. J.; Bieniasz, P. D. Identification of interferon-stimulated genes with antiretroviral activity. *Cell Host & Microbe* **2016**, *20* (3), 392–405. https://doi.org/10.1016/j.chom.2016.08.005.

158. Vicenzi, E.; Poli, G. The interferon-stimulated gene TRIM22: a double-edged sword in HIV-1 infection. *Cytokine & Growth Factor Reviews* **2018**, *40*, 40–47. https://doi.org/10.1016/j.cytogfr.2018.02.001.

159. Scagnolari, C.; Antonelli, G. Type I interferon and HIV: subtle balance between antiviral activity, immunopathogenesis and the microbiome. *Cytokine & Growth Factor Reviews* **2018**, *40*, 19–31. https://doi.org/10.1016/j.cytogfr.2018.03.003.

160. Loucif, H.; Gouard, S.; Dagenais-Lussier, X.; Murira, A.; Stäger, S.; Tremblay, C.; Van Grevenynghe, J. Deciphering natural control of HIV-1: a valuable strategy to

achieve antiretroviral therapy termination. *Cytokine & Growth Factor Reviews* **2018**, *40*, 90–98. https://doi.org/10.1016/j.cytogfr.2018.03.010.

161. Borrego, P.; Marcelino, J.; Rocha, C.; Doroana, M.; Antunes, F.; Maltez, F.; Gomes, P.; Novo, C.; Barroso, H.; Taveira, N. The role of the humoral immune response in the molecular evolution of the envelope C2, V3 and C3 regions in chronically HIV-2 infected patients. *Retrovirology* **2008**, *5* (1), 78. https://doi.org/10.1186/1742-4690-5-78.

162. Peeters, M.; Toure-Kane, C.; Nkengasong, J. N. Genetic diversity of HIV in Africa: impact on diagnosis, treatment, vaccine development and trials. *AIDS* **2003**, *17* (18), 2547–2560.

163. Travers, K.; Mboup, S.; Marlink, R.; Gueye-Nidaye, A.; Siby, T.; Thior, I.; Traore, I.; Dieng-Sarr, A.; Sankale, J.; Mullins, C.; *et al*. Natural protection against HIV-1 infection provided by HIV-2. *Science* **1995**, *268* (5217), 1612–1615. https://doi.org/10.1126/science.7539936.

164. Travers, K. U.; Eisen, G. E.; Marlink, R. G.; et al. Protection from HIV-1 infection by HIV-2. *AIDS* **1998** Jan 22; 12 (2): 224-5.

165. Esbjörnsson, J.; Månsson, F.; Kvist, A.; Isberg, P.-E.; Nowroozalizadeh, S.; Biague, A. J.; da Silva, Z. J.; Jansson, M.; Fenyö, E. M.; Norrgren, H.; *et al*. Inhibition of HIV-1 disease progression by contemporaneous HIV-2 infection. *N. Engl. J. Med.* **2012**, *367* (3), 224–232. https://doi.org/10.1056/NEJMoa1113244.

166. Esbjörnsson, J.; Månsson, F.; Kvist, A.; Isberg, P.-E.; Nowroozalizadeh, S.; Biague, A. J.; Da Silva, Z. J.; Jansson, M.; Fenyö, E. M.; Norrgren, H.; *et al*. Effect of

HIV-2 infection on HIV-1 disease progression and mortality. *AIDS* **2014**, *28* (4), 615. https://doi.org/10.1097/QAD.0000000000000139.

167. Garrett, E. D.; Cullen, B. R. Comparative Analysis of Rev Function in Human Immunodeficiency Virus Types 1 and 2. *J. Virol.* **1992**, *66* (7), 4288–92.

168. Matsuda, Z.; Yu, X.; Yu, Q. C.; Lee, T. H.; Essex, M. A virion-specific inhibitory molecule with therapeutic potential for human immunodeficiency virus type 1. *Proc. Natl. Acad. Sci. USA* **1993**, *90* (8), 3544–8. https://doi.org/10.1073/pnas.90.8.3544.

169. Rappaport, J.; Arya, S. K.; Richardson, M.; Baier-Bitterlich, G.; Klotman, P. HIV-1 inhibition by HIV-2. *J. Mol. Med.* **1995**, *73*, 583–589.

170. Arya, S. K.; Gallo, R. C. Human immunodeficiency virus (HIV) type 2-mediated inhibition of HIV type 1: A new approach to gene therapy of HIV infection. *Proc. Natl. Acad. Sci. USA* **1996**, *93* (9), 4486–4491. https://doi.org/10.1073/pnas.93.9.4486.

171. Browning, C. M.; Cagnon, L.; Good, P. D.; Rossi, J.; Engelke, D. R.; Markovitz, D. M. Potent Inhibition of Human Immunodeficiency Virus Type 1 (HIV-1) Gene Expression and Virus Production by an HIV-2 Tat Activation-Response RNA Decoy. *J. Virol.* **1999**, *73*, 5.

172. Michienzi A, Li S, Zala JA, et al. A nucleolar TAR decoy inhibitor of HIV-1 replication. *PNAS* **2002** Oct 29; *22*(99):1407-52.

173. Mahdi, M.; Szojka, Z.; Mótyán, J. A.; Tőzsér, J. Inhibitory effects of HIV-2 Vpx on replication of HIV-1. *J. Virol.* **2018**, *92* (14), e00554-18, /jvi/92/14/e00554-18.atom. https://doi.org/10.1128/JVI.00554-18.

174. Platt, E. J.; Wehrly, K.; Kuhmann, S. E.; Chesebro, B.; Kabat, D. Effects of CCR5 and CD4 cell surface concentrations on infections by macrophage tropic isolates of

human immunodeficiency virus type 1. *Journal of Virology* **1998**, *72* (4), 2855–64. https://doi.org/10.1128/JVI.72.4.2855-2864.1998.

175. Derdeyn, C. A.; Decker, J. M.; Sfakianos, J. N.; Wu, X.; O'Brien, W. A.; Ratner, L.; Kappes, J. C.; Shaw, G. M.; Hunter, E. Sensitivity of human immunodeficiency virus type 1 to the fusion inhibitor T-20 is modulated by coreceptor specificity defined by the V3 Loop of Gp120. *Journal of Virology* **2000**, *74* (18), 8358–67. https://doi.org/10.1128/JVI.74.18.8358-8367.2000.

176. Wei, X.; Decker, J. M.; Liu, H.; Zhang, Z.; Arani, R. B.; Kilby, J. M.; Saag, M. S.; Wu, X.; Shaw, G. M.; Kappes, J. C. Emergence of resistant human immunodeficiency virus type 1 in patients receiving fusion inhibitor (T-20) monotherapy. *Antimicrobial Agents and Chemotherapy* **2002**, *46* (6), 1896–1905. https://doi.org/10.1128/AAC.46.6.1896-1905.2002.

177. Takeuchi, Y.; McClure, M. O.; Pizzato, M. Identification of gammaretroviruses constitutively released from cell lines used for human immunodeficiency virus research. *Journal of Virology* **2008**, *82* (24), 12585–8. https://doi.org/10.1128/JVI.01726-08.

178. Rosa, A.; Chande, A.; Ziglio, S.; De Sanctis, V.; Bertorelli, R.; Goh, S. L.; McCauley, S. M.; Nowosielska, A.; Antonarakis, S. E.; Luban, J.; *et al*. HIV-1 Nef promotes infection by excluding SERINC5 from virion incorporation. *Nature* **2015**, *526* (7572), 212–7. https://doi.org/10.1038/nature15399.

179. Osada, N.; Kohara, A.; Yamaji, T.; Hirayama, N.; Kasai, F.; Sekizuka, T.; Kuroda, M.; Hanada, K. The genome landscape of the African green monkey kidney-derived Vero cell line. *DNA Res.* **2014**, *21* (6), 673–83. https://doi.org/10.1093/dnares/dsu029.

180. Adachi, A., Gendelman, H. E., Koenig, S., et al. Production of acquired immunodeficiency syndrome-associated retrovirus in human and nonhuman cells transfected with an infectious molecular clone. *J. Virol.* **1986**, *59*(2), 284-291

181. Kong L.I., Lee S-W, Kappes JC, et al. West African HIV-2-related human retrovirus with attenuated cytopathicity. *Science* **1988**, *240*:1525-1529.

182. Kumar P, Hui HX, Kappes JC, et al. Molecular characterization of an attenuated human immunodeficiency virus type 2 isolate. *J. Virol.* **1990**, *64*(2):890.

183. Calvanese V, Chavez L, Laurent T, et al. Dual-color HIV reporters trace a population of latently infected cells and enable their purification. *Virology* **2013** Nov; *446*(1-2):283-92

184. Good, P.; Krikos, A.; Li, S.; Bertrand, E.; Lee, N.; Giver, L.; Ellington, A.; Zaia, J.; Rossi, J.; *et al*. Expression of small, therapeutic RNAs in human cell nuclei. *Gene Ther.* **1997**, *4* (1), 45–54. https://doi.org/10.1038/sj.gt.3300354.

185. Integrated DNA Technology (IDT). UNAFold tool. Coralville, Indiana, USA **2019**. Available from *https://www.idtdna.com/UNAFold* (Accessed on 3-5-2019)

186. Chesebro, B.; Wehrly, K.; Nishio, J.; Perryman, S. Macrophage-tropic human immunodeficiency virus isolates from different patients exhibit unusual V3 envelope sequence homogeneity in comparison with T-cell-tropic isolates: Definition of critical amino acids involved in cell tropism. *J. Virol.* **1992**, *66* (11): 6547-54.

187. Lanman, J.; Sexton, J.; Sakalian, M.; Prevelige, P. E. Kinetic analysis of the role of intersubunit interactions in human immunodeficiency virus type 1 capsid protein assembly in vitro. *J. Virol.* **2002**, *76* (14), 6900–8. https://doi.org/10.1128/JVI.76.14.6900-6908.2002.

188. Gres, A. T.; Kirby, K. A.; KewalRamani, V. N.; Tanner, J. J.; Pornillos, O.; Sarafianos, S. G. X-ray crystal structures of native HIV-1 capsid protein reveal conformational variability. *Science* **2015**, *349* (6243), 99–103. https://doi.org/10.1126/science.aaa5936.

189. Cummins, L. M.; Weinhold, K. J.; Matthews, T. J.; Langlois, A. J.; Perno, C. F.; Condie, R. M.; Allain, J. P. Preparation and characterization of an intravenous solution of IgG from human immunodeficiency virus-seropositive donors. *Blood* **1991**, *77* (5), 1111-7

190. Mashiba, M.; Collins, K. Molecular mechanisms of HIV immune evasion of the innate immune response in myeloid cells. *Viruses* **2012**, *5* (1), 1–14. https://doi.org/10.3390/v5010001.

191. Cheng X, Ratner L. HIV-2 Vpx protein interacts with interferon regulatory factor 5 (IRF5) and inhibits its function. *J. Biol. Chem.* **2014**; *289*: 9146–9157.

192. Royle, C. M., Graham, D. R., Sharma, S. et al. HIV-1 and HIV-2 differentially mature plasmacytoid dendritic cells into IFN-producing cells or APCs. *J. Immunol.* **2014**; 193: 3538–3548.

193. Sauter, D.; Kirchhoff, F. Multilayered and versatile inhibition of cellular antiviral factors by HIV and SIV accessory proteins. *Cytokine & Growth Factor Reviews* **2018**, *40*, 3–12. https://doi.org/10.1016/j.cytogfr.2018.02.005.

194. Fenrick, R.; Malim, M. H.; Hauber, J.; Cullen, B. R. Functional analysis of the Tat transactivator of human immunodeficiency virus type 2. *J. Virol.* **1989**, *63* (12), 5006–5012.

195. Popper, S. J.; Sarr, A. D.; Guèye-Ndiaye, A.; Mboup, S.; Essex, M. E.; Kanki, P. J. Low plasma human immunodeficiency virus type 2 viral load is independent of proviral load: low virus production in vivo. *J. Virol.* **2000**, *74* (3), 1554–1557. https://doi.org/10.1128/JVI.74.3.1554-1557.2000.

196. O'Donovan, D.; Ariyoshi, K.; Milligan, P.; Ota, M.; Yamuah, L.; Sarge-Njie, R.; Whittle, H. Maternal plasma viral RNA levels determine marked differences in mother-to-child transmission rates Of HIV-1 and HIV-2 in the Gambia: *AIDS* **2000**, *14* (4), 441–448. https://doi.org/10.1097/00002030-200003100-00019.

197. Marchant, D. Human Immunodeficiency Virus Types 1 and 2 Have Different Replication Kinetics in Human Primary Macrophage Culture. *J. Gen. Virol.* **2006**, *87* (2), 411–418. https://doi.org/10.1099/vir.0.81391-0.

198. Chauveau, L.; Puigdomenech, I.; Ayinde, D.; Roesch, F.; Porrot, F.; Bruni, D.; Visseaux, B.; Descamps, D.; Schwartz, O. HIV-2 infects resting CD4+ T cells but not monocyte-derived dendritic cells. *Retrovirology* **2015**, *12* (1), 2. https://doi.org/10.1186/s12977-014-0131-7.

199. Lenzi, G. M.; Domaoal, R. A.; Kim, D.-H.; Schinazi, R. F.; Kim, B. Mechanistic and kinetic differences between reverse transcriptases of Vpx coding and non-coding Lentiviruses. *J. Biol. Chem.* **2015**, *290* (50), 30078–30086. https://doi.org/10.1074/jbc.M115.691576.

200. Patel, S. S.; Wong, I.; Johnson, K. A. Pre-steady-state kinetic analysis of processive DNA replication including complete characterization of an exonuclease-deficient mutant. *Biochemistry* **1991**, *30*:511–525

201. Mizrahi, V.; Henrie, R. N.; Marlier, J. F.; Johnson, K. A.; Benkovic, S. J. Rate-limiting steps in the DNA polymerase I reaction pathway. *Biochemistry* **1985**, *24*, 4010 – 4018

202. Arien, K. K.; Abraha, A.; Quinones-Mateu, M. E.; Kestens, L.; Vanham, G.; Arts, E. J.; 2005. The replicative fitness of primary human immunodeficiency virus type 1 (HIV-1) group M, HIV-1 group O, and HIV-2 isolates. *J. Virol.* **2005**, *79*, 8979–8990.

203. Hawkins, P. G.; Morris, K. V. Transcriptional regulation of Oct4 by a long non-coding RNA antisense to Oct4-pseudogene 5. *Transcription* **2010**, *1*: 165–175.

204. Johnsson, P.; Ackley, A.; Vidarsdottir, L.; Lui, W. O.; Corcoran, M.; Grandér, D.; *et al.* A pseudogene long-noncoding-RNA network regulates PTEN transcription and translation in human cells. *Nat Struct Mol Biol* **2013**, *20*: 440–446.

205. Morris, K. V.; Santoso, S.; Turner, A. M.; Pastori, C.; Hawkins, P. G. Bidirectional transcription directs both transcriptional gene activation and suppression in human cells. *PLoS Genet* **2008**, *4*: e1000258.

206. Yu, W.; Gius, D.; Onyango, P.; Muldoon-Jacobs, K.; Karp, J.; Feinberg, A. P.; *et al.* Epigenetic silencing of tumor suppressor gene p15 by its antisense RNA. *Nature* **2008**, *451*: 202–206.

207. Lee, J. T. Epigenetic regulation by long noncoding RNAs. *Science* **2012** *338*: 1435–1439.

208. Landry, S.; Halin, M.; Lefort, S.; Audet, B.; Vaquero, C.; Mesnard, J. M.; *et al*. Detection, characterization and regulation of antisense transcripts in HIV-1. *Retrovirology* **2007** *4*: 71.

209. Ludwig, L. B.; Ambrus, J. L. Jr.; Krawczyk, K. A.; Sharma, S.; Brooks, S.; Hsiao, C. B.; *et al*. Human immunodeficiency virus-type 1 LTR DNA contains an intrinsic gene producing antisense RNA and protein products. *Retrovirology* **2006**, *3*: 80.

210. Schopman, N. C.; Willemsen, M.; Liu, Y. P.; Bradley, T.; van Kampen, A.; Baas, F.; *et al*. Deep sequencing of virus-infected cells reveals HIV-encoded small RNAs. *Nucleic Acids Res* **2012**, 40: 414–427.

211. Kobayashi-Ishihara, M.; Yamagishi, M.; Hara, T.; Matsuda, Y.; Takahashi, R.; Miyake, A.; *et al*. HIV-1-encoded antisense RNA suppresses viral replication for a prolonged period. *Retrovirology* **2012**, *9*: 38.

212. Saayman, S.; Ackley, A.; Turner, A.-M. W.; Famiglietti, M.; Bosque, A.; Clemson, M.; Planelles, V.; Morris, K. V. An HIV-encoded antisense long noncoding RNA epigenetically regulates viral transcription. *Molecular Therapy* **2014**, *22* (6), 1164–1175. https://doi.org/10.1038/mt.2014.29.

VITA

Assi V. D. P. Yapo was born in Adzope, Cote d'Ivoire in 1976. After my High School Diploma in 1995, I was admitted to the Department of Pharmaceutical and Biological Sciences of the Felix Houphouet Boigny University of Abidjan, Cote d'Ivoire. There I was trained as a pharmacist specialized in medical biology. I got a Pharmacy Doctorate (PharmD) in 2004, and went on to do a residency in medical biology in several teaching hospitals in Cote d'Ivoire for 4 years. During my residency time, I earned several certificates in Hematology, Bacteriology, Virology, and Clinical Biochemistry. In 2012, I successfully completed a Post-Graduate Diploma in Human Tropical Biology.

In 2005, I was recruited and posted to the Central Medical Laboratory of the Teaching Hospital of Yopougon, Abidjan. Two years later, I joined a research team at the leading research center on HIV/AIDS in Cote d'Ivoire, the Center for Diagnostic and research on HIV/AIDS and Opportunistic Infections (CeDReS). The same year, I was recruited as a Teaching Assistant by the Department that did my initial training at the university. As member of the research team aforementioned, I have authored 11 peer-reviewed papers including one first author article in 2013.

In 2014, I became a grantee of the Foreign Student Fulbright Board with a two-year scholarship to start a PhD program in the USA. I joined the Molecular Pathogenesis and Therapeutics (M.P.T.) PhD program and the Sarafianos lab in the Fall of the same year. There I was fortunate to be under the mentorship of Stefan G. Sarafianos, PhD, and Marc C. Johnson, PhD. I met terrific scientists in my committee members, the Sarafianos lab, the Johnson lab, and the various core facilities at the Christopher Bond Life Sciences Center. I fulfilled the requirements for the Doctor of Philosophy in the Spring 2020.